TECHNISCHE UNIVERSITÄT WIEN

VIENNA UNIVERSITY OF TECHNOLOGY

DISSERTATION

OFDM Multi-User Communication Over Time-Variant Channels

ausgeführt zum Zwecke der Erlangung des akademischen Grades
eines Doktors der technischen Wissenschaften

eingereicht an der
Technischen Universität Wien
Fakultät für Elektrotechnik und Informationstechnik

von

Dipl.-Ing. Thomas Zemen
Maurer Lange Gasse 87/2, 1230 Wien
geboren in Mödling am 20. Jänner 1970
Matrikelnr. 8925585

Wien, im July 2004 .....

Supervisor

Prof. Ernst Bonek

Institut für Nachrichtentechnik und Hochfrequenztechnik

Technische Universität Wien

Examiner

Prof. Markus Rupp

Institut für Nachrichtentechnik und Hochfrequenztechnik

Technische Universität Wien

Kurzfassung

Die Verfügbarkeit hoher Datenraten für mobile Teilnehmer ist eine der wichtigsten Eigenschaften zukünftiger Mobilfunksysteme. Wir untersuchen ein MC-CDMA (multi-carrier code division multiple access) System bei dem eine OFDM (orthogonal frequency division multiplexing) basierte Mehrträgerübertragung mit der Spreizung der Datensymbol im Frequenzbereich verbunden wird. Die Spreizsequenz dient zur Identifikation der Benutzer und ermöglicht die Ausnützung der Mehrwegediversität des Mobilfunkkanals. Die Übertragung ist blockorientiert, wobei sich ein Block aus OFDM Pilot- und OFDM Datensymbolen zusammensetzt.

Für Schrittgeschwindigkeit kann der Mobilfunkkanal als konstant für die Dauer eines Datenblocks modelliert werden. Wir verwenden ein iteratives Mehrbenutzerdetektionsverfahren. Hierbei werden Softsymbole aus den Ausgangsdaten des Dekoders gewonnenen. Mittels dieser Softsymbole kann die Interferenz, die durch andere Benutzer verursacht wird, reduziert werden. Wir entwickeln ein iteratives Kanalschätzverfahren das die zurückgeführten Softsymbole zur Verbesserung der Kanalschätzung verwendet. Die Bitfehlerrate des iterativen Empfängers kommt der Einbenutzergrenze nahe. Die Einbenutzergrenze ist die Bitfehlerrate die der Empfänger für einen einzelnen Benutzer und bei perfekter Kanalkenntnis erreicht.

Zur weiteren Verbesserung der Kanalschätzung nützen wir den geschätzten Mittelwert und die geschätzte Varianz der Softsymbole. Diese Informationen können aus den Dekoderausgangsdaten abgeleitet werden da die Datensymbole aus einem Alphabet mit konstantem Betrag stammen. Die iterative Kanalschätzung die diese Informationen zur Minimierung des quadratischen Fehlers (MMSE, minimum mean square error) nützt, führt zu verbesserter Konvergenz des iterativen Empfängers.

Bei Fahrzeuggeschwindigkeit ändert sich der Kanal signifikant über die Dauer eines Datenblocks. Wir benötigen daher eine adäquate Beschreibung seiner zeitlichen Veränderung. Wir untersuchen Algorithmen die den zeitvarianten Kanal schätzen können, ohne genaue Information über seine Statistik zweiter Ordnung zu benötigen. Es wird nur die Kenntnis der maximalen Dopplerbandreite in einem Mobilfunksystem, die durch die Trägerfrequenz und die maximale Geschwindigkeit der Benutzer bestimmt ist, angenommen.

Wir untersuchen zuerst zeitvariante frequenzflache Kanäle und analysieren die

Fourier Basisentwicklung für die zeitvariante Kanalschätzung. Die Analyse zeigt, dass die Fensterung durch die begrenzte Blocklänge zu spektraler Verschmierung führt und die beschränkte Dimension der Fourier Basisentwicklung einen Effekt ähnlich dem Gibbs Phänomen verursacht. Beide Mechanismen zusammen sind der Grund für systematische Schätzfehler.

Slepians Theorie der zeitkonzentrierten und bandlimitierten Sequenzen eröffnet einen neuen Ansatz für die zeitvariante Kanalschätzung. Diese Theorie ermöglicht das Design von doppelt orthogonalen DPS (discrete prolate spheroidal) Sequenzen die an die Datenblocklänge und die maximale Dopplerbandbreite angepasst sind. Die DPS Sequenzen werden zur Definition der Slepian Basisentwicklung verwendet. Wir beweisen analytisch, dass der systematische Schätzfehler der Slepian Basisentwicklung mindestens eine Zehnerpotenz kleiner ist als der der Fourier Basisentwicklung.

Die Slepian Basisentwicklung verliert ihre Orthogonalität für pilotbasierte Kanalschätzung und ihr systematischer Schätzfehler wächst mit sinkender Pilotanzahl. Wir lösen dieses Problem durch das Design neuer endlicher Sequenzen die auch auf dem Pilotraster orthogonal sind und weiterhin bandlimitiert und zeitkomprimiert bleiben. Die generalisierte endliche Slepian Basisentwicklung, die auf den resultierenden generalisierten FDPS (finite discrete prolate spheroidal) Sequenzen aufbaut, zeigt die beste Leistung für pilotbasierte Kanalschätzung. Wir beweisen dies durch analytische Ergebnisse und präsentieren numerische Simulationen.

Wir verwenden die generalisierte endliche Slepian Basisentwicklung für die Kanalschätzung eines zeitvarianten frequenzselektiven Kanals in einem MC-CDMA System in der Abwärtstrecke. Simulationsergebnisse zeigen die hervorragende Leistung dieses Kanalschätzverfahrens speziell für eine geringe Anzahl an Pilotsymbolen. Der zeitvariante frequenzselektive Kanal bietet Mehrwegediversität und Dopplerdiversität. Ein MC-CDMA System kann beide Diversitätsquellen durch Verschachtelung und Kodierung der Datensymbole ausnützen. Wir leiten ein analytisches Maß für die Dopplerdiversität ab und untersuchen mit Simulationsergebnissen wie viel Diversität ein MC-CDMA System tatsächlich nützen kann.

Wir entwickeln in dieser Dissertation eine iterative Empfängerarchitektur für die Aufwärtsstrecke mit Mehrbenutzerdekodierung für zeitvariante Mobilfunkkanäle. Dieser Empfänger nähert sich der Einbenutzergrenze bis auf 2.5 dB unter voller Last mit 64 Benutzern, für ein Signal zu Rauschverhältnis von 14 dB und mit mobilen Benutzern die sich mit einer Geschwindigkeit im Bereich von 0 bis 100 km/h bewegen.

Abstract

Wireless broadband communications for users moving at vehicular speed is a cornerstone of future fourth generation (4G) mobile communication systems. We investigate a multi-carrier (MC) code division multiple access (CDMA) system which is based on orthogonal frequency division multiplexing (OFDM). A spreading sequence is used in the frequency domain in order to distinguish individual users and to take advantage of the multipath diversity of the wireless channel. The transmission is block oriented. A block consists of OFDM pilot and OFDM data symbols.

At pedestrian velocities the channel can be modelled as block fading. We apply iterative multi-user detection and channel estimation. In iterative receivers soft symbols are derived from the output of an soft-input soft-output decoder. These soft symbols are used in order to reduce the interference from other users and to enhance the channel estimates. We develop an iterative channel estimation scheme for MC-CDMA. The iterative MC-CDMA receiver achieves a performance close to the single-user bound in moderately overloaded systems. The single-user bound is defined as the performance for one user and perfect channel knowledge.

In order to obtain enhanced iterative channel estimates we take advantage of additional information like the estimated mean and variance of the soft symbols, which can be obtained from the decoder output since the used symbol alphabet has constant modulus. Using these information a linear minimum mean square error (MMSE) channel estimator is derived. The iterative receiver achieves enhanced convergence towards the single-user bound with the linear MMSE channel estimator.

At vehicular velocities, the channel can not be treated as block fading for the duration of a data block. Instead, its temporal variation must be modelled adequately. We investigate channel estimation algorithms that do *not* need the knowledge of complete second order statistics. We assume an upper bound for the Doppler bandwidth only, which is determined by the carrier frequency and the maximum supported velocity. This approach is motivated by the fact that existent wireless channels do *not* adhere to Jakes' model.

First, we deal with time-variant frequency-flat channels. We analyze the Fourier basis expansion, i.e. a truncated discrete Fourier transform (DFT), for time-variant channel estimation. The analysis shows that the windowing due to the block-based

transmission leads to spectral leakage and the truncation of the DFT gives rise to an effect similar to the Gibbs phenomenon. Both mechanisms together lead to biased channel estimates.

Slepian's theory of time-concentrated and bandlimited sequences allows a new approach for time-variant channel estimation. It enables the design of doubly orthogonal discrete prolate spheroidal (DPS) sequences with just two parameters; the block length and the maximum Doppler bandwidth. The DPS sequences are used to define a Slepian basis expansion. We give analytic results showing that the bias of the Slepian basis expansion is at least one magnitude smaller compared to the Fourier basis expansion.

The Slepian basis expansion performance degrades for pilot based channel estimation because the orthogonality of the basis functions is lost due to the pilot grid. We tackle this problem by designing a new set of finite sequences that are orthogonal over the pilot index positions but keep their bandlimited and time-concentrated properties. The resulting generalized finite Slepian basis expansion achieves best performance for pilot based time-variant channel estimation which is proven by analytical results and shown in numerical simulations.

We apply the generalized finite Slepian basis expansion for time-variant frequency-selective channel estimation in an MC-CDMA downlink and discuss simulation results. The time-variant frequency-selective channel offers Doppler diversity in addition to multipath diversity. An MC-CDMA system can take advantage of the Doppler diversity through interleaving and coding over a data block. We derive an analytic measure for the Doppler diversity of a time-variant channel and support it by simulation results.

In this thesis, we design an iterative receiver-architecture for an MC-CDMA uplink with multi-user decoding for time-variant mobile radio channels. It is shown that this receiver type reaches the single-user bound up to 2.5 dB under full load with $N = 64$ users, at an $E_\mathrm{b}/N_0 = 14\,\mathrm{dB}$, and for mobile users moving with velocities in the range from 0 to 100 km/h.

Acknowledgment

I would like to thank Christoph Mecklenbräuker for his continuous support and encouragement. His subtle guidance together with Professor Ernst Bonek, Professor Markus Rupp and Ralf Müller helped me to discover new grounds in mobile communications.

A significant part of funding for this research was provided by Siemens AG Austria from the department for radio communication devices (PSE PRO RCD). I would like to thank Werner Schladofsky, Martin Birgmeier, Leopold Faltin, Alfred Pohl and Günther Hraby for their support.

I am grateful to all my colleagues at the Telecommunication Research Center Vienna (ftw.) especially to Joachim Wehinger, Florian Hammer, Helmut Hofstetter and Maja Lončar. The collaboration with them was a constant source of new ideas, chocolate, coffee and entertaining hours. The professional, inspiring, and open work environment at ftw., shaped by Markus Kommenda and Horst Rode, provided the basis for the work on this thesis.

I would like to thank my family and my friends for their continuous sympathy in my research adventure, and Dada for being the smiling sun in my life.

Contents

1 Introduction

Wireless broadband communication for users moving at vehicular speed is the cornerstone of future fourth generation (4G) mobile communication systems. Current systems like UMTS [1] provide a maximum bit rate of 384 kbit/s for mobile users while wireless local area network (LAN) systems like IEEE 802.11a [29] provide more than 10 Mbit/s under ideal conditions in an office environment. Figure 1.1 shows the mobility bit-rate regions for different communication systems [58].

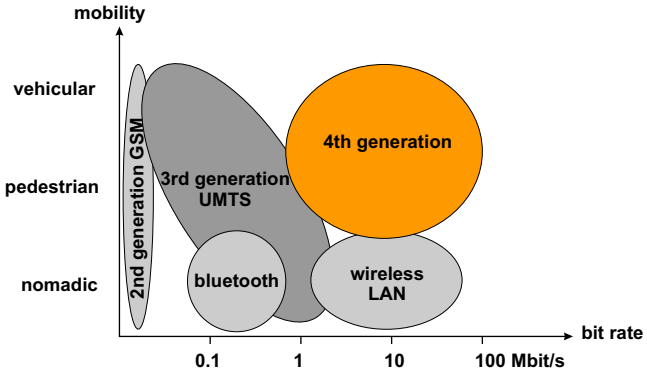

Figure 1.1: Mobility versus bit rate for existing and future wireless communication systems [58].

Users moving at vehicular speed communicate over a wireless channel that exhibits time-variant frequency-selective characteristics due to multipath propagation and Doppler effects. Thus, accurate channel state information at the receiver side, an appropriate modulation format, an efficient multiple access scheme and low complexity equalization algorithms are necessary to enable high bit rate transmission.

In this thesis we develop solutions for these challenging problems based on orthogonal frequency division multiplexing (OFDM) [81] which uses multiple orthogonal subcarriers to transmit information. OFDM is used in state of the art wireless high bit rate applications like digital video broadcast terrestrial (DVB-T) [59, 19], digital audio broadcast (DAB) [18], digital radio mondial (DRM) [20] and in wireless LANs according to the IEEE 802.11a standard. For high bit-rate downlink applications

a UMTS extension based on OFDM is under discussion [2]. IEEE 802.20 [30] is another currently developed high bit-rate communication standard for mobile users that will be based on OFDM too.

1.1 Outline and Contributions

The thesis is organized in the following chapters and the author's contributions are as follows:

Chapter 2: Multi-Carrier Code Division Multiple Access (MC-CDMA)

Starting with multipath propagation in wireless channels the dependence of the inter-symbol interference on the delay spread and the bit rate is discussed. In order to avoid the high complexity of time domain equalizers at high bit-rates OFDM [11] has been introduced. In OFDM the information is transmitted over a set of orthogonal subcarriers which enables low complexity equalization of frequency-selective channels.

Linear precoding [16], i.e. spreading, has been introduced in order to avoid the influence of strongly attenuated subcarriers [96] which are caused by the frequency-selective nature of the wireless channel. The spreading operation additionally distinguishes the individual users in a multi-user system [34]. A short introduction of multi-user detection [75, 50] is given before iterative multi-user detection based on parallel interference cancellation and minimum mean square error (MMSE) filtering is introduced [51, 80].

Chapter 3: Iterative Channel Estimation for Block-Fading Channels

Accurate channel estimation is crucial for the performance of a multi-user receiver. In this chapter we assume that the wireless channel has block-fading frequency-selective characteristic, i.e. the channel stays constant for the duration of a data block. A data block consists of OFDM pilot and OFDM data symbols.

We design an iterative least-square channel estimation scheme for the MC-CDMA uplink where deterministic pilot information is combined with soft-symbols in order to obtain enhanced channel estimates [91]. The soft-symbols are derived from the output of a soft-input soft-output decoder, implemented using the BCJR algorithm [6]. An MC-CDMA receiver using this scheme achieves a performance close to the single-user bound. The single-user bound is defined as the receiver performance for one user and perfect channel knowledge at the receiver side.

The channel estimation performance degrades if the number of users is bigger than the degrees of freedom for the spreading sequence (overloaded system). In order to

accommodate to this situation we derive an improved channel estimator based on the linear MMSE criterion. This estimator exploits statistical information, like the mean and the variance of the soft-symbols, which can be derived from the decoder output. Hence, we achieve a monotonically decreasing channel estimation error with increasing number of iterations in overloaded systems and at low signal to noise ratios [84].

Chapter 4: Time-Variant Frequency-Flat Channel Estimation

The variation in time of the wireless channel is caused by user mobility and multipath propagation. In this chapter we limit our considerations to time-variant frequency-flat channels, i.e. the symbol duration is longer than the delay spread of the channel. In this case the channel is memory-less. We discuss different time-variant channel estimation methods highlighting their applicability for receivers with block processing. In this thesis we focus on algorithms that do not need *complete* knowledge of the second order statistics of the fading process. This is due to the fact that real wireless channels do not adhere to Jakes' model [92]. However, we do exploit the fact that the variation of a frequency-flat channel over the duration of a data block is upper bounded by the maximum Doppler bandwidth which is determined by the maximum velocity of the users and the carrier frequency. We analyze the well-known Fourier basis expansion [9] and show its weaknesses [88].

To overcome the drawbacks of the Fourier basis expansion we exploit results from the theory of time-concentrated and bandlimited sequences [70, 69] and apply a Slepian basis expansion for time-variant frequency-flat channel estimation. The Slepian basis functions are designed according to the block length and the maximum Doppler bandwidth. We establish analytic results for the mean square error per subcarrier enabling an easy comparison between the Slepian basis expansion and any other set of basis functions [52]. The bias of the Slepian basis expansion is shown to be at least one magnitude smaller compared to the Fourier basis expansion.

The Slepian basis expansion is biased when a pilot grid is used for channel estimation. We develop a generalized finite Slepian basis expansion using basis functions that are time-concentrated, bandlimited, and orthogonal on the pilot grid. This enables time-variant frequency-flat channel estimation with extremely low complexity [85, 87]. We develop analytic expressions for the bias and variance of pilot-based basis expansion channel estimators [87] extending the concepts of [52].

We describe a simulation model for time-variant channels with Jakes' spectrum based on [93]. This simulation model generates channels with correct Rayleigh fading statistic for the full velocity range [86] and converges to a block fading channel for zero velocity. We use Jakes' model for the purpose of performance evaluation in order to enable easy comparisons with existing results in the literature only.

Chapter 5: Time-Variant Frequency-Selective Channel Estimation

We develop a channel estimator for an MC-CDMA downlink by generalizing the results from Chapter 4 for frequency-selective channels [87]. An upper bound for the Doppler diversity of a time-variant channel [86] is derived and we give simulation results demonstrating the ability of MC-CDMA to take advantage of Doppler diversity if the channel estimation is based on the finite Slepian basis expansion. The receiver performs *better* with increasing speed of the user.

Chapter 6: Iterative Time-Variant Channel Estimation and Data Detection

We present an iterative multi-user detector and time-variant channel estimator for an MC-CDMA uplink. We apply the Slepian basis expansion for pilot based time-variant frequency-selective channel estimation and combine it with the iterative scheme developed in Chapter 3. Thus, we combine deterministic pilot information with soft symbols so that we obtain enhanced time-variant channel estimates. An iterative linear MMSE estimation algorithm for the basis expansion coefficients in a multi-user system is derived. The consistent performance of the iterative receiver for a wide range of velocities is validated by simulations [90, 89].

1.2 Notation

We use the notation presented in Table 1.1 throughout this thesis:

Symbol	Description
$f(t)$	function of a continuous variable
$f[m]$	function of a discrete variable
$\boldsymbol{a}$	column vector
$a[i]$	i-th element of $\boldsymbol{a}$
$\boldsymbol{A}$	matrix
$[\boldsymbol{A}]_{i,\ell}$	i,ℓ-th element of $\boldsymbol{A}$
$\boldsymbol{A}_{P\times Q}$	upper left part of $\boldsymbol{A}$ with dimension $P \times Q$
$\boldsymbol{A}^{\mathrm{T}}$	transpose of $\boldsymbol{A}$
$\boldsymbol{A}^{\mathrm{H}}$	conjugate transpose of $\boldsymbol{A}$
$\mathrm{diag}(\boldsymbol{a})$	diagonal matrix with entries $a[i]$
$\boldsymbol{I}_Q$	$Q \times Q$ identity matrix
$\boldsymbol{F}_Q$	$Q \times Q$ unitary Fourier matrix
$\boldsymbol{1}_Q$	$Q \times 1$ column vector with all ones
$\boldsymbol{0}_Q$	$Q \times 1$ column vector with all zeros
a^*	complex conjugate of a
$\lfloor a \rfloor$	largest integer, lower or equal than $a \in \mathbb{R}$
$\lceil a \rceil$	smallest integer, greater or equal than $a \in \mathbb{R}$
$\lvert a \rvert$	absolute value of a
$\lVert \boldsymbol{a} \rVert$	ℓ_2 norm of vector $\boldsymbol{a}$
$\lVert \boldsymbol{A} \rVert_{\mathrm{F}}$	Frobenius norm of matrix $\boldsymbol{A}$
$\mathrm{vec}(\boldsymbol{A})$	stacks all columns of matrix $\boldsymbol{A}$ in a single vector
j	$\sqrt{-1}$
$\delta_{i\ell}$	1 for $i = \ell$, 0 otherwise

Table 1.1: Notation used throughout this thesis.

2 Multi-Carrier Code Division Multiple Access (MC-CDMA)

Electromagnetic waves are the medium of choice for the transmission of information between two remote locations if one side or both sides are moving. However, the flexibility of wireless communication does not come at no cost.

2.1 Why Multi-Carrier Transmission?

Electromagnetic waves, transmitted from an antenna, arrive at the receiving antenna via different paths. Figure 2.1 gives a simplified schematic representation of such a wireless multipath wave propagation scenario.

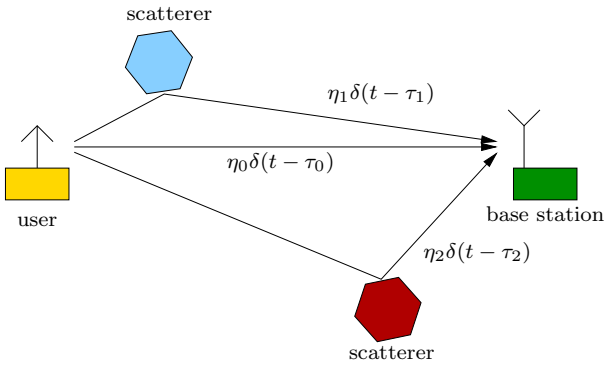

Figure 2.1: Wireless multipath propagation. Every path ℓ has attenuation η_ℓ and time delay τ_ℓ.

Every path ℓ experiences a specific attenuation η_ℓ and time delay τ_ℓ corresponding to the runtime of the electromagnetic wave. This is why the channel impulse response is made up by the sum of L' different paths, mathematically described by

$$h'(t) = \sum_{\ell=0}^{L'-1} \eta_\ell \delta(t-\tau_\ell)\,. \tag{2.1}$$

Throughout this thesis we use an equivalent sampled baseband description for the wireless channel. Thus, we combine the effect of the up-converter, the transmit filter $h_{\mathrm{T}}(t)$, the channel $h'(t)$, the matched receive filter $h_{\mathrm{R}}(t)$ and the down-converter into the equivalent, complex-valued impulse response

$$h(t) = h_{\mathrm{T}}(t) * h'(t) * h_{\mathrm{R}}(t) \tag{2.2}$$

where $*$ denotes convolution. The sampling operation at rate $1/T_{\mathrm{C}}$ is denoted by

$$h[\ell] = h(\ell T_{\mathrm{C}}) \tag{2.3}$$

where discrete time $\ell \in \{0, \ldots, L-1\}$ with L denoting the essential support of the sampled impulse response. We assume Rayleigh fading characteristics [54],

$$\mathbb{E}\left\{|h[\ell]|^2\right\} = \eta^2[\ell]$$

and an exponential decaying power delay profile $\eta^2[l]$ according to COST 259 [15]

$$\eta^2[\ell] = \frac{\mathrm{e}^{-\frac{\ell}{L_{\mathrm{D}}}}}{\sum_{\ell'=0}^{L-1} \mathrm{e}^{-\frac{\ell'}{L_{\mathrm{D}}}}} \tag{2.4}$$

where

$$L_{\mathrm{D}} = T_{\mathrm{D}}/T_{\mathrm{C}}$$

denotes the root mean square delay spread T_{D} normalized to the sampling rate $1/T_{\mathrm{C}}$. In this thesis the term delay spread is used as short form for root mean square delay spread, throughout. In the special case of an exponential power delay profile (2.4) the delay spread gives the time after which the power delay profile has decayed to $1/e$. For the case of a general impulse response the delay spread is defined as the second central moment of the power delay profile [56]

$$T_{\mathrm{D}} = \sqrt{\frac{\sum_{\ell=0}^{L'-1} \eta_\ell^2 \tau_\ell}{\sum_{\ell=0}^{L'-1} \eta_\ell^2} - \left(\frac{\sum_{\ell=0}^{L'-1} \eta_\ell^2 \tau_\ell^2}{\sum_{\ell=0}^{L'-1} \eta_\ell^2}\right)^2}$$

We neglect path loss and assume perfect power control

$$\sum_{\ell=0}^{L-1} \eta^2[\ell] = 1\,. \tag{2.5}$$

Topology	Delay spread T_D	Max. path length difference
office building	40ns	15m
corridor	120ns	35m
typical urban	400ns	120m

Table 2.1: Root mean square delay spread T_D in different topologies for a single reflecting cluster according to COST259 [15].

The essential support of the sampled impulse response L is selected according to the signal to noise ratio at which the wireless communication system will operate:

$$L \geq 1 + T_\mathrm{D}/T_\mathrm{C} \ln\left(\frac{E_\mathrm{b}}{N_0}\right) . \tag{2.6}$$

Hence, components of the channel impulse response that are smaller than the signal to noise ratio are not taken into account. We also assume perfect time- and frequency synchronization.

The delay spread T_D is mainly influenced by the topology and the material of the surrounding area. Table 2.1 lists typical values for the delay spread of a single reflecting cluster [15]. These values are further increased if metallic reflectors are present. In COST 259 scenarios like bad urban or hilly terrain the possibility of further reflecting clusters is high. This leads to longer impulse responses consisting of a superposition of several individual exponential decaying components. For the sake of simplicity we use the typical urban scenario and model the channel with one reflecting cluster, only.

Figure 2.2 shows the channel impulse response magnitude $|h(t)|$ of a typical urban scenario in Oslo. The impulse response was obtained by channel sounder measurements [27]. Additionally, Figure 2.2 shows the sampled impulse response magnitude $|h[n]|$ sampled at the UMTS sampling rate $1/T_\mathrm{C} = 3.84 \cdot 10^6\,\mathrm{s}^{-1}$.

In a simple communication system the sequence of symbols $d[n]$ is directly transmitted over the multipath channel $h[n]$ where n denotes discrete time at rate $1/T_\mathrm{C}$. The received signal is given by the convolution of the symbol sequence with the channel impulse response:

$$x[n] = \sum_{\ell=0}^{L-1} h[\ell]d[n-\ell] = h[0]d[n] + \underbrace{\sum_{\ell=1}^{L-1} h[\ell]d[n-\ell]}_{\text{ISI}} \tag{2.7}$$

From (2.6) and Figure 2.2 it becomes clear that the number of samples L that represent the impulse response increase linearly with increasing sample rate $1/T_\mathrm{C}$. Thus,

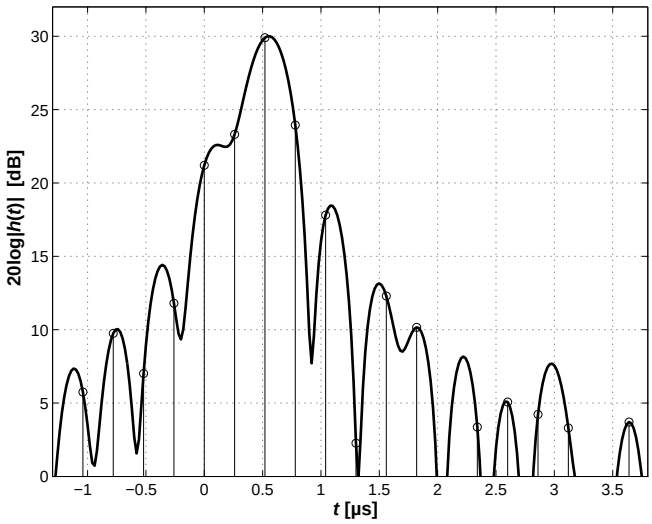

Figure 2.2: Impulse response magnitude $|h(t)|$ obtained through channel sounder measurement in an urban scenario in Oslo [27]. Additionally, we also depict the sampled impulse response magnitude $|h[\ell]|$ sampled at the UMTS sampling rate $1/T_C = 3.84 \cdot 10^6\,\mathrm{s}^{-1}$. The time origin was placed at τ_0, the time delay of the first arriving wavefront.

the inter-symbol interference (ISI) described by the second term in (2.7) increases too. The application of a time-domain equalizer is the classical approach to remove the inter-symbol interference. However, a time-domain equalizer gets prohibitively complex with increasing data rate since the number of operations necessary grows with $\mathcal{O}(L^2)$.

In the next section we will introduce orthogonal frequency division multiplexing (OFDM). This is a technique that is able to avoids inter-symbol interference completely [11].

2.2 Orthogonal Frequency Division Multiplexing (OFDM)

The basic idea of OFDM is to transmit N symbols in parallel over N different subcarriers [81] while enlarging the symbol duration N times. Figure 2.3 visualizes the OFDM principle through a rotation of the time-frequency plane. In a single-carrier system each symbol occupies the full bandwidth. In an multi-carrier system the symbol duration is enlarged N times and simultaneously the bandwidth consumption of each symbol is reduced by the same factor N. The overall data-rate

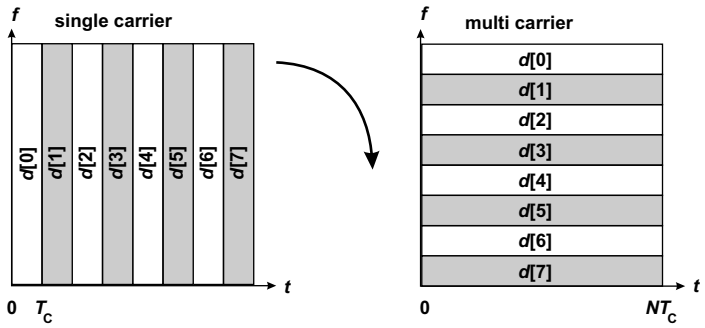

Figure 2.3: We illustrate the difference between a single-carrier and a multi-carrier system through a rotation of the time-frequency plane. The transmitted data symbols are denoted $d[1] \ldots d[8]$. The multi-carrier system uses $N = 8$ subcarriers.

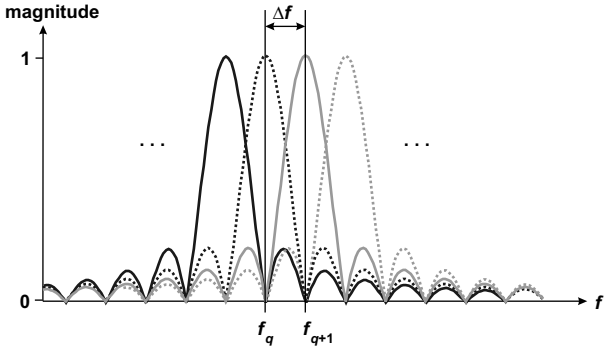

Figure 2.4: Subcarrier frequency-spectra in an OFDM system. The subcarrier have bandwidth Δf. The center frequency of subcarrier q is denoted by f_q.

and bandwidth consumption is kept constant trough parallel transmission over N independent subcarriers.

The subcarrier spectra overlap, as depicted in Figure 2.4. However, if the center frequency of each subcarrier q is chosen as

$$f_q = q/(NT_C) \tag{2.8}$$

for $q \in \{0, \ldots, N-1\}$ the subcarriers are orthogonal despite their overlapping spectra. OFDM is a special case of a multi-carrier scheme with overlapping but orthogonal subcarriers.

Figure 2.5 shows all operations that are necessary for OFDM. Each subcarrier is modulated by a symbol (from a binary phase shift keying (BPSK) alphabet in this example) and the resulting signals are summed up. These operations are equivalent to an inverse discrete Fourier transform (DFT). The inverse DFT can be efficiently

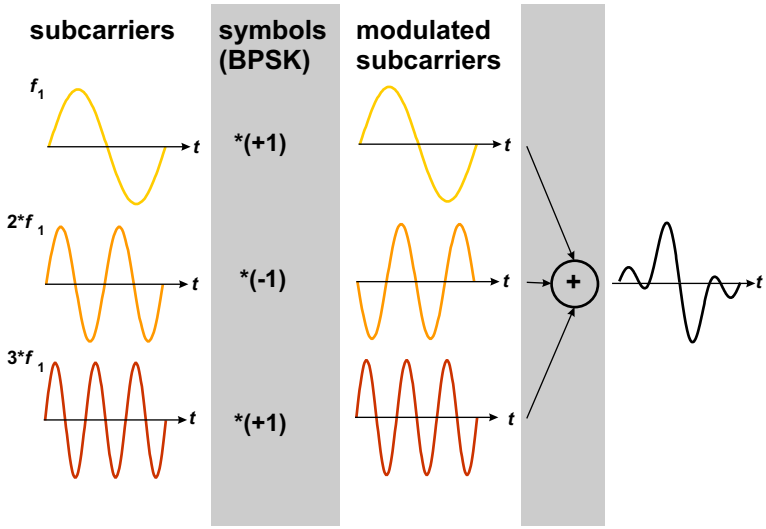

Figure 2.5: OFDM needs the following processing steps: First the subcarriers are multiplied by the individual data symbols, then the resulting signals are added together.

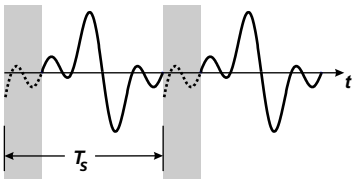

Figure 2.6: Cyclic prefix insertion: A copy of the signal tail is inserted at the beginning of each OFDM symbol.

implemented by means of the inverse fast Fourier transform. The existence of such an efficient algorithm for the actual implementation is one major reason for the widespread application of OFDM.

OFDM enlarges the symbol duration by a factor of N, as depicted in Figure 2.3, which results in reduced inter-symbol interference. However, in order to completely remove the inter-symbol interference a cyclic prefix is inserted in front of every OFDM symbol. The cyclic prefix is a copy of the OFDM symbol tail. We illustrate this operation in Figure 2.6. A mathematically more thorough explanation of the cyclic prefix follows in the next section. For complete inter-symbol interference removal the length of the cyclic prefix G must be longer than the essential support of the channel impulse response L,

$$G \geq L\,. \tag{2.9}$$

The length of the OFDM symbol in chips after insertion of the cyclic prefix is denoted by $P = N + G$.

After this treatment of OFDM at a glance we give a more detailed and mathematical description of OFDM for the single-user case in the following section.

2.3 Single-User Signal Model

OFDM maps a symbol vector $\boldsymbol{d}[m] \in \mathbb{C}^N$ into a chip vector according to

$$\boldsymbol{\mu}[m] = \boldsymbol{T}_{\mathrm{CP}} \boldsymbol{F}_N^{\mathrm{H}} \boldsymbol{d}[m] \,. \tag{2.10}$$

After parallel to serial conversion the chips are serially transmitted over the multipath channel. We denote discrete time at rate $1/T_{\mathrm{S}}$ by m. The unitary DFT matrix $\boldsymbol{F}_N \in \mathbb{C}^{N \times N}$ has elements

$$[\boldsymbol{F}_N]_{i,\ell} = \frac{1}{\sqrt{N}} \, \mathrm{e}^{\frac{-\mathrm{j}2\pi i \ell}{N}} \,, \qquad i, \ell \in \{0, \ldots, N-1\} \,. \tag{2.11}$$

The cyclic prefix insertion is described via matrix

$$\boldsymbol{T}_{\mathrm{CP}} = \begin{bmatrix} \boldsymbol{I}_{\mathrm{CP}} \\ \boldsymbol{I}_N \end{bmatrix} \in \mathbb{R}^{P \times N} \,.$$

This matrix replicates the last G chips of each OFDM symbol to the front. $\boldsymbol{I}_{\mathrm{CP}} \in \mathbb{R}^{G \times N}$ denotes the last G rows of the identity matrix $\boldsymbol{I}_N \in \mathbb{R}^{N \times N}$ [94, 78].

We formulate the parallel to serial conversion of the chip vector as

$$\boldsymbol{\mu}[m] = \begin{bmatrix} \mu[mP] \\ \vdots \\ \mu[mP + P - 1] \end{bmatrix} \in \mathbb{C}^P \,.$$

The chip sequence $\mu[n]$ with chip rate $1/T_{\mathrm{C}}$ is transmitted over a multipath Rayleigh fading channel with block-fading characteristic. We assume the channel to remain constant for M OFDM symbols. The chip rate is P-times the symbol rate

$$\frac{1}{T_{\mathrm{C}}} = P \frac{1}{T_{\mathrm{S}}} \,.$$

The multipath fading channel $h[\ell]$ has an essential support of length L. We assume that the components of $h[\ell]$ for $\ell \geq L$ do not contribute to the inter-symbol interference since they are below the signal to noise ratio (see (2.6)). We express the channel impulse response in vector notation as

$$\boldsymbol{h} = \begin{bmatrix} h[0] \\ \vdots \\ h[L-1] \end{bmatrix} \in \mathbb{C}^L \,.$$

The resulting signal at the receiver input without noise is given by

$$x[n] = \sum_{\ell=0}^{L-1} h[\ell]\mu[n-\ell]\,. \tag{2.12}$$

The received signal in the presence of complex additive white Gaussian noise $z[n]$ with zero mean and variance σ_z^2 can be written as

$$r[n] = x[n] + z[n].$$

Following the lines of [78, 94] we convert the serial representation of (2.12) into vector-matrix form. We define the vector

$$\boldsymbol{x}[m] = \begin{bmatrix} x[mP] \\ \vdots \\ x[mP+P-1] \end{bmatrix} \in \mathbb{C}^P$$

and equivalently

$$\boldsymbol{z}'[m] = \begin{bmatrix} z[mP] \\ \vdots \\ z[mP+P-1] \end{bmatrix} \in \mathbb{C}^P.$$

Let

$$\boldsymbol{H}^{(0)} = \begin{bmatrix} h[0] & 0 & & & \dots & 0 \\ \vdots & \ddots & & & & \vdots \\ h[L-1] & & & & & \\ 0 & \ddots & & & & \\ \vdots & \ddots & & & & 0 \\ 0 & \dots & 0 & h[L-1] & \dots & h[0] \end{bmatrix} \in \mathbb{C}^{P\times P}$$

be the lower triangular Toeplitz channel matrix and let

$$\boldsymbol{H}^{(1)} = \begin{bmatrix} 0 & \dots & 0 & h[L-1] & \dots & h[1] \\ & \ddots & & \ddots & \ddots & \vdots \\ & & & & & h[L-1] \\ & & & & & 0 \\ \vdots & & & & & \vdots \\ 0 & \dots & & & & 0 \end{bmatrix} \in \mathbb{C}^{P\times P}$$

be the upper triangular Toeplitz channel matrix. We can write (2.12) as

$$\boldsymbol{x}[m] = \boldsymbol{H}^{(0)}\boldsymbol{\mu}[m] + \boldsymbol{H}^{(1)}\boldsymbol{\mu}[m-1]$$

where the second term represents the inter-symbol interference between two consecutive OFDM symbols.

At the receiver the cyclic prefix of length G is removed, and a DFT is performed on the remaining N chips. The cyclic prefix removal can be represented by the matrix

$$\boldsymbol{R}_{\mathrm{CP}} = [\boldsymbol{0}_{N\times G}\boldsymbol{I}_N] \in \mathbb{R}^{N\times P}$$

which removes the first G entries from the vector $\boldsymbol{x}[m] \in \mathbb{C}^P$ if the product $\boldsymbol{R}_{\mathrm{CP}}\boldsymbol{x}[m]$ is formed. As long as (2.9) holds,

$$\boldsymbol{R}_{\mathrm{CP}}\boldsymbol{H}^{(1)} = \boldsymbol{0}_{N\times P},$$

which indicates that the inter-symbol interference between two consecutive OFDM symbols is completely eliminated.

Finally, the received signal can be written as:

$$\begin{aligned}\boldsymbol{y}[m] &= \boldsymbol{F}\boldsymbol{R}_{\mathrm{CP}}(\boldsymbol{x}[m]+\boldsymbol{z}'[m]) = \boldsymbol{F}\boldsymbol{R}_{\mathrm{CP}}\boldsymbol{H}^{(0)}\boldsymbol{\mu}[m] + \boldsymbol{F}\boldsymbol{R}_{\mathrm{CP}}\boldsymbol{z}'[m]\\ &= \boldsymbol{F}\boldsymbol{R}_{\mathrm{CP}}\boldsymbol{H}^{(0)}\boldsymbol{T}_{\mathrm{CP}}\boldsymbol{F}^{\mathrm{H}}\boldsymbol{d}[m] + \boldsymbol{F}\boldsymbol{R}_{\mathrm{CP}}\boldsymbol{z}'[m]\\ &= \boldsymbol{F}\bar{\boldsymbol{H}}\boldsymbol{F}^{\mathrm{H}}\boldsymbol{d}[m] + \boldsymbol{F}\boldsymbol{R}_{\mathrm{CP}}\boldsymbol{z}'[m] \qquad (2.13)\end{aligned}$$

where $\bar{\boldsymbol{H}} \in \mathbb{C}^{N\times N}$ is the overall circulant channel matrix. This matrix can be decomposed as

$$\bar{\boldsymbol{H}} = \boldsymbol{R}_{\mathrm{CP}}\boldsymbol{H}^{(0)}\boldsymbol{T}_{\mathrm{CP}} = \boldsymbol{F}^{\mathrm{H}}\mathrm{diag}(\boldsymbol{g})\boldsymbol{F} \qquad (2.14)$$

where the frequency response $\boldsymbol{g} \in \mathbb{C}^N$ is defined as the DFT of the channel impulse response

$$\boldsymbol{g} = \sqrt{N}\boldsymbol{F}_{N\times L}\boldsymbol{h}\,.$$

Equation (2.14) describes the essential mathematical footing of OFDM. The Toeplitz structure channel matrix $\boldsymbol{H}^{(0)}$ is circularized by insertion of the cyclic prefix. Therefore, the columns of the DFT matrix are exact eigenvectors and the resulting channel matrix $\mathrm{diag}\,(\boldsymbol{g})$ has diagonal structure. The inversion of $\mathrm{diag}\,(\boldsymbol{g})$, which is necessary for channel equalization, has complexity $\mathcal{O}(N)$. In contrast, the channel matrix in a single-carrier system has full Toeplitz structure. The inversion of a Toeplitz matrix is an operation with complexity $\mathcal{O}(N^2)$.

Using (2.14) we write (2.13) as

$$\boldsymbol{y}[m] = \mathrm{diag}(\boldsymbol{g})\boldsymbol{d}[m] + \boldsymbol{z}[m], \qquad (2.15)$$

where the elements of $\boldsymbol{z}[m] = \boldsymbol{F}\boldsymbol{R}_{\mathrm{CP}}\boldsymbol{z}'[m]$, denoted by $z[m,q]$, are white with variance σ_z^2. Hence, the covariance matrix of $\boldsymbol{z}[m]$ has diagonal structure with identical elements

$$\begin{aligned}\boldsymbol{R}_{\boldsymbol{z}[m]} &= \mathbb{E}\{\boldsymbol{F}\boldsymbol{R}_{\mathrm{CP}}\boldsymbol{z}[m]\boldsymbol{z}[m]^{\mathrm{H}}\boldsymbol{R}_{\mathrm{CP}}^{\mathrm{H}}\boldsymbol{F}^{\mathrm{H}}\}\\ &= \sigma_z^2\boldsymbol{F}\boldsymbol{R}_{\mathrm{CP}}\boldsymbol{I}_P\boldsymbol{R}_{\mathrm{CP}}^{\mathrm{H}}\boldsymbol{F}^{\mathrm{H}}\\ &= \sigma_z^2\boldsymbol{I}_N.\end{aligned}$$

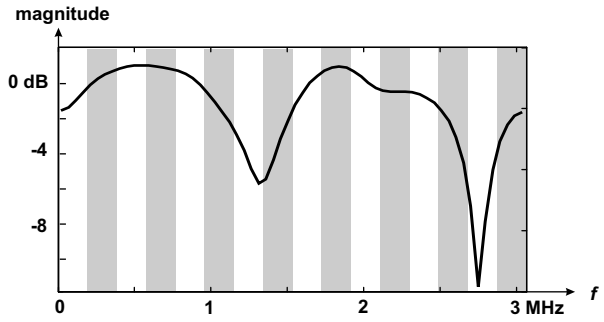

Figure 2.7: Frequency response of a multipath channel in baseband description.

In an OFDM system, according to (2.15), every element of the symbol vector $\boldsymbol{d}[m]$ is transmitted over an individual frequency-flat subcarrier. Figure 2.7 shows the frequency response of a typical wireless multipath channel. It is evident that subcarriers which are located near the fading dips of the frequency response are strongly attenuated. These attenuated subcarriers will dominate the bit error rate of the overall system [96]. In wireline applications of OFDM, like in the asymmetric digital subscriber line (ADSL), channel state information is usually available at the transmitter side. With this information optimal water pouring [54, Sec. 12.2.1] can be performed, thus avoiding the strong performance reduction through highly attenuated subcarriers. The same approach is in general not possible for wireless applications, since the fading channel changes too rapidly.

Applying a convolutional code and performing appropriate interleaving in the frequency domain is one possible solution in order to tackle the problem of highly attenuated subcarriers [21]. In such a coded OFDM system the information which is lost due to some strong attenuated subcarriers can be reconstructed at the receiver side through the additional information provided by the code [96]. Additionally, the code allows to exploit multipath diversity too. Coded OFDM is the method of choice for OFDM broadcast systems like DVB-T [19] or for multi-user systems which use time division multiple access (TDMA) like IEEE 802.11a [29].

A second method that allows to deal with strongly attenuated subcarriers is to spread each single data symbol over all N subcarriers through the application of a spreading code. This method is also known as linear precoding for OFDM [16]. The spreading operation reduces the negative influence of some strongly attenuated subcarriers and enables the utilization of the full multipath diversity of the channel. Additionally, the spreading operation allows to distinguish between individual users in a multi-user system. Multi-carrier code division multiple access (MC-CDMA) is the term which is most often used in literature in order to describe a system that combines OFDM with spreading over subcarriers [34].

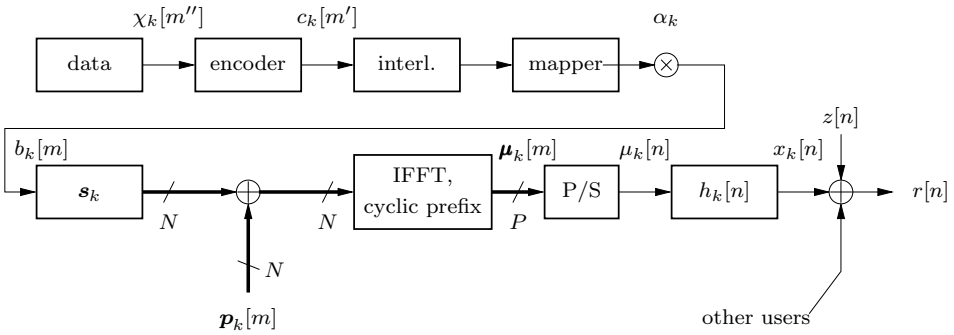

Figure 2.8: Model for the MC-CDMA transmitter and block-fading channel in the uplink.

Because of all these mentioned benefits we will use MC-CDMA as the basic transmission concept throughout this thesis. In the next section we introduce MC-CDMA in more detail for the multi-user case in the uplink.

2.4 Multi-User Signal Model

Figure 2.8 shows the block structure of an MC-CDMA transmitter for the uplink. The transmission is block oriented, a data block consists of $M - J$ OFDM data symbols and J OFDM pilot symbols. Each user transmits quadrature phase shift keying (QPSK) modulated symbols $b_k[m]$ with symbol rate $1/T_\mathrm{S}$. There are K users in the system, the user index is denoted by k. Each symbol is spread by a user specific spreading sequence $\boldsymbol{s}_k \in \mathbb{C}^N$. The spreading sequence $\boldsymbol{s}_k$ has independent identically distributed (i.i.d.) elements $s[n]$ chosen with equal probability from the QPSK constellation set[1] $\{\pm 1 \pm \mathrm{j}\}/\sqrt{2N}$. Therefore, the spreading sequence fulfills

$$\|\boldsymbol{s}_k\|^2 = 1 \quad \text{for} \quad k \in \{1, \ldots, K\}\,.$$

In Section 2.5.1 we will treat the spreading sequence selection in more detail.

The data symbols $b_k[m]$ result from the convolutionally encoded, randomly interleaved and QPSK modulated (with symbol mapper rate $R_\mathrm{S} = 2$) binary information sequence $\chi_k[m'']$ of length $R_\mathrm{S} R_\mathrm{C}(M - J)$ by applying Gray labelling. The code rate is denoted by R_C. The amplitude of user k is denoted by α_k. We do not take into account path loss and assume perfect power control, thus

$$\alpha_k = 1 \quad \text{for} \quad k \in \{1, \ldots, K\}\,.$$

[1]The expression $\{\pm 1 \pm \mathrm{j}\}$ is a shorthand notation for the set $\{+1 + \mathrm{j}, +1 - \mathrm{j}, -1 - \mathrm{j}, -1 + \mathrm{j}\}$.

To allow for pilot symbol insertion at the beginning of each data block the $M - J$ data symbols for a block of length M satisfy

$$b_k[m] \in \{\pm 1 \pm \mathrm{j}\}\frac{1}{\sqrt{2}} \quad \text{for} \quad m \in \{J, \ldots, M-1\}\,,$$

and

$$b_k[m] = 0 \quad \text{for} \quad m \in \{0, \ldots, J-1\}\,.$$

After the spreading operation a pilot symbol vector $\boldsymbol{p}_k[m] \in \mathbb{C}^N$ with elements $p_k[m, q]$ is added

$$\boldsymbol{d}_k[m] = \boldsymbol{s}_k b_k[m] + \boldsymbol{p}_k[m]\,. \tag{2.16}$$

The elements of the pilot vector $p_k[m, q]$ are i.i.d. chosen with equal probability from the QPSK symbol set $\{\pm 1 \pm \mathrm{j}\}/\sqrt{2N}$ for $m \in \{0, \ldots, J-1\}$, otherwise

$$\boldsymbol{p}_k[m] = \boldsymbol{0}_N \quad \text{for} \quad m \in \{J, \ldots, M-1\}\,.$$

Finally, an N point inverse DFT is performed and a cyclic prefix of length G is inserted. We insert (2.16) into (2.10) and obtain the transmitted chip sequence for user k

$$\boldsymbol{\mu}_k[m] = \boldsymbol{T}_{\mathrm{CP}}\boldsymbol{F}_N^{\mathrm{H}}\left(\boldsymbol{s}_k b_k[m] + \boldsymbol{p}_k[m]\right).$$

The received signal for user k after the DFT operation and the cyclic prefix removal can be expressed as

$$\boldsymbol{y}_k[m] = \mathrm{diag}\left(\boldsymbol{g}_k\right)\left(\boldsymbol{s}_k b_k[m] + \boldsymbol{p}_k[m]\right) + \boldsymbol{z}[m]\,, \tag{2.17}$$

where

$$\boldsymbol{g}_k = \sqrt{N}\boldsymbol{F}_{N\times L}\boldsymbol{h}_k$$

with elements $g_k[q]$ for $q \in \{0, \ldots, N-1\}$. We define the effective spreading sequence

$$\tilde{\boldsymbol{s}}_k = \mathrm{diag}(\boldsymbol{g}_k)\boldsymbol{s}_k \tag{2.18}$$

and represent the multi-user system by

$$\boldsymbol{y}[m] = \tilde{\boldsymbol{S}}\boldsymbol{b}[m] + \sum_{k=1}^{K}\mathrm{diag}(\boldsymbol{g}_k)\boldsymbol{p}_k[m] + \boldsymbol{z}[m] \tag{2.19}$$

where the effective spreading matrix is defined as

$$\tilde{\boldsymbol{S}} = [\tilde{\boldsymbol{s}}_1, \ldots, \tilde{\boldsymbol{s}}_K] \in \mathbb{C}^{N\times K}$$

and

$$\boldsymbol{b}[m] = \begin{bmatrix} b_1[m] \\ \vdots \\ b_K[m] \end{bmatrix} \in \mathbb{C}^K \tag{2.20}$$

contains the information symbols for K users at time index m.

2.5 Multi-User Detection

At the base station the multi-user detector has the task to find the most likely transmitted sequence of data vectors $\boldsymbol{b}[m]$ given the received vectors $\boldsymbol{y}[m]$. This is a special class of a vector-classification problem that is generally np-complete. A bank of K linear filters matched to the K effective spreading sequences form a set of sufficient statistics for the estimation of all users data [75]:

$$\boldsymbol{\xi}[m] = \tilde{\boldsymbol{S}}^{\mathrm{H}} \boldsymbol{y}[m]. \tag{2.21}$$

This means that by using $\boldsymbol{\xi}[m]$ no information is lost. If we define the correlation matrix

$$\boldsymbol{R}_{\tilde{\boldsymbol{S}}} = \tilde{\boldsymbol{S}}^{\mathrm{H}} \tilde{\boldsymbol{S}} \tag{2.22}$$

the MC-CDMA system can be described by

$$\boldsymbol{\xi}[m] = \boldsymbol{R}_{\tilde{\boldsymbol{S}}} \boldsymbol{b}[m] + \tilde{\boldsymbol{S}}^{\mathrm{H}} \boldsymbol{z}[m]. \tag{2.23}$$

2.5.1 Spreading Sequences

As already mentioned, the aim of the spreading operation is twofold: First, it distributes the information of the transmitted data symbol over all subcarrier and second, it is used in order to differentiate the individual users. For orthogonal Walsh-Hadamard spreading sequences and frequency-flat channels the correlation matrix $\boldsymbol{R}_{\tilde{\boldsymbol{S}}}$ will be the identity matrix and user separation will be optimal. For frequency-selective channels this is not true anymore because of (2.18). For sequences with length N there exist N different orthogonal sequences. The maximum number of users is therefore limited to N. We define the load as

$$\beta = \frac{K}{N}.$$

For random spreading sequences with length N there exist 2^N different sequences (for a BPSK alphabet). Thus, by using random spreading sequences the load can be increased above 1. The lost orthogonality of the spreading sequences is of no great impact, since the effective spreading sequences are not orthogonal anyway.

2.5.2 Linear Detector Types

The optimum maximum likelihood detector operating on $\boldsymbol{\xi}[m]$ is prohibitively complex. Hence, we resort to suboptimum linear multi-user detectors [50]. After linear

filtering, denoted by matrix $\boldsymbol{L}$, a hard decision is performed to obtain an estimate for the transmitted symbols

$$\hat{\boldsymbol{b}}[m] = \underset{\mathcal{X}}{\text{quant}}(\boldsymbol{L}\boldsymbol{\xi}[m]),$$

with

$$\underset{\mathcal{X}}{\text{quant}}(w) = \underset{\tilde{w}\in\mathcal{X}}{\text{argmin}}\,|w - \tilde{w}|$$

where $\mathcal{X}$ denotes the symbol set. For the QPSK constellation we define

$$\mathcal{X} = \{\pm 1 \pm \mathrm{j}\}/\sqrt{2}.$$

The matched-filter receiver is optimal with respect to the signal to noise ratio for orthogonal spreading sequences $\boldsymbol{s}_k$ in frequency-flat channels. The output of the filter bank $\boldsymbol{\xi}[m]$ (the sufficient statistics) is directly used in order to detect the data symbols, i.e.

$$\boldsymbol{L} = \boldsymbol{I}.$$

In a frequency-selective channel the orthogonality of the spreading sequences is destroyed by the effect of the channel, mathematically described by (2.18). Therefore, a simple matched-filter receiver has poor performance that degrades rapidly when the number of users is increased because of the multi-access interference.

Better performance can be achieved with the decorrelating receiver. The decorrelator (also known as zero forcing solution) follows from the approximation $\mathcal{X} \approx \mathbb{C}$ and is given by

$$\boldsymbol{L} = \boldsymbol{R}_{\tilde{\boldsymbol{S}}}^{-1}.$$

The decorrelator completely suppresses all interference but enhances the noise [75, Sec. 5]. This effect can be seen in Figure 2.9. In the low signal to noise region the decorrelating detector performs even worse than the matched filter.

A common approach in estimation theory is to choose a function $L(\boldsymbol{\xi})$ that minimizes the mean square error. Because vector $\boldsymbol{b}[m]$ is not Gaussian the exact solution is challenging. It is common to minimize the mean square error

$$\mathbb{E}\{(\boldsymbol{b}[m] - \boldsymbol{L}\boldsymbol{\xi}[m])^{\mathrm{H}}(\boldsymbol{b}[m] - \boldsymbol{L}\boldsymbol{\xi}[m])\} \tag{2.24}$$

within the restricted set of linear functions that can be represented by matrix $\boldsymbol{L}$. The solution of the minimization problem results in the linear MMSE filter given by

$$\boldsymbol{L} = \left(\boldsymbol{R}_{\tilde{\boldsymbol{S}}} + \sigma_z^2 \boldsymbol{I}\right)^{-1}.$$

The complexity of the linear MMSE filter is identical to the one of the decorrelator but the performance for low signal to noise ratios is enhanced.

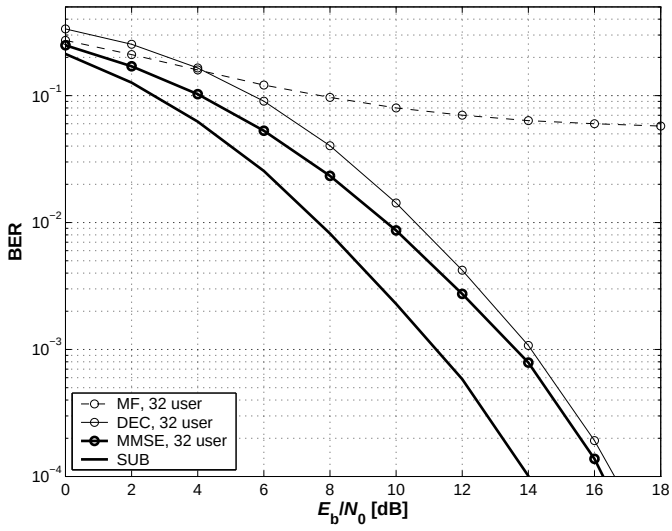

Figure 2.9: Bit error rate (BER) versus E_b/N_0 for an MC-CDMA uplink with $K = 32$ users and spreading length $N = 64$ for different linear multi-user detectors: matched-filter (MF), decorrelator (DEC), and linear MMSE filter. The single-user bound (SUB) is shown for the linear MMSE filter.

We demonstrate this with the comparison in Figure 2.9 where the performance of the matched-filter, the decorrelator, and the linear MMSE filter is shown in terms of bit error rate versus E_b/N_0. The energy per bit is denoted by E_b and N_0 denotes the noise power spectral density. We simulate an MC-CDMA uplink with $K = 32$ user and spreading length $N = 64$. The Rayleigh fading channel is perfectly known to the receiver. The single-user bound is defined as the performance for one user with perfect channel knowledge. The single-user bound was simulated using the linear MMSE detector. The comparison makes clear, that the linear MMSE detector performs best and the performance difference to the decorrelator is largest in the low signal to noise region. Based on this performance results and its moderate complexity we will use the linear MMSE detector throughout this thesis.

2.6 Iterative Multi-User Detection

In iterative receivers, the information gained about the transmitted symbols is used in subsequent iterations in order to reduce the interference from other users [14]. Soft symbols $\tilde{b}_k[m]$ instead of hard decisions $\hat{b}_k[m]$ are used to avoid error propagation. A convolutional code is used and the BCJR algorithm [6] is applied in order to obtain soft output values on the received code symbols. The iterative MC-CDMA receiver

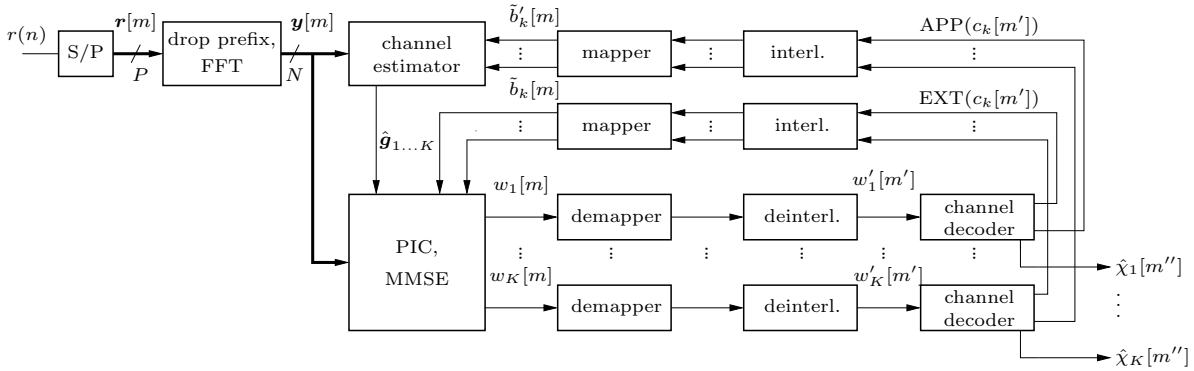

Figure 2.10: Schematic model of an MC-CDMA receiver that performs iterative joint channel-estimation and multi-user detection.

detects the data $\boldsymbol{b}[m]$ using the received vector $\boldsymbol{y}[m]$, the effective spreading matrix $\tilde{\boldsymbol{S}}^{(i)}$, and the feedback extrinsic probability (EXT) on the code bits at iteration step i denoted by $\Pr^{(\mathrm{EXT})}\{c_k^{(i)}[m'] = +1\}$. Figure 2.10 shows the structure of this iterative receiver.

The frequency-selective nature of the channel implies to build a filter which is matched to the effective spreading sequence $\tilde{\boldsymbol{s}}_k^{(i)}$. For the moment, it is only of interest that the channel estimator supplies an estimate $\hat{\boldsymbol{g}}_k$ for the channel frequency response of every user. The general optimization problem is therefore reduced to the estimation of $\boldsymbol{b}[m]$. In order to cancel the multi-access interference, we perform soft parallel interference cancellation for user k:

$$\tilde{\boldsymbol{y}}_k^{(i)}[m] = \boldsymbol{y}[m] + \tilde{\boldsymbol{s}}_k^{(i)}\tilde{b}_k^{(i)}[m] - \tilde{\boldsymbol{S}}^{(i)}\tilde{\boldsymbol{b}}^{(i)}[m]. \tag{2.25}$$

Vector $\tilde{\boldsymbol{b}}^{(i)}[m]$ contains the soft symbol estimates that are computed from the extrinsic probability supplied by the decoding stage. When the extrinsic probabilities get better from iteration to iteration and the channel is correctly estimated the parallel interference cancelling removes the interference from all other users completely and the detection problem is reduced to a single-user detection in Gaussian noise.

The soft symbol mapping for the QPSK alphabet is given by

$$\tilde{b}_k[m] = \mathop{\mathbb{E}}_{b}^{(\mathrm{EXT})}\{b_k[m]\} = \mathop{\mathbb{E}}_{c}^{(\mathrm{EXT})}\{c_k[2m]\} + \mathrm{j}\mathop{\mathbb{E}}_{c}^{(\mathrm{EXT})}\{c_k[2m+1]\} \tag{2.26}$$

where

$$\begin{aligned}\mathop{\mathbb{E}}_{c}^{(\mathrm{EXT})}\{c_k[m']\} &= \Pr^{(\mathrm{EXT})}\{c_k[m'] = +1\} - \Pr^{(\mathrm{EXT})}\{c_k[m'] = -1\} \\ &= 2\Pr^{(\mathrm{EXT})}\{c_k[m'] = +1\} - 1\end{aligned} \tag{2.27}$$

calculates the expectation over the alphabet of c which is $\{-1, +1\}$ and $\Pr^{(\mathrm{EXT})}\{c_k[m'] = +1\}$ is the extrinsic probability supplied by the BCJR decoder.

The notation $\mathbb{E}^{(\mathrm{EXT})}$ is chosen to explicitly show that extrinsic probabilities are used for the calculation of the expectation. In the next chapter about channel estimation we will use soft symbols based on a-posteriori probabilities which will be indicated through the notation $\mathbb{E}^{(\mathrm{APP})}$.

The $\tilde{\boldsymbol{y}}_k^{(i)}[m]$ are further cleaned from noise and multi-access interference with a successive linear MMSE filter

$$w_k^{(i)}[m] = (\boldsymbol{f}_k^{(i)})^{\mathrm{H}} \tilde{\boldsymbol{y}}_k^{(i)}[m] \tag{2.28}$$

to obtain an estimate of the transmitted symbols $b_k[m]$. An unbiased MMSE filter for the MC-CDMA system can be found similarly to the MMSE detector given in [14, 51, 80]. We omit the iteration index $(\cdot)^{(i)}$ to allow for simpler notation,

$$\boldsymbol{f}_k^{\mathrm{H}} = \frac{\tilde{\boldsymbol{s}}_k^{\mathrm{H}} (\sigma_z^2 \boldsymbol{I} + \tilde{\boldsymbol{S}} \boldsymbol{V} \tilde{\boldsymbol{S}}^{\mathrm{H}})^{-1}}{\tilde{\boldsymbol{s}}_k^{\mathrm{H}} (\sigma_z^2 \boldsymbol{I} + \tilde{\boldsymbol{S}} \boldsymbol{V} \tilde{\boldsymbol{S}}^{\mathrm{H}})^{-1} \tilde{\boldsymbol{s}}_k} \,. \tag{2.29}$$

Matrix $\boldsymbol{V}$ denotes the error covariance matrix of the soft symbols

$$\boldsymbol{V} = \mathbb{E}\{(\boldsymbol{b}[m] - \tilde{\boldsymbol{b}}[m])(\boldsymbol{b}[m] - \tilde{\boldsymbol{b}}[m])^{\mathrm{H}}\}$$

with diagonal elements

$$V_{k,k} = \mathbb{E}\{1 - |\tilde{b}_k[m]|^2\} \tag{2.30}$$

which are constant during iteration i, the other elements are assumed to be zero. In this case we calculate the variance from all symbols in the block belonging to user k and call the filter unconditional.

The expectation operator in (2.30) is implemented as empirical mean

$$V_{k,k} = \mathbb{E}\{1 - |\tilde{b}_k[m]|^2\} = \frac{1}{M} \sum_{m=0}^{M-1} (1 - |\tilde{b}_k[m]|^2) \,, \tag{2.31}$$

which is the case for all expectation operators in numerical simulations in this thesis, if not noted otherwise.

2.7 Decoder

The iterative receiver feeds back soft values on code bits $c_k[m']$ in order to get better detection results and better channel estimates. The soft feedback values are either computed from the so-called a-posteriori probability (APP) or the extrinsic probability (EXT) of the code bits through mapping to QPSK symbols. The soft-symbol mapping from extrinsic probabilities is given in (2.26). A similar mapping from a-posteriori probabilities (3.5) is used for the iterative channel estimation algorithm that will be treated in the next chapter [35, 80].

A soft-input soft-output decoder for binary convolutional codes, implemented using the BCJR algorithm [6], supplies these measures. The input values to the decoder are the so called channel values $w'_k[m']$ derived from the linear MMSE-filter outputs after demapping and deinterleaving. Additionally the decoder also needs an estimate of the noise variance

$$\hat{\sigma}^2_{z,k} = \frac{1}{2M} \sum_{m'=0}^{2M-1} \left| w'_k[m'] - \hat{\mu}_{w',k} \right|^2 ,$$

where the mean value of the absolute channel values is estimated through

$$\hat{\mu}_{w',k} = \frac{1}{2M} \sum_{m'=0}^{2M-1} \left| w'_k[m'] \right| .$$

The explicit estimation of $\hat{\mu}_{w',k}$ is necessary because during the first iterations the channel estimates are not accurate and thus the linear MMSE filter (2.29) is not truly unbiased.

The a-posteriori probability for the code symbol being $+1$ if the channel value $w'_k[m']$ is observed is given by

$$\Pr^{(\mathrm{APP})} \{c_k[m'] = +1\} = \Pr \{c_k[m'] = +1 \mid w'_k[m']\} . \tag{2.32}$$

The link between a-posterior probability and extrinsic probability is established via

$$\Pr^{(\mathrm{APP})} \{c_k[m'] = +1\} \propto \Pr^{(\mathrm{EXT})} \{c_k[m'] = +1\} \Pr \{w'_k[m'] \mid c_k[m'] = +1\} , \tag{2.33}$$

where the last expression denotes the channel transition function, which is as conditional Gaussian probability density function

$$\Pr \{w'_k[m'] \mid c_k[m'] = +1\} = \frac{1}{\sqrt{2\pi\sigma^2_{z,k}}} \exp \left(- \frac{\left| w'_k[m'] - \hat{\mu}_{w',k} \right|^2}{2\hat{\sigma}^2_{z,k}} \right) . \tag{2.34}$$

Estimating $\hat{\sigma}^2_{z,k}$ after the linear MMSE filter we model the residual multiple access interference as additive Gaussian noise (2.34).

3 Iterative Channel Estimation for Block-Fading Channels

Accurate channel estimation is crucial for the performance of any type of multi-user receiver. This is made obvious by (2.18); a filter matched to the effective spreading sequence depends directly on the quality of the channel estimate.

Various blind channel estimation schemes have been proposed in the literature for MC-CDMA. All these schemes suffer from an inherent phase ambiguity [73]. For coherent detection, which is necessary for multi-user detection schemes, it would be necessary to introduce some sort of pilot symbols to resolve this ambiguity. Furthermore, the popular blind subspace method limits the maximum number of users in the system to $K \leq N - L$, see [33, 44, 45, 82]. We propose a new iterative pilot based channel estimation scheme that can be applied to overloaded systems $K > N$ and allows for coherent detection.

3.1 Iterative Least-Square Channel Estimation

We use a random time domain pilot sequence $p_k[m, q]$ with i.i.d. elements that is J symbols long and unique for every user k and subcarrier q. This approach was inspired by equivalent approaches for direct sequence (DS)-CDMA in [13, 80] and the analysis in [94].

Figure 3.1 gives a schematic representation of the channel estimation scheme. Please note that the pilot sequence is a sequence in time while the spreading sequence, which is used to spread the information of a data symbol $b_k[m]$ over all subcarriers, is applied in the frequency domain. Therefore, this scheme allows to decouple the user specific identification sequences that are used for data detection and for channel estimation.

The MC-CDMA transmission described by the signal model (2.17) takes place over N independent parallel frequency-flat channels respectively subcarriers. We

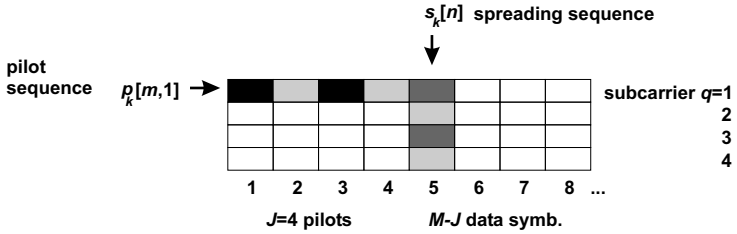

Figure 3.1: Channel estimation scheme for an iterative MC-CDMA receiver. The pilot sequence in time for user k on subcarrier q is denoted by $p_k[m,q]$ where m denotes discrete time. The spreading sequence $s_k[n]$ is applied in the frequency domain.

rewrite (2.17) as a set of equations for every subcarrier $q \in \{0,\ldots,N-1\}$,

$$y[m,q] = \sum_{k=1}^{K} g_k[q]d_k[m,q] + z[m,q]\,,$$

where

$$d_k[m,q] = s_k[q]b_k[m] + p_k[m,q]\,. \tag{3.1}$$

Hence, a least-square estimate of the subcarrier coefficients $\hat{g}_k[q]$ can be obtained jointly for all K users but individually for every subcarrier q.

We define the vector

$$\boldsymbol{g}_q = \begin{bmatrix} g_1[q] \\ \vdots \\ g_K[q] \end{bmatrix} \in \mathbb{C}^K$$

containing the channel coefficients of all K users for subcarrier q. Furthermore, we introduce the notation

$$\boldsymbol{y}_q = \begin{bmatrix} y[0,q] \\ \vdots \\ y[M-1,q] \end{bmatrix} \in \mathbb{C}^M$$

denoting the received symbol sequence on subcarrier q for a single data block. With these definitions we can write

$$\boldsymbol{y}_q = \boldsymbol{D}_q\boldsymbol{g}_q + \boldsymbol{z}_q\,, \tag{3.2}$$

where the matrix $\boldsymbol{D}_q \in \mathbb{C}^{M\times K}$ is defined as

$$\boldsymbol{D}_q = \begin{bmatrix} d_1[0,q] & \ldots & d_K[0,q] \\ \vdots & \ddots & \vdots \\ d_1[M-1,q] & \ldots & d_K[M-1,q] \end{bmatrix}, \tag{3.3}$$

containing the transmitted symbols for all K users on subcarrier q.

For the channel estimation task the J pilot symbols $p_k[m,q]$ for $m \in \{0,\ldots,J-1\}$ in (3.1) are known. The remaining $M-J$ data symbols $b_k[m]$ for $m \in \{J,\ldots,M-1\}$ are not known. We replace them by soft symbols $\tilde{b}'_k[m]$ that are calculated from the a-posteriori probabilities obtained in the previous iteration. This enables us to obtain refined channel estimates if the soft symbols gets more certain from iteration to iteration. For the first iteration the soft symbols $\tilde{b}'_k[m]$ are set to zero.

We define the soft symbol matrix $\tilde{\boldsymbol{D}}_q \in \mathbb{C}^{M\times K}$ equivalent to (3.3) by replacing $d_k[m,q]$ with

$$\tilde{d}_k[m,q] = s_k[q]\tilde{b}'_k[m] + p_k[m,q]\,. \tag{3.4}$$

The soft symbols $\tilde{b}'_k[m]$ are defined according to

$$\tilde{b'}_k[m] = \underset{b}{\mathbb{E}}^{(\mathrm{APP})}\{b_k[m]\} = \underset{c}{\mathbb{E}}^{(\mathrm{APP})}\{c_k[2m]\} + \mathrm{j}\underset{c}{\mathbb{E}}^{(\mathrm{APP})}\{c_k[2m+1]\} \tag{3.5}$$

where

$$\begin{aligned}\underset{c}{\mathbb{E}}^{(\mathrm{APP})}\{c_k[m']\} &= \Pr^{(\mathrm{APP})}\{c_k[m'] = +1\} - \Pr^{(\mathrm{APP})}\{c_k[m'] = -1\}\\ &= 2\Pr^{(\mathrm{APP})}\{c_k[m'] = +1\} - 1\,,\end{aligned}$$

and $\Pr^{(\mathrm{APP})}\{c_k[m'] = +1\}$ is the a-posteriori probability supplied by the BCJR decoder. The code bits $c[m']$ are from the set $\{+1,-1\}$.

Finally, the least-square channel estimator is given by

$$\hat{\boldsymbol{g}}'_q = \left(\tilde{\boldsymbol{D}}_q^{\mathrm{H}}\tilde{\boldsymbol{D}}_q\right)^{-1}\tilde{\boldsymbol{D}}_q^{\mathrm{H}}\boldsymbol{y}_q. \tag{3.6}$$

After estimating the subcarrier coefficients for all subcarriers we can further reduce the noise by exploiting their correlation since the channel impulse response in the time domain $\boldsymbol{h}_k$ possesses $L < N$ taps:

$$\hat{\boldsymbol{g}}_k = \boldsymbol{F}_{N\times L}\boldsymbol{F}_{N\times L}^{\mathrm{H}}\hat{\boldsymbol{g}}'_k. \tag{3.7}$$

The estimates $\hat{\boldsymbol{g}}_k$ are inserted in (2.18) to calculate the effective spreading sequences which in turn are used by the parallel interference canceller (2.25) and the linear MMSE detector (2.28).

The least square solution in (3.6) expects deterministic values in matrix $\tilde{\boldsymbol{D}}$. However, this is not the case since we combine deterministic pilots with soft symbols. The absolute values of the soft symbols in matrix $\tilde{\boldsymbol{D}}_q$ can be very small, particularly during the first iteration and in overloaded systems, where

$$\beta = K/N > 1\,, \tag{3.8}$$

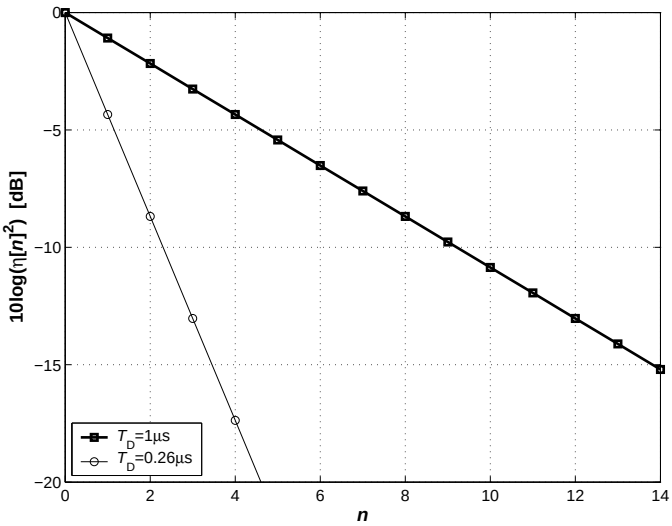

Figure 3.2: Power delay profile $\eta^2[\ell]$ with (root mean square) delay spread $T_\mathrm{D} \in \{0.26, 1\}\mu$s sampled at rate $1/T_\mathrm{C} = 3.84 \cdot 10^6\,\mathrm{s}^{-1}$. The normalized delay spread $L_\mathrm{D} = T_\mathrm{D}/T_\mathrm{C} \in \{1, 4\}$. We plot $L = 15$ significant channel taps.

due to strong interference. This leads to strongly biased channel estimates and slow convergence of the iterative receiver. We apply a partial heuristic solution through scaling by $\sqrt{N/L}$ in the first iteration, i.e.

$$\hat{\boldsymbol{g}}_k^{(1)} = \boldsymbol{F}_{N\times L}\boldsymbol{F}_{N\times L}^\mathrm{H}\hat{\boldsymbol{g}}_k'^{(1)}\sqrt{\frac{N}{L}}.$$

Furthermore, we normalize each column of $\tilde{\boldsymbol{D}}_q$ to $\sqrt{M/N}$, so that the Frobenius norm $\|\tilde{\boldsymbol{D}}_q\|_\mathrm{F}$ stays constant. In Section 3.2 we will present a more systematic solution based on the MMSE theory.

3.1.1 Simulation Parameters

The realizations of the Rayleigh fading channel are calculated using the exponential power delay profile (2.4) with a delay spread $T_\mathrm{D} \in \{0.26, 1\}\mu$s. We use a chip rate of $1/T_\mathrm{C} = 3.84{\cdot}10^6\,\mathrm{s}^{-1}$ as in UMTS. The normalized delay spread $L_\mathrm{D} = T_\mathrm{D}/T_\mathrm{C} \in \{1, 4\}$. We obtain an essential support of the channel impulse response (2.6) of $L = 15$ for a maximum $E_\mathrm{b}/N_0 = 15\,\mathrm{dB}$.

The OFDM transmission uses $N = 64$ subcarriers and each OFDM symbol including the cyclic prefix has length of $P = G + N = 79$ chips. The spreading sequence has length $N = 64$ equal to the number of subcarriers. The convolutional code used is a non-systematic, non-recursive, four state, rate $R_\mathrm{C} = 1/2$ code with generator

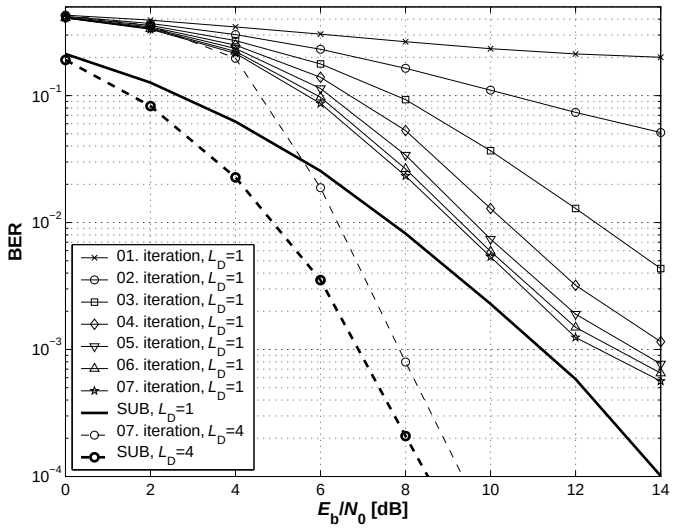

Figure 3.3: Receiver performance in terms of bit error rate (BER) versus E_b/N_0 for $K = 64$ users with least-square channel estimation. The channel has an exponential power delay profile with normalized delay spread $L_\mathrm{D} \in \{1, 4\}$. The single-user bounds (SUB) are shown as reference.

polynomial $(5, 7)_8$. The data block has length $M = 256$ including $J = 20$ pilot symbols. The energy of the transmitted QPSK symbols is normalized to 1, therefore the E_b/N_0 is defined as

$$\frac{E_\mathrm{b}}{N_0} = \frac{1}{R_\mathrm{S} R_\mathrm{C} \sigma_z^2} \frac{P}{N} \frac{M}{M - J}. \tag{3.9}$$

In (3.9) we also take into account the loss through the cyclic prefix and the pilot symbols. The single-user bound is taken as a reference for the multi-user receiver performance. The single-user bound is defined as the receiver performance for one user with perfect channel knowledge.

3.1.2 Simulation Results

Figure 3.3 shows the receiver performance in terms of bit error rate versus E_b/N_0 for full load $\beta = K/N = 1$. The simulations are averaged over 100 independent channel realizations. The number of iterations is limited to 7. The bit error rate decreases after each iteration and converges towards the single-user bound up to 1 dB after 7 iterations.

The strong influence of the delay spread on the receiver performance is displayed in Figure 3.3 too. The larger the delay spread the more multipath diversity (respectively frequency diversity) can be used at the receiver side, enhancing the receiver

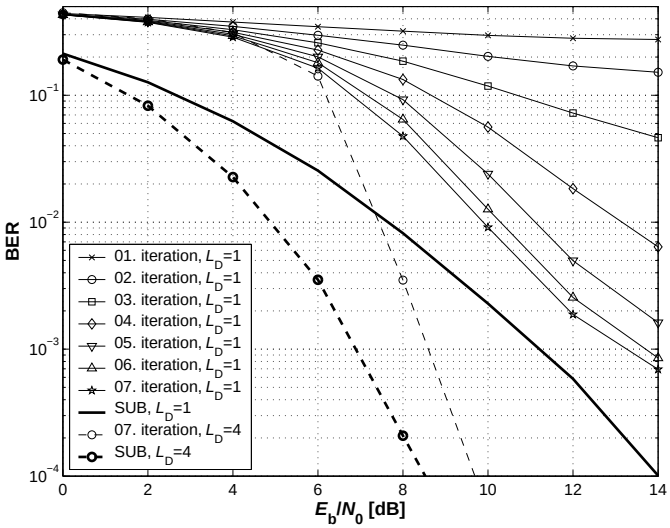

Figure 3.4: Receiver performance in terms of bit error rate (BER) versus E_b/N_0 for $K = 80$ users with least-square channel estimation. The channel has an exponential decaying power delay profile with normalized delay spread $L_\mathrm{D} \in \{1, 4\}$.

performance.

Figure 3.4 shows the same results for a moderately overloaded system with load $\beta = 1.25$ for $K = 80$ users and normalized delay spread $L_\mathrm{D} \in \{1, 4\}$. The bit rate per user is 44.8 kbit/s, the net bit rate per cell is 2.87 Mbit/s for 64 users and 3.58 Mbit/s for 80 users.

The iterative receiver uses pilot symbols only for channel estimation in the first iteration. These channel estimates are used in the multi-user detector in order to calculate the effective spreading sequence and perform data detection. This is why the bit error rate curve of the first iteration is identical with the performance of a non-iterative linear MMSE multi-user detectors with imperfect channel knowledge.

In the second iteration soft symbols are supplied by the BCJR decoder which are used in the parallel interference canceller in order to reduce the interference by other users. Additionally, the soft symbols also help to enhance the channel estimation quality. This leads to continuous performance improvements between iteration 1 and iteration 7 as can be clearly seen in Figure 3.3 and Figure 3.4. In a fully loaded system and even in an overloaded system the reduction in bit error rate is in the orders of 3 magnitudes after 7 iterations.

3.1.3 Comparison Between MC-CDMA and DS-CDMA

It is well-known that the signal-models for MC-CDMA and DS-CDMA are similar [50], and therefore many multi-user detection algorithms are applicable to both MC-CDMA and DS-CDMA. However, the computational complexity of the channel estimation algorithm for an MC-CDMA receiver is smaller than the one needed for DS-CDMA.

In MC-CDMA the inter-symbol interference is removed through insertion of the cyclic prefix, and channel equalization is performed in the frequency domain. The complexity for the channel estimation is growing by $\mathcal{O}(NK^3)$ in MC-CDMA where N denotes the number of subcarriers and K the number of users. The term K^3 is due to the necessary matrix inversion with dimension $K \times K$ which has to be performed for N subcarriers individually.

In comparable DS-CDMA systems for UMTS time division duplex (TDD) the complexity grows with $\mathcal{O}(L^3K^3)$ since the matrix to be inverted has dimension $LK \times LK$ [80]. The time-domain channel estimation in DS-CDMA has to estimate L channel taps for all K users jointly, thus raising its complexity. Whereas, in an OFDM system the coefficients for every subcarrier can be estimated separately.

The essential support of the channel L determines the length of the cyclic prefix. The number of subcarriers N is usually $N > 5L$, so that the spectral efficiency of the system is still acceptable. The spectral efficiency of the system is determined by the ratio $L/(N+L)$. Thus, the channel estimation complexity advantage of MC-CDMA is especially important at high data rates when L gets large.

3.1.4 Channel Estimation Error

Figure 3.4 presents the performance of an MC-CDMA system with load $\beta = 1.25$ in terms of bit error rate versus E_b/N_0. The distance to the single-user bound is increased compared to the results for load $\beta = 1$ that are shown in Figure 3.3. We know from theoretical results that with perfect channel knowledge the performance difference between $K = 64$ and $K = 80$ users should be much smaller [14]. Thus, we analyze the channel estimation error in this section.

We define the mean square error of the channel estimates, so that we obtain a measure of the channel estimation quality:

$$\mathrm{MSE}_\mathrm{BF} = \frac{1}{KL} \sum_{k=1}^{K} \left\| \hat{\boldsymbol{h}}_k - \boldsymbol{h}_k \right\|^2 .$$

In Figure 3.5 we plot the mean square error of the channel estimate versus the iteration number for a channel with exponential decaying power delay profile with normalized delay spread $L_\mathrm{D} = 1$. It can be clearly seen, that the mean square error

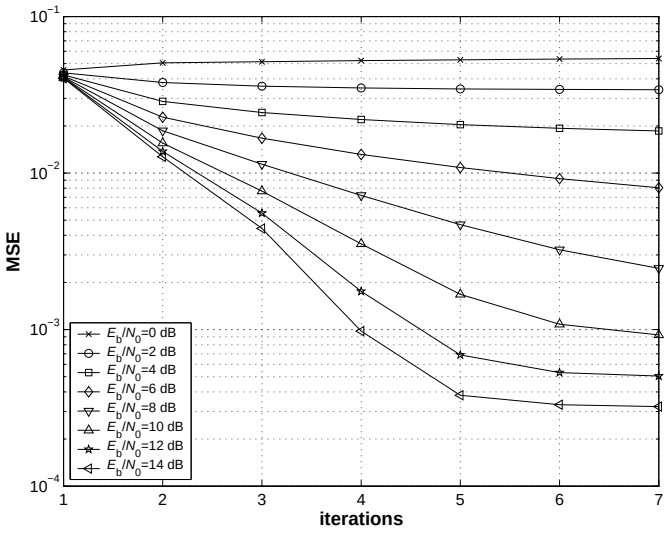

Figure 3.5: Mean square error (MSE) of the channel estimates for $K = 80$ users with least-square channel estimation for normalized delay spread $L_{\mathrm{D}} = 1$.

slightly increases after the 2nd iteration especially for a low signal to noise ratio. This is due to the already mentioned fact, that the soft symbols in matrix $\tilde{\boldsymbol{D}}_q$ have very small absolute values, particularly during the first iteration and in overloaded systems (3.8) due to strong interference.

In the next section we develop an iterative channel estimation scheme based on the MMSE theory in order to avoid this degradation of the channel estimation performance with increasing number of users.

3.2 Iterative Linear Minimum Mean Square Error Channel Estimation

Equation (3.5) makes clear, that the soft symbols are actually the expectation of the data symbols given the received data vector and the current channel estimate after the decoding process. Since the data symbols are from a constant modulus alphabet we know their variance too,

$$\mathrm{var}\{b_k[m]\} = \mathop{\mathbb{E}}_{\boldsymbol{b}}\left\{\left(b_k[m] - \mathop{\mathbb{E}}_{\boldsymbol{b}}\{b_k[m]\}\right)^2\right\} = 1 - \tilde{b}_k^2[m]. \tag{3.10}$$

We take advantage of this information in the following, deriving a linear MMSE multi-user channel estimator, enhancing the overall performance especially for over-

loaded systems. See also [74] for a related approach in a single-user scenario. Independently in [3] a similar algorithm was derived using the concept of expectation maximization (EM).

The individual subcarriers in an OFDM system are orthogonal. For this reason we are able to estimate the subcarrier coefficient $g_k[q]$ individually for every subcarrier q but jointly for all K users. We repeat the signal model (3.2) for the received symbol block $\boldsymbol{y}_q$ on subcarrier q which is given by

$$\boldsymbol{y}_q = \boldsymbol{D}_q \boldsymbol{g}_q + \boldsymbol{z}_q \,.$$

In the previous section we obtained the channel coefficients using a least-square estimator by approximating $\boldsymbol{D}_q$ with $\tilde{\boldsymbol{D}}_q$. The matrix $\tilde{\boldsymbol{D}}_q$ contains deterministic pilot symbols and statistical information in terms of expectation (3.5) about the transmitted data symbols.

The minimization of the mean square estimation error is a widely used optimization criterion in parameter estimation. We use this approach in order to estimate the channel coefficients. In general, for a linear data model, if the observed data and the unknown parameters are jointly Gaussian distributed, the resulting MMSE estimator is a linear function of the data. In the model (3.2), we assume that the channel coefficients in the vector $\boldsymbol{g}_q$ are independent, complex Gaussian distributed random variables, with zero mean and unit variance (which corresponds to Rayleigh fading), while the symbols in the matrix $\boldsymbol{D}_q$ have a discrete distribution determined by the QPSK symbol alphabet. The resulting distribution of the observed vector $\boldsymbol{y}_q$ is not Gaussian, thus the MMSE estimator is not linear. Due to the shape of the probability density function $f(\boldsymbol{y}_q)$, the derivation of the exact MMSE estimator is a complicated task. Therefore, we constrain the channel estimator to be linear in $\boldsymbol{y}_q$. We will omit the index q in the following derivations to simplify the notation.

The linear estimator can be expressed as

$$\hat{\boldsymbol{g}}_{\mathrm{LMMSE}} = \boldsymbol{A}\boldsymbol{y},$$

where the matrix $\boldsymbol{A}$ satisfies the Wiener-Hopf equation

$$\boldsymbol{C}_{\boldsymbol{y}\boldsymbol{y}} \boldsymbol{A}^{\mathrm{H}} = \boldsymbol{C}_{\boldsymbol{y}\boldsymbol{g}} \,.$$

The covariance matrices are given by ($\boldsymbol{y}$, $\boldsymbol{g}$ and $\boldsymbol{z}$ are zero-mean and statistically independent)

$$\boldsymbol{C}_{\boldsymbol{y}\boldsymbol{y}} = \mathop{\mathbb{E}}_{\boldsymbol{b}} \mathop{\mathbb{E}}_{\boldsymbol{g}} \mathop{\mathbb{E}}_{\boldsymbol{z}} \left\{ \boldsymbol{y}\boldsymbol{y}^{\mathrm{H}} \right\} = \mathop{\mathbb{E}}_{\boldsymbol{b}} \left\{ \boldsymbol{D}\boldsymbol{D}^{\mathrm{H}} \right\} + \sigma_z^2 \boldsymbol{I}_M \tag{3.11}$$

$$\boldsymbol{C}_{\boldsymbol{y}\boldsymbol{g}} = \mathop{\mathbb{E}}_{\boldsymbol{b}} \mathop{\mathbb{E}}_{\boldsymbol{g}} \mathop{\mathbb{E}}_{\boldsymbol{z}} \left\{ \boldsymbol{y}\boldsymbol{g}^{\mathrm{H}} \right\} = \mathop{\mathbb{E}}_{\boldsymbol{b}} \left\{ \boldsymbol{D} \right\} \triangleq \tilde{\boldsymbol{D}}, \tag{3.12}$$

where the index under the expectation operator denotes the random variable with respect to which the expectation is taken. Expectations with respect to $\boldsymbol{b}$ are computed using APPs of data symbols, see (3.5). The linear MMSE estimator is then:

$$\begin{aligned}\hat{\boldsymbol{g}}_{\mathrm{LMMSE}} &= \boldsymbol{C_{yg}}^{\mathrm{H}} \boldsymbol{C_{yy}}^{-1} \boldsymbol{y} \\ &= \tilde{\boldsymbol{D}}^{\mathrm{H}} \left(\mathop{\mathbb{E}}_{\boldsymbol{b}} \left\{ \boldsymbol{D}\boldsymbol{D}^{\mathrm{H}} \right\} + \sigma_z^2 \boldsymbol{I}_M \right)^{-1} \boldsymbol{y}. \end{aligned} \tag{3.13}$$

If we want to calculate $\mathop{\mathbb{E}}_{\boldsymbol{b}}\{\boldsymbol{D}\boldsymbol{D}^{\mathrm{H}}\}$ we have to take into account that due to the independence of the users and the data symbols within one block, it holds:

$$\mathop{\mathbb{E}}_{\boldsymbol{b}}\{b_k'[m']b_k[m]\} = \begin{cases} \tilde{b}_k'[m']\tilde{b}_k[m], & k' \neq k, m' \neq m \\ 1, & k' = k, m' = m \end{cases} \tag{3.14}$$

for $k, k' \in \{1, ..., K\}$ and for $m, m' \in \{0, 1, ..., M-1\}$. Please refer to (3.5) for the definition of the soft symbols $\tilde{b}_k[m]$.

With (3.14) we are able to write the expectation of the product $\mathop{\mathbb{E}}_{\boldsymbol{b}}\{\boldsymbol{D}\boldsymbol{D}^{\mathrm{H}}\}$ as product of expectations plus a correcting diagonal matrix $\boldsymbol{\Lambda}$ which takes (3.14) into account

$$\mathop{\mathbb{E}}_{\boldsymbol{b}}\{\boldsymbol{D}\boldsymbol{D}^{\mathrm{H}}\} = \mathop{\mathbb{E}}_{\boldsymbol{b}}\{\boldsymbol{D}\} \mathop{\mathbb{E}}_{\boldsymbol{b}}\{\boldsymbol{D}^{\mathrm{H}}\} + \boldsymbol{\Lambda} = \tilde{\boldsymbol{D}}\tilde{\boldsymbol{D}}^{\mathrm{H}} + \boldsymbol{\Lambda}. \tag{3.15}$$

The elements of the diagonal matrix $\boldsymbol{\Lambda}$ are defined as

$$[\boldsymbol{\Lambda}]_{m,m} = \sum_{k=1}^{K} \mathrm{var}\{b_k[m]\}, \tag{3.16}$$

where the soft-symbol variance from (3.10) is used.

Inserting (3.15) into (3.13) we obtain

$$\hat{\boldsymbol{g}}_{\mathrm{LMMSE}} = \tilde{\boldsymbol{D}}^{\mathrm{H}} \left(\tilde{\boldsymbol{D}}\tilde{\boldsymbol{D}}^{\mathrm{H}} + \underbrace{\boldsymbol{\Lambda} + \sigma_z^2 \boldsymbol{I}_M}_{\triangleq \boldsymbol{\Delta}} \right)^{-1} \boldsymbol{y}. \tag{3.17}$$

For the evaluation of this estimator it is necessary to invert an M-dimensional matrix, which is computationally expensive. In order to reduce complexity we apply the matrix inversion lemma to (3.17). The final expression yields

$$\hat{\boldsymbol{g}}_{\mathrm{LMMSE}} = \left(\tilde{\boldsymbol{D}}^{\mathrm{H}} \boldsymbol{\Delta}^{-1} \tilde{\boldsymbol{D}} + \boldsymbol{I}_K \right)^{-1} \tilde{\boldsymbol{D}}^{\mathrm{H}} \boldsymbol{\Delta}^{-1} \boldsymbol{y}. \tag{3.18}$$

The rows of matrix $\tilde{\boldsymbol{D}}$ are scaled by the diagonal matrix $\boldsymbol{\Delta}$, taking into account the variance of the noise and the variances of the soft-symbol estimates.

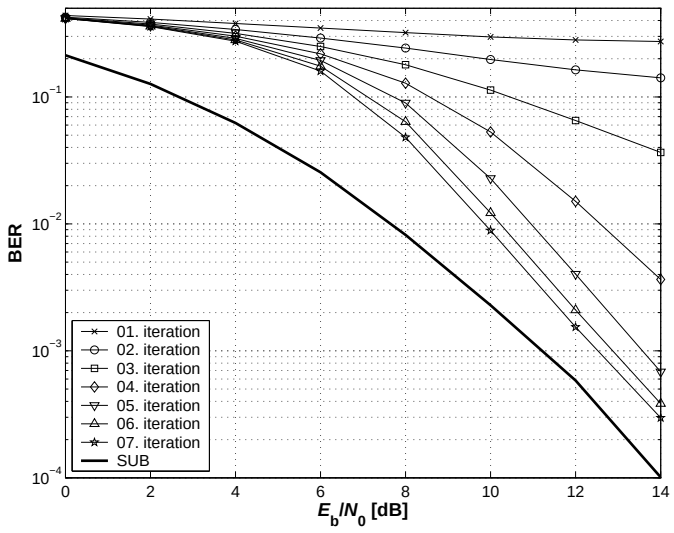

Figure 3.6: Receiver performance in terms of bit error rate (BER) versus E_b/N_0 for $K = 80$ users with linear MMSE channel estimation and normalized delay spread $L_\mathrm{D} = 1$. For reference the single-user bound (SUB) is shown too.

If the data symbols are known, then

$$\tilde{b}_k[m] = b_k[m],$$

thus $\boldsymbol{\Lambda} = \mathbf{0}$, $\boldsymbol{\Delta} = \sigma_z^2 \boldsymbol{I}_K$ and the estimator (3.18) becomes the exact MMSE estimator (conditioned on the given $\boldsymbol{D}$, $\boldsymbol{g}$ and $\boldsymbol{y}$ are jointly Gaussian, thus the linear MMSE coincides with the exact MMSE estimator which becomes linear for jointly Gaussian variables):

$$\hat{\boldsymbol{g}}_{\mathrm{MMSE}|\boldsymbol{D}} = \left(\boldsymbol{D}^\mathrm{H}\boldsymbol{D} + \sigma_z^2 \boldsymbol{I}_K\right)^{-1} \boldsymbol{D}^\mathrm{H}\boldsymbol{y}. \tag{3.19}$$

For the training part of the data block (the first J symbols), the estimator will equal the exact MMSE estimator for the given pilot symbols. For the data part the variances of the estimates of the unknown data symbols are taken into account by the matrix $\boldsymbol{\Delta}$.

3.2.1 Simulation Results

The simulation results for this estimator are given in Figure 3.6 and Figure 3.7. The parameters are the same as in the least-square case (see Section 3.1). If Figure 3.7 is compared with the results obtained with the least-square estimator in Figure 3.5, it can be clearly seen that the mean square error is a monotonic decreasing function of the iteration number and the E_b/N_0, now. The bit error rate performance in

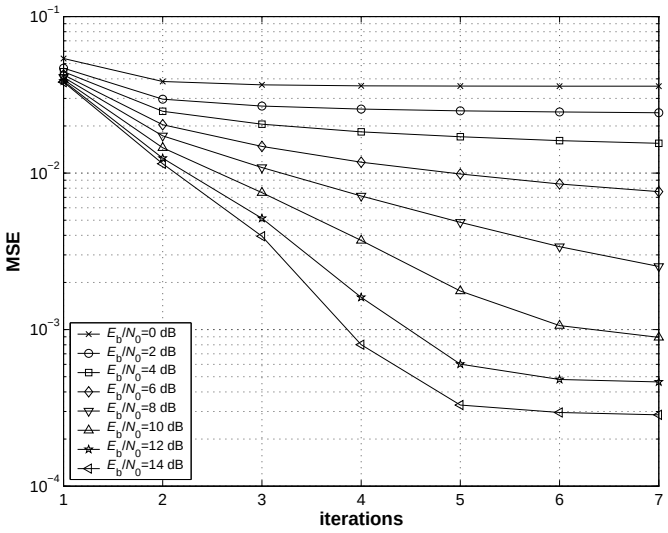

Figure 3.7: MSE of the channel estimates for $K = 80$ users with linear MMSE channel estimation for normalized delay spread $L_{\mathrm{D}} = 1$.

Figure 3.6 is enhanced and the error floor behavior visible in Figure 3.4 is removed. The single user bound is reached up to 1 dB after 7 iterations at $E_{\mathrm{b}}/N_0 = 14\,\mathrm{dB}$ with the linear MMSE based channel estimation compared to the least-square estimator where the distance is 2 dB.

3.2.2 Other Communication Systems

The iterative linear MMSE channel estimation scheme is not limited to MC-CDMA systems. It is straight forward to apply this scheme in DS-CDMA and MIMO systems as well. The required modifications are to take into account the different structure of the matrix $\boldsymbol{D}$, and to properly apply the rule in (3.14) for the soft symbol estimates. For further details see [79] and [46].

3.3 Block Interleaving

We interleave the transmitted data over B data blocks in order to enhance the receiver performance. We assume independent channel realizations for every data block of length M. The transmitter is changed in the way that the uncoded bit sequence $\chi[m'']$ has length $B(M-J)R_{\mathrm{C}}R_{\mathrm{S}}$. This sequence is coded with a convolutional code, randomly interleaved and mapped to a QPSK symbol constellation. The resulting symbol sequence $b[m]$ with length $B(M-J)$ is partitioned in B sequences with length $M-J$.

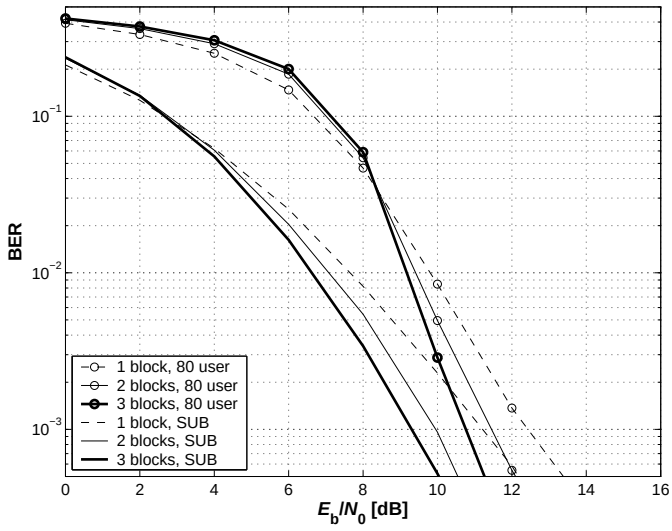

Figure 3.8: Receiver performance in terms of bit error rate (BER) versus E_b/N_0 for $K = 80$ users with linear MMSE channel estimation and block interleaving for $B \in \{1, 2, 3\}$ after the 7th iteration for normalized delay spread $L_\mathrm{D} = 1$. For reference the single-user bounds (SUB) are shown too.

At the receiver all B block are received. Than the channel is estimated for every block separately. The output of the MMSE filter for all B blocks is concatenated demapped, deinterleaved and jointly decoded by the BCJR algorithm. The output of the BCJR is again interleaved and mapped and then partitioned in B sequences with length $M - J$ that are used do perform the second iteration for all B received data blocks separately. The joint coding and interleaving over B blocks is expected to increases the diversity by B. See also [39] for a related approach using a serial interference cancellation scheme.

We apply the same simulation parameters as in the previous section. In Figure 3.8 we plot the result after the 7th iteration with block interleaver length $B \in \{1, 2, 3\}$. Additionally the single-user bounds are given too. Figure 3.8 shows that the bit error rate decreases with increasing block interleaver length B. The diversity is defined as the slope of the bit error rate versus E_b/N_0 curve in log-log scale. The slope increase from $B = 1$ to $B = 3$ does not reach the expected factor of 3. This is linked to the constrained length of the applied code. Some experimental results on appropriate code selection for block interleaving are given in [39].

4 Time-Variant Channel Estimation

The key feature of future 4th generation mobile communication systems will be their ability to deliver high data rates to users moving at vehicular speed. User mobility together with multipath propagation and scatterer movement are the main reasons for the variation of a wireless channel over the duration of a data block.

Figure 4.1 shows the extension of the model from Figure 2.1 to the time-variant case. The Doppler shifts f_ℓ on the individual paths ℓ depend on the user's direction and velocity v, the carrier frequency f_C, and the scattering environment.

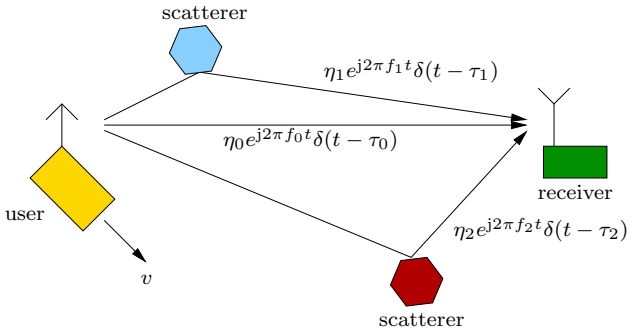

Figure 4.1: Time-variant multipath propagation model. The user moves with velocity v, every path ℓ has attenuation η_ℓ, time delay τ_ℓ and Doppler shift f_ℓ.

The maximum variation in time of the wireless channel is upper bounded by the maximum (one sided) normalized Doppler bandwidth

$$\nu_{\mathrm{Dmax}} = \frac{v_{\max} f_C}{c_0} T_{\mathrm{S}} \geq |f_\ell T_{\mathrm{S}}|\,, \tag{4.1}$$

where $v_{\max}$ is the maximum supported velocity, T_{S} is the symbol duration, and c_0 denotes the speed of light.

4.1 How to Deal With Time Variation?

A two dimensional Wiener filter was proposed by [34] for time-variant channel estimation in an OFDM system for the downlink case where all users share a common channel. Exact knowledge of the second order statistics was assumed for the initial design of the Wiener filter. However, for the actual simulation a worst case power spectral density is used and the performance degradation in the mismatched case is analyzed. The same procedure is applied in [17] where a rank reduced Wiener Filter was applied exploiting the frequency correlation, and in [68] where the expectation maximization (EM) algorithm based on the Karhunen-Loève transform was used.

In [37] a Kalman filter is applied and the Doppler spectrum is assumed to adhere to Jakes' model [32]. The Jakes' spectrum is valid for a dense scatterer model in the limit of an infinite number of scatterers around a linear omnidirectional antenna [56] [52, Sec. 2.5.2]. This assumption is not fulfilled if a few dominant propagation paths are present only. It was shown by measurements in [92] that wireless channels at 5.3 GHz do *not* have a Jakes spectrum. Furthermore, the actual velocity of the user and the angles of arrival enter the autocorrelation as parameters and have to be estimated explicitly.

Another approach is to use a Wiener filter and estimate and track the channel statistics online [64, 62, 63, 65]. However, it was shown by channel sounder measurements that wireless fading channels show stationary behavior for less than 70 wavelengths in a pedestrian typical-urban environment [77]. We doubt that meaningful short-term fading characteristics (second order statistics to begin with) can be acquired in a multi-user system when users move at vehicular speed.

We pursue a channel estimation approach for an OFDM system that exploits the band-limitation of the time-variant subcarrier coefficients only. Hence, we make no assumption about the shape of the power spectral density (i.e. the autocorrelation). We take advantage of Slepian's basic result [69] that time-limited parts (snapshots) of bandlimited sequences span a low-dimensional subspace. The *basis functions of this subspace are the discrete prolate spheroidal sequences*. Using these results from the theory of time-concentrated and bandlimited sequences we represent every time-variant subcarrier, that is frequency-flat, through a Slepian basis expansion of low dimensionality. It can be shown [85,87] that the bias of the Slepian basis expansion is more than a magnitude smaller than the bias of the Fourier basis expansion [61, 60] (i.e. a truncated discrete Fourier transform) since the frequency leakage effect of the Fourier transform is avoided.

This chapter is structured in the following way:

Section 4.2 introduces a channel model for the time-variant channel. A signal model for the special case of transmission over a time-variant frequency-flat channel is given in Section 4.3. We discuss the deficiencies of the Fourier basis expansion in Section 4.4 using a single path channel.

In Section 4.5 the Slepian basis expansion is introduced and we analyze its performance for a multipath channel in comparison to the Fourier basis expansion. We assume that noisy channel observations are available for this analysis, which is typically the case in decision feedback equalizers or in iterative receivers.

In the case of pilot based channel estimation, noisy channel observations are available on a pilot grid only. The corresponding signal model is introduced in Section 4.6. We derive a generalized finite Slepian basis expansion that takes the pilot grid into account in Section 4.7. Analytic and numeric performance results for pilot based channel estimation are provided in Section 4.8.

4.2 Time-Variant Channel Model

Figure 4.1 shows the discrete multipath channel model [26, 7] for a moving user at velocity v. The time-variant channel impulse response

$$h'(t,\tau) = \sum_{\ell=0}^{L'-1} \eta_\ell e^{\mathrm{j}2\pi f_\ell t} \delta(\tau - \tau_\ell) \tag{4.2}$$

is given by the sum of L' different paths with path delay τ_ℓ, Doppler shift

$$|f_\ell| < B_{\mathrm{Dmax}} = \nu_{\mathrm{Dmax}}/T_{\mathrm{S}} \tag{4.3}$$

and complex attenuation η_ℓ. Oncoming traffic in a tunnel would be one of the rare cases where (4.3) may be violated. Equation (4.2) is a deterministic channel description that depends in a nonlinear manner on the Doppler frequencies of each individual path. This prevents the direct application of (4.2) for channel equalization.

We extend the concepts from Section 2.1 to the time-variant case. The equivalent, complex-valued, baseband time-variant impulse response is given by

$$h(t,\tau) = h_{\mathrm{T}}(\tau) * h'(t,\tau) * h_{\mathrm{R}}(\tau). \tag{4.4}$$

Throughout this chapter we will deal with the case where the symbol duration is much longer than the delay spread of the time-variant impulse response

$$T_{\mathrm{S}} \gg T_{\mathrm{D}}\,.$$

In this case no inter-symbol interference occurs. Thus, the channel is frequency-flat [56] and we can focus on the task of time-variant channel estimation. We apply no OFDM since its advantages are specific to frequency selective channels.

In Chapter 5 we will extend the results to time-variant frequency-selective channels where $T_\mathrm{S} \leq T_\mathrm{D}$.

4.3 Signal Model for a Frequency-Flat Channel

We consider the transmission of a symbol sequence $d[m]$ with symbol rate $1/T_\mathrm{S}$. The channel is considered frequency-flat since we assume

$$T_\mathrm{S} \gg T_\mathrm{D}\,.$$

We define the time-variant channel, sampled at the symbol rate $1/T_\mathrm{S}$, by

$$h[m] \triangleq h(mT_\mathrm{S}, 0)\,. \tag{4.5}$$

The symbols $d[m]$ are chosen i.i.d. with equal probability from a QPSK symbol set $\{\pm 1 \pm \mathrm{j}\}/\sqrt{2}$. The symbol energy $E_\mathrm{S} = 1$. The received sequence $y[m]$ is given by the multiplication of the symbol sequence and the sampled time-variant channel plus additional circular symmetric complex white Gaussian noise $z[m]$ with zero mean and variance σ_z^2,

$$y[m] = h[m]d[m] + z[m]\,. \tag{4.6}$$

For coherent detection we need an estimate of $h[m]$ at the receiver side. The classic approach [9] to represent $h[m]$ is the channel spreading function in the Doppler domain which is obtained by means of the Fourier transform.

4.4 Fourier Basis Expansion and its Deficiencies

The channel spreading function is defined as

$$S'_{\boldsymbol{H}}(\nu) = \sum_{m=-\infty}^{\infty} h[m]\mathrm{e}^{-\mathrm{j}2\pi m\nu}\,, \tag{4.7}$$

where $-1/2 \leq \nu < 1/2$. Please note that $h[m]$, as defined in (4.5), represents a sequence of sampled channel coefficients from a time-variant frequency-flat channel. This is why the channel spreading function $S'_{\boldsymbol{H}}(\nu)$ is now one-dimensional and coincides with the Doppler spectrum of the frequency-flat channel.

For a wireless system the maximum normalized Doppler bandwidth ν_{Dmax} is known so that $S'_{\boldsymbol{H}}(\nu)$ is bandlimited, and vanishes for $|\nu| > \nu_{\mathrm{Dmax}}$. This can be expressed by

$$h[m] = \int_{-\nu_{\mathrm{Dmax}}}^{\nu_{\mathrm{Dmax}}} S'_{\boldsymbol{H}}(\nu) \mathrm{e}^{\mathrm{j}2\pi m\nu} \mathrm{d}\,\nu\,. \tag{4.8}$$

In order to enable block based processing we limit the observation time to $m \in \{0, \ldots, M-1\}$ which results in rectangular windowing of $h[m]$, thus

$$S_{\boldsymbol{H}}(\nu) = \sum_{m=0}^{M-1} h[m] \mathrm{e}^{-\mathrm{j}2\pi m\nu}\,. \tag{4.9}$$

We are able to represent $h[m]$ for $m \in \{0, \ldots, M-1\}$ uniquely by sampling in the frequency-domain

$$S_{\boldsymbol{H}}[d] = \sum_{m=0}^{M-1} h[m] \mathrm{e}^{-\mathrm{j}2\pi md/M} = S_{\boldsymbol{H}}(d/M), \tag{4.10}$$

for $d \in \{-M/2, \ldots, M/2-1\}$ and M even, a representation well-known as DFT.

The rectangular windowing in (4.10) results in spectral leakage [55, Sec. 5.4] [53, Sec. 3.7]. This means, the energy from low frequency Fourier coefficients leaks to the full frequency range. Therefore, the support region of $S_{\boldsymbol{H}}[d]$ is not limited to $|d| \leq \lceil \nu_{\mathrm{Dmax}} M \rceil$. However, $S_{\boldsymbol{H}}[d]$ will decay with increasing $|d|$.

4.4.1 Numerical Example

Figure 4.2 illustrates the spectral leakage effect by plotting the magnitude of the sampled channel-spreading function $S_{\boldsymbol{H}}[d]$ (and an interpolated version $S_{\boldsymbol{H}}(\nu)$) which arises in an actual communication system after time windowing to $m \in \{0, \ldots, M-1\}$. For comparison the channel spreading function without windowing $S'_{\boldsymbol{H}}(\nu)$ is shown too. We consider a transmission with carrier frequency $f_{\mathrm{C}} = 2\,\mathrm{GHz}$ at a symbol rate $1/T_{\mathrm{S}} = 48.6 \cdot 10^3\,\mathrm{s}^{-1}$. The data block has length of $M = 256$ symbols. These parameters match the one of the MC-CDMA system defined in Section 3.1.1. The maximum speed of the user $v_{\max} = 102.5\,\mathrm{km/h}$ which results in a maximum normalized Doppler frequency $\nu_{\mathrm{Dmax}} = 3.9 \cdot 10^{-3}$. We assume a dense scattering environment. The system parameters result in a time-bandwidth product $\nu_{\mathrm{Dmax}} M = 1$.

Figure 4.3 shows the difference between the energy in the index set $\{-U, \ldots, U\}$ and the total energy for varying U which is identical to the mean square error

$$\mathrm{MSE} = \sum_{d=-U}^{U} |S_{\boldsymbol{H}}[d]|^2 - \sum_{d=-M/2}^{M/2-1} |S_{\boldsymbol{H}}[d]|^2\,, \tag{4.11}$$

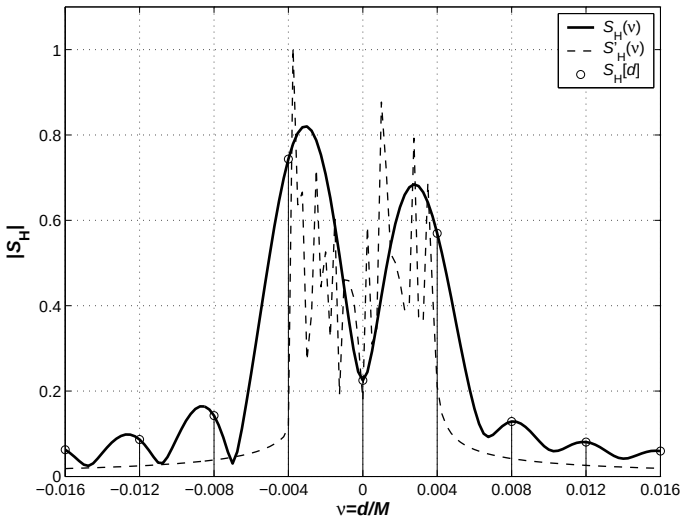

Figure 4.2: Sampled channel-spreading function magnitude $|S_{\boldsymbol{H}}[d]|$ (and an interpolated version $|S_{\boldsymbol{H}}(\nu)|$). The user moves at $v = 102.5\,\mathrm{km/h}$ in a dense scattering environment. Information is transmitted at $f_\mathrm{C} = 2\,\mathrm{GHz}$ with rate $1/T_\mathrm{S} = 48 \cdot 10^3\,\mathrm{s}^{-1}$ in blocks of length $M = 256$. For comparison the channel spreading function without windowing $|S'_{\boldsymbol{H}}(\nu)|$ is shown too.

for M even. We can see that most of the energy of $S_{\boldsymbol{H}}[d]$ is concentrated between $|d| \leq \lceil \nu_{\mathrm{Dmax}} M \rceil = 1$. However, the energy in $S_{\boldsymbol{H}}[d]$ for $|d| > \lceil \nu_{\mathrm{Dmax}} M \rceil$ is still significant. Signal energy from low frequency Fourier coefficients leaks to the full frequency range because of the time-windowing applied in (4.10). Nevertheless, the signal concentration in the index range $\{-\lceil \nu_{\mathrm{Dmax}} M \rceil, \ldots, \lceil \nu_{\mathrm{Dmax}} M \rceil\}$ is exploited for the definition of the Fourier basis expansion [61, 60].

4.4.2 Definition of the Fourier Basis Expansion

The Fourier basis expansion [61, 60] is defined as

$$h[m] \approx \tilde{h}^{(\mathrm{F})}[m] = \sum_{i=0}^{D^{(\mathrm{F})}-1} \gamma_i^{(\mathrm{F})} u_i^{(\mathrm{F})}[m], \quad m \in \{0, \ldots, M-1\},$$

where

$$u_i^{(\mathrm{F})}[m] = \frac{1}{\sqrt{M}} \mathrm{e}^{\frac{\mathrm{j}2\pi(i-(D^{(\mathrm{F})}-1)/2)m}{M}} \tag{4.12}$$

defines the basis functions for $i \in \{0, \ldots, D^{(\mathrm{F})} - 1\}$ and

$$2\lceil \nu_{\mathrm{Dmax}} M \rceil + 1 \leq D^{(\mathrm{F})} \leq M - 1$$

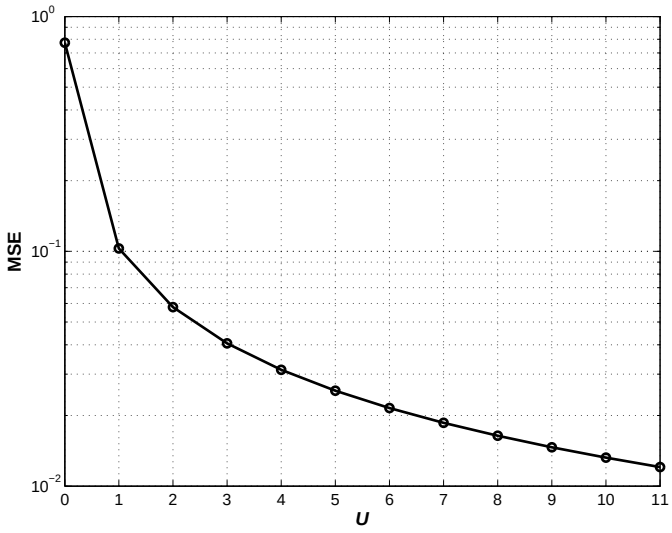

Figure 4.3: Mean square error caused by limiting $S_{\boldsymbol{H}}[d]$ to $|d| \leq U$.

defines the dimension of the basis expansion.

Wherever possible we will use a generic notation for the basis expansion quantities $u_i[m]$, D, γ_i, and $\tilde{h}[m]$ to indicate that the expression is applicable to any set of orthonormal basis functions $u_i[m]$. If we want to specifically reference the Fourier basis expansion we use the superscript $(\cdot)^{(\mathrm{F})}$.

By choosing D we can control the mean square error of the Fourier basis expansion that is defined as

$$\mathrm{MSE}_M = \frac{1}{M} \sum_{m=0}^{M-1} \mathbb{E}\left\{ \left| h[m] - \tilde{h}[m] \right|^2 \right\} . \tag{4.13}$$

The basis expansion parameters are calculated according to

$$\gamma_i = \sum_{m=0}^{M-1} h[m] u_i{}^*[m], \quad i \in \{0, \ldots, D-1\} . \tag{4.14}$$

However, equation (4.14) is of limited practical relevance, because at the receiver side the channel coefficients $h[m]$ will be available in the form of noisy observations. Furthermore, observations of the channel can be only obtained at index positions where known pilots are transmitted. These pilot positions are a subset of $\{0, \ldots, M-1\}$.

We will treat all these issues throughout the remainder of this chapter. For now let us assume that we know the channel $h[m]$ and that the channel is defined by one propagation path only. Using this most simple channel we analyze the mean square error of the Fourier basis expansion for $D < M$ in the following section.

4.4.3 Performance Results for Single Path Channel

We are interested to analyze the mean square error of the Fourier basis expansion for a single-path time-variant frequency-flat channel

$$h[m] = \mathrm{e}^{\mathrm{j}2\pi\nu_{\mathrm{D}}m} \tag{4.15}$$

for $m \in \{0, \ldots, M-1\}$ and $0 < \nu_{\mathrm{D}} < \nu_{\mathrm{Dmax}}$.

The time-variant channel coefficients $h[m]$ result from a sampled complex exponential with normalized frequency ν_{D}. Thus, we are interested in the frequency response of the Fourier basis expansion. The (instantaneous) frequency response of an orthonormal basis expansion is defined as [52]:

$$H(m,\nu) = \boldsymbol{f}^{\mathrm{T}}[m] \sum_{\ell=0}^{M-1} \boldsymbol{f}^{*}[\ell]\mathrm{e}^{-\mathrm{j}2\pi\nu(m-\ell)} \tag{4.16}$$

for $m \in \{0, \ldots, M-1\}$, $|\nu| < \nu_{\mathrm{Dmax}}$. The instantaneous values of the basis functions are collected in vector

$$\boldsymbol{f}[m] = \begin{bmatrix} u_0[m] \\ \vdots \\ u_{D-1}[m] \end{bmatrix} \in \mathbb{C}^{D}\,.$$

In (4.16) the sum $\sum_{\ell=0}^{M-1} \boldsymbol{f}^{*}[\ell]\mathrm{e}^{-\mathrm{j}2\pi\nu(m-\ell)}$ projects the complex exponential onto the basis function, i.e. we calculate the inner product with every basis function. Then, the realization at time instant m is calculated by left multiplying with $\boldsymbol{f}^{\mathrm{T}}[m]$.

The complex exponential in (4.16) is shifted by m, thus $|H(m,\nu)|$ is the instantaneous amplitude response of the basis expansion at time instant m. The phase of $H(m,\nu)$, expressed by $\arg(H(m,\nu))$, is the instantaneous phase shift of the basis expansion at time index m. The design goal for a basis expansion is to have no amplitude error $|H(m,\nu)| = 1$ and no phase error $\arg(H(m,\nu)) = 0$, i.e. $H(m,\nu) = 1$. Therefore, the instantaneous error (energy) characteristic of the basis expansion is defined as

$$E(m,\nu) = |1 - H(m,\nu)|^2\,. \tag{4.17}$$

For the single path channel as defined in (4.15) the mean square error at time index m is identical to the instantaneous error characteristic of the basis expansion for $\nu = \nu_{\mathrm{D}}$

$$\mathrm{MSE}[m] = E(m,\nu_{\mathrm{D}})\,. \tag{4.18}$$

We define the mean square error for a block of length M as

$$\mathrm{MSE}_M = E_M(\nu_{\mathrm{D}}) \tag{4.19}$$

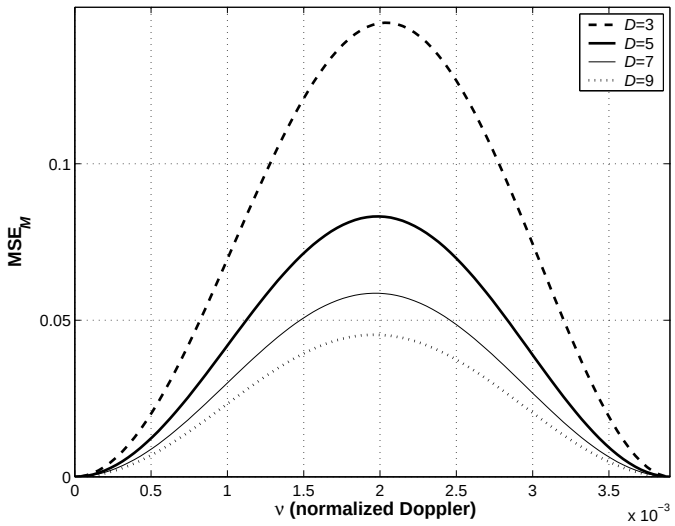

Figure 4.4: Mean square error of the Fourier basis expansion for a single path channel. The Fourier basis expansion is designed for $\lceil \nu_{\mathrm{Dmax}} M \rceil = 1$ and has dimension $D^{(\mathrm{F})} \in \{3, 5, 7, 9\}$. The normalized Doppler frequency is varied in the range $0 \leq \nu_{\mathrm{D}} \leq \nu_{\mathrm{Dmax}} = 3.9 \cdot 10^{-3}$.

where the mean error characteristic

$$E_M(\nu) = \frac{1}{M} \sum_{m=0}^{M-1} E(m, \nu)\,. \tag{4.20}$$

We use the parameters from the example in Section 4.4.1 to evaluate (4.19) numerically. The speed of the user is varied in the range $0 < v < v_{\max} = 102.5\,\mathrm{km/h}$ which results in a normalized Doppler frequency $0 \leq \nu_{\mathrm{D}} \leq 3.9 \cdot 10^{-3}$ for the single path channel defined in (4.15). The dimension of the Fourier basis expansion with these parameters is $D^{(\mathrm{F})} \geq 3$.

Figure 4.4 shows the mean square error MSE_M for a Fourier basis expansion with dimension $D^{(\mathrm{F})} \in \{3, 5, 7, 9\}$. With increasing $D^{(\mathrm{F})}$ the mean square error decreases. At $\nu_{\mathrm{D}} = 0.0018 = 1/(2M)$ the error obtains a maximum since ν_{D} lies exactly in between two frequencies of the chosen Fourier base.

Figure 4.5 plots the trajectory of $h[m]$ for $m \in \{0, \ldots, M-1\}$ in the complex plane to give more insights in the detailed approximation behavior. We compare $h[m]$ with the reconstruction through the Fourier basis expansion $\tilde{h}^{(\mathrm{F})}[m]$ for $\nu_{\mathrm{D}} = 1/(2M)$ where MSE_M is maximum. We show results for $D^{(\mathrm{F})} \in \{3, 12\}$.

In Figure 4.6 we plot the absolute phase error $\left|\arg\left(H^{(\mathrm{F})}(m, \nu_{\mathrm{D}})\right)\right|$ which is an important measure for equalization. The phase error for $\nu_{\mathrm{D}} = 1/(2M)$ at the beginning and at the end of the block is greater than 45 degree for a Fourier basis expansion

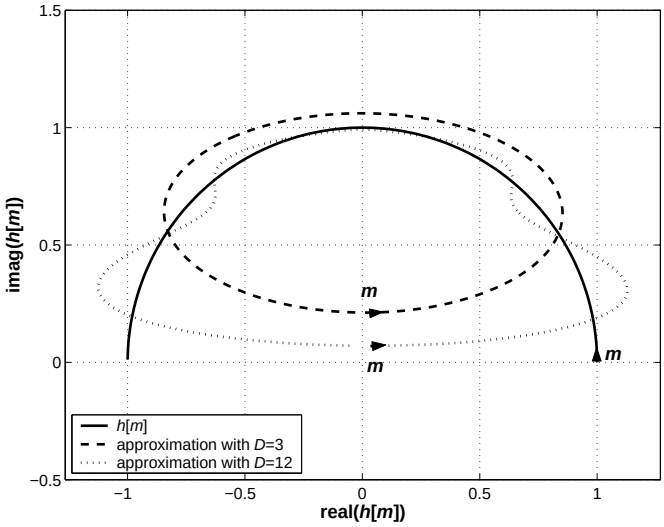

Figure 4.5: Trajectory of $h[m]$ and its approximation by the Fourier basis expansion $\tilde{h}^{(\mathrm{F})}[m]$. The trajectories are plotted for discrete index values $m \in \{0, \ldots, M-1\}$. The Fourier basis expansion has dimension $D^{(\mathrm{F})} \in \{3, 12\}$, is designed for $\lceil \nu_{\mathrm{Dmax}} M \rceil = 1$, and is evaluated for a complex exponential with $\nu_{\mathrm{D}} = 1/(2M)$.

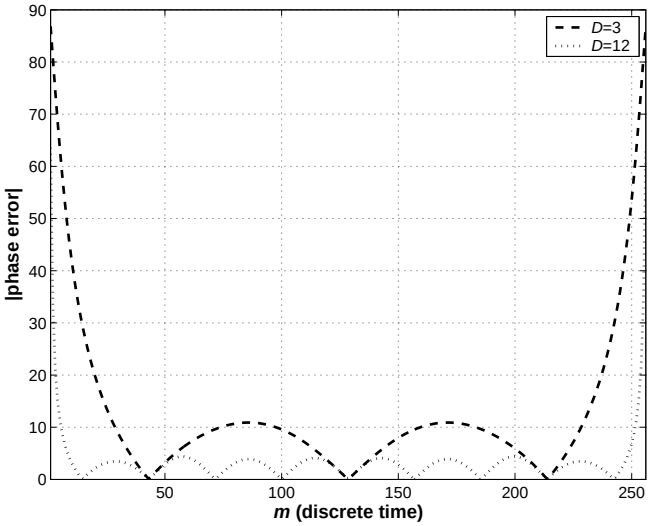

Figure 4.6: Absolute phase error $\left|\arg\left(H^{(\mathrm{F})}(m, \nu_{\mathrm{D}})\right)\right|$ for $m \in \{0, \ldots, M-1\}$. The Fourier basis expansion has dimension $D^{(\mathrm{F})} \in \{3, 12\}$, is designed for $\lceil \nu_{\mathrm{Dmax}} M \rceil = 1$, and is evaluated for a complex exponential with $\nu_{\mathrm{D}} = 1/(2M)$.

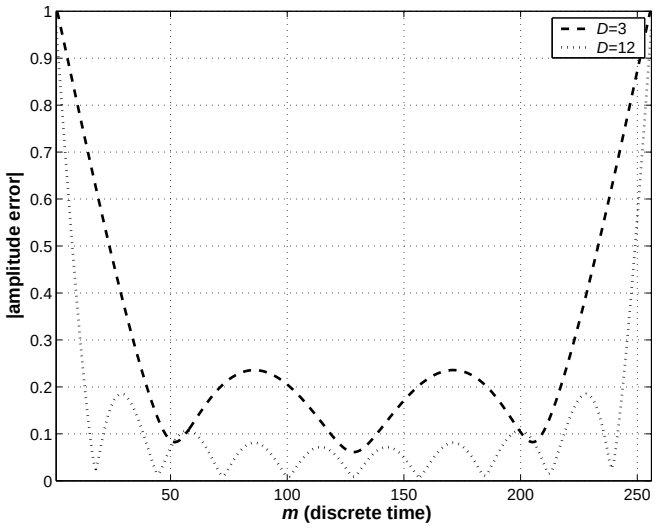

Figure 4.7: Absolute amplitude error $\left|1-\left|H^{(\mathrm{F})}(m,\nu_{\mathrm{D}})\right|\right|$ for $m \in \{0,\ldots,M-1\}$. The Fourier basis expansion has dimension $D^{(\mathrm{F})} \in \{3,12\}$, is designed for $\lceil \nu_{\mathrm{Dmax}} M \rceil = 1$, and is evaluated for a complex exponential with $\nu_{\mathrm{D}} = 1/(2M)$.

with a dimension of $D^{(\mathrm{F})} \in \{3,12\}$. With increasing $D^{(\mathrm{F})}$ the phase error at both ends of the interval decays faster but the initial value stays the same. A symbol alphabet, like QPSK, that encodes information in the phase is sensible to phase errors in the channel estimation. Thus, decision errors will result from the phase error inherent to the Fourier basis expansion leading to an error floor at higher signal to noise ratios.

Figure 4.7 plots the absolute amplitude error

$$\left|1-\left|H^{(\mathrm{F})}(m,\nu_{\mathrm{D}})\right|\right|$$

for $\nu_{\mathrm{D}} = 1/(2M)$. The behavior depicted in Figure 4.6 and Figure 4.7 is similar to the well-known Gibbs phenomenon [55, Sec. 8.2.2]. If the DFT is truncated at $\lceil \nu_{\mathrm{Dmax}} M \rceil$ the Gibbs effect together with spectral leakage leads to significant phase and amplitude errors at the beginning and at the end of the data block. These (deterministic) errors will result in an error floor at higher signal to noise ratios for a single-user detector if the Fourier basis expansion is used for time-variant channel equalization as was shown in [8] and by the author in [88]. We can conclude that the dimension of the Fourier basis expansion $2\lceil \nu_{\mathrm{Dmax}} M \rceil + 1$ that is reported in [61, 60, 4, 42, 47] is not sufficient for error free detection. In Section 5 we will analyze the effect of the Fourier basis expansion in the context of multi-user detection algorithms.

The analysis in this section shows clearly that the Fourier basis expansion has several drawbacks and a different set of better suited basis functions must be found. The theory of time-concentrated and bandlimited sequences developed by Slepian [69] enables a new approach for the time-variant channel estimation problem which we will pursue in the next section.

4.5 Slepian Basis Expansion

Slepian [69] asked which sequences are bandlimited to the frequency range $[-\nu_{\mathrm{Dmax}}, \nu_{\mathrm{Dmax}}]$ and simultaneously most concentrated in a certain time interval of length M. The associated optimization problem was solved first for continuous time in [70] and later for discrete time in [69]. In both cases Slepian found that the desired set of orthogonal sequence are the eigenfunctions of an integral operator and simultaneously of a commuting differential operator [71]. These special results enable the numerical calculation for practical applications.

We are interested in the discrete time case. The sequences $u[m]$ we are seeking shall have their maximum energy concentration in an interval with length M

$$\lambda = \frac{\sum_{m=0}^{M-1} |u[m]|^2}{\sum_{m=-\infty}^{\infty} |u[m]|^2}\,, \tag{4.21}$$

while being bandlimited to ν_{Dmax}, hence

$$u[m] = \int_{-\nu_{\mathrm{Dmax}}}^{\nu_{\mathrm{Dmax}}} U(\nu) \mathrm{e}^{\mathrm{j}2\pi m\nu} \mathrm{d}\,\nu \tag{4.22}$$

where

$$U(\nu) = \sum_{m=-\infty}^{\infty} u[m] \mathrm{e}^{-\mathrm{j}2\pi m\nu}\,. \tag{4.23}$$

We see that $0 \leq \lambda \leq 1$.

The solutions of this constrained maximization problem are the discrete prolate spheroidal (DPS) sequences [69]. The DPS sequences $u_i^{(\mathrm{S})}[m, \nu_{\mathrm{Dmax}}, M]$ are defined as the real solution of

$$\sum_{\ell=0}^{M-1} \frac{\sin(2\pi\nu_{\mathrm{Dmax}}(\ell - m))}{\pi(\ell - m)} u_i^{(\mathrm{S})}[\ell, \nu_{\mathrm{Dmax}}, M] = \lambda_i(\nu_{\mathrm{Dmax}}, M) u_i^{(\mathrm{S})}[m, \nu_{\mathrm{Dmax}}, M] \tag{4.24}$$

for $i \in \{0, \ldots, M-1\}$ and $m \in \{-\infty, \ldots, \infty\} = \mathbb{Z}$ [69]. We drop the explicit dependence of $u_i^{(\mathrm{S})}[m]$ on ν_{Dmax} and M which we consider fixed system parameters for the remainder of the entire thesis.

The DPS sequence $u_0[m]$ is the unique sequence that is bandlimited and most time-concentrated in a given interval with length M, $u_1[m]$ is the next sequence having maximum energy concentration among the DPS sequences orthogonal to $u_0[m]$, and so on. Thus, the DPS sequences are a set of orthogonal sequences. Each DPS sequence is exactly band-limited and simultaneously possess a high (but not complete) time-concentration in a certain interval with length M. The eigenvalues λ_i are a measure for this energy concentration expressed by (4.21).

The DPS sequences are not only orthogonal with respect to the index set $\{-\infty, \ldots, \infty\} = \mathbb{Z}$ but also with respect to $\{0, M-1\}$, thus they are *doubly* orthogonal in the following sense

$$\sum_{m=0}^{M-1} u_i^{(\mathrm{S})}[m] u_\ell^{(\mathrm{S})}[m] = \lambda_i \sum_{m=-\infty}^{\infty} u_i^{(\mathrm{S})}[m] u_\ell^{(\mathrm{S})}[m] = \delta_{i\ell}\,,$$

where $i, \ell \in \{0, \ldots, M-1\}$. Please note that the DPS sequences are defined as orthonormal for the index set $\{0, \ldots, M-1\}$.

The eigenvalues λ_i are clustered near 1 for $i \leq \lceil 2\nu_{\mathrm{Dmax}} M \rceil$ and rapidly decay to zero for $i > \lceil 2\nu_{\mathrm{Dmax}} M \rceil$. Therefore, the approximate signal space dimension [69, Sec. 3.3] of time-limited snapshots of a bandlimited signal is given by

$$D' = \lceil 2\nu_{\mathrm{Dmax}} M \rceil + 1\,. \tag{4.25}$$

All these properties described so far enable parameter estimation without the drawbacks of windowing as in the case of the Fourier basis expansion [69, Sec. 3.3].

For our application we are interested at $u_i^{(\mathrm{S})}[m]$ for the index set $\{0, \ldots, M-1\}$ only. We introduce the term Slepian sequences for the index limited DPS sequences and define the vector $\boldsymbol{u}_i^{(\mathrm{S})} \in \mathbb{R}^M$ with elements $u_i^{(\mathrm{S})}[m]$ for $m \in \{0, \ldots, M-1\}$. The Slepian sequences $\boldsymbol{u}_i^{(\mathrm{S})}$ are eigenvectors of the matrix $\boldsymbol{C} \in \mathbb{R}^{M \times M}$ fulfilling

$$\boldsymbol{C}\boldsymbol{u}_i^{(\mathrm{S})} = \lambda_i \boldsymbol{u}_i^{(\mathrm{S})}\,. \tag{4.26}$$

The eigenvalues λ_i are identical to the one in (4.24). Matrix $\boldsymbol{C}$ is defined as

$$[\boldsymbol{C}]_{i,\ell} = \frac{\sin\left[2\pi(i-\ell)\nu_{\mathrm{Dmax}}\right]}{\pi(i-\ell)}\,, \tag{4.27}$$

where $i, \ell \in \{0, \ldots, M-1\}$. Equation (4.26) is not suited for the numerical calculation of $\boldsymbol{u}_i^{(\mathrm{S})}$ because matrix $\boldsymbol{C}$ is rank deficient and the eigenvalues are clustered around 1 and 0. However, the already mentioned commuting differential operator

offers an numerically fast and stable way for the calculation of $\boldsymbol{u}_i^{(\mathrm{S})}$. Please refer to [69] and [53, Section 8.3] for more details on the numerical calculation of the Slepian sequences. We will come back to the utility of (4.26) later.

Concluding, the Slepian sequences span an orthonormal basis which allows to represent time-limited snapshots of bandlimited sequences through a basis expansion. The Slepian basis expansion expands the sequence $h[m]$ in terms of Slepian sequences $u_i^{(\mathrm{S})}[m]$

$$h[m] \approx \tilde{h}^{(\mathrm{S})}[m] = \sum_{i=0}^{D^{(\mathrm{S})}-1} u_i^{(\mathrm{S})}[m]\gamma_i^{(\mathrm{S})}\,, \tag{4.28}$$

where $m \in \{0, \ldots, M-1\}$. The dimension of this basis expansion fulfills

$$D' \leq D^{(\mathrm{S})} \leq M\,.$$

By choosing $D^{(\mathrm{S})}$ we can control the mean square error defined in (4.13).

In order to highlight the utility of the Slepian basis expansion in terms of dimension reduction we give a numerical example of an actual communication system. Again, we use the parameters from Section 4.4.1 that are: carrier frequency $f_\mathrm{C} = 2\,\mathrm{GHz}$, symbol rate $1/T_\mathrm{S} = 48.6 \cdot 10^3\,\mathrm{s}^{-1}$, maximum speed of the user $v_\mathrm{max} = 102.5\,\mathrm{km/h}$, maximum normalized Doppler frequency $\nu_\mathrm{Dmax} = 3.9 \cdot 10^{-3}$, and data block length $M = 256$. With these system parameters the approximate dimension of the signal space $D' = \lceil 2\nu_\mathrm{Dmax} M \rceil + 1 = 3$. Therefore, the dimension of the estimation problem is reduced by a factor of $256/3 = 85$ which is a very considerable saving. In Figure 4.8 the DPS eigenvalue spectrum is given. The corresponding Slepian sequences $\boldsymbol{u}_i$ for $i \in \{0, \ldots, 4\}$ are depicted in Figure 4.9.

4.5.1 Parameter Estimation From Noisy Observations

We insert the basis expansion (4.28) in the signal model (4.6),

$$y[m] = h[m]d[m] + z[m] = \left(\sum_{i=0}^{D-1} u_i[m]\gamma_i\right) d[m] + z[m]\,. \tag{4.29}$$

Hence, we can visualize the communication system as depicted in Figure 4.10. The transmission takes place over D parallel channels with fixed complex attenuation γ_i followed by modulation with the orthonormal sequences $u_i[m]$.

For now we assume that the receiver has knowledge of all transmitted data symbols in a data block, which is typically the case in iterative receiver structures. Since the data symbols have constant modulus $|d[m]| = \sqrt{E_\mathrm{S}} = 1$ we obtain a noisy estimate of the instantaneous channel values through

$$\hat{h}[m] = y[m]d^*[m] = h[m] + z[m]d^*[m]\,.$$

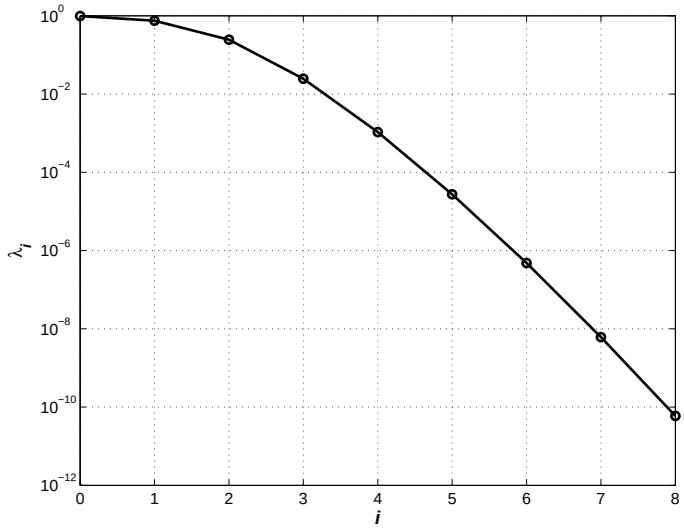

Figure 4.8: Eigenvalue spectrum λ_i for the Slepian sequences, ordered from the largest eigenvalue λ_0 to the smallest λ_{M-1}. The Slepian sequences are designed for block length $M = 256$ and a maximum Doppler bandwidth $\nu_{\mathrm{Dmax}} = 3.9 \cdot 10^{-3}$. The approximate dimension of the signal space evaluates to $D' = \lceil 2\nu_{\mathrm{Dmax}} M \rceil + 1 = 3$.

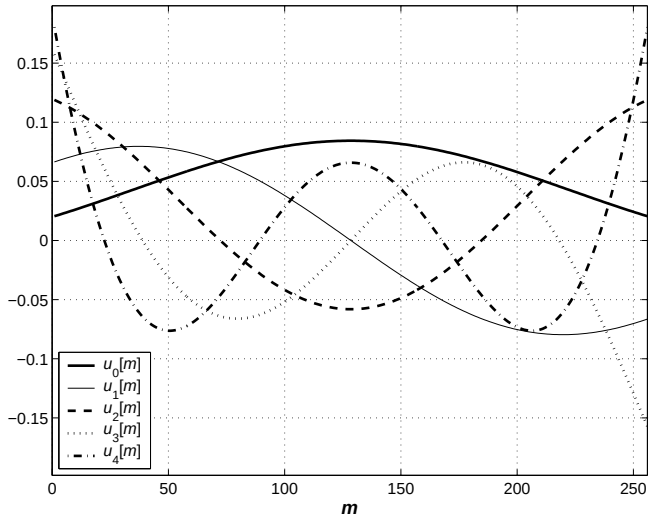

Figure 4.9: Slepian sequences $u_i[m]$ for $M = 256$ and $\nu_{\mathrm{Dmax}} = 3.9 \cdot 10^{-3}$.

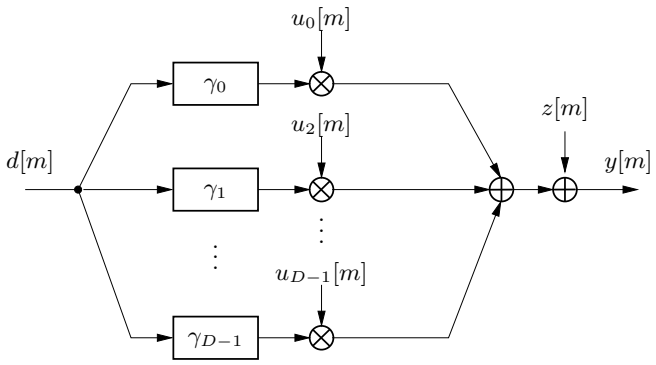

Figure 4.10: Representation of a linear time-variant frequency-flat channel $h[m]$ using time-invariant weighting coefficients γ_i and modulation with orthonormal basis functions $u_i[m]$. This model is valid for $m \in \{0, \ldots, M-1\}$.

Considering the model in Figure 4.10 we can estimate the unknown coefficients in (4.28) through

$$\hat{\gamma}_i = \sum_{m=0}^{M-1} \hat{h}[m] u_i^*[m] = \sum_{m=0}^{M-1} y[m] d^*[m] u_i^*[m] \tag{4.30}$$

for $i \in \{0, \ldots, D^{(\mathrm{S})} - 1\}$.

The mean square error (4.13) of the basis expansion can be described by the sum of a square bias and a variance term

$$\mathrm{MSE}_M = \mathrm{bias}_M^2 + \mathrm{var}_M \,. \tag{4.31}$$

We will see in the next section that bias_M^2 is depending on the actual set of basis functions and var_M depends linearly on the noise variance σ_z^2 and the dimension D of the basis expansion.

4.5.2 Analytic Performance Results

For the purposes of performance *analysis* for a *nominal* ensemble of channel realizations of $h[m]$, let us specify a Doppler power spectral density

$$S_{hh}(\nu) = \sum_{\tilde{m}=-\infty}^{\infty} R_{hh}[\tilde{m}] \mathrm{e}^{-\mathrm{j}2\pi\tilde{m}\nu} \,,$$

where the autocorrelation is defined as

$$R_{hh}[\tilde{m}] = \mathbb{E}\{h^*[m+\tilde{m}] h[m]\} \,. \tag{4.32}$$

The square bias of the basis expansion can be expressed [52] by integrating the single path error expression (4.18) over the Doppler power spectrum,

$$\text{bias}^2[m] = \int_{-\frac{1}{2}}^{\frac{1}{2}} E(m,\nu) S_{hh}(\nu) \mathrm{d}\,\nu\,. \tag{4.33}$$

The square bias for a block of length M is defined as

$$\text{bias}^2_M \triangleq \frac{1}{M} \sum_{m=0}^{M-1} \text{bias}^2[m] = \int_{-\frac{1}{2}}^{\frac{1}{2}} E_M(\nu) S_{hh}(\nu) \mathrm{d}\,\nu\,, \tag{4.34}$$

where the mean error characteristic (4.20)

$$E_M(\nu) = \frac{1}{M} \sum_{m=0}^{M-1} E(m,\nu)\,. \tag{4.35}$$

The bias^2_M is defined as the mean square error (4.31) in the absence of noise ($\sigma_z^2 = 0$), see also [66, Sec. 9.9].

The parameter estimation in (4.30) is operating with noisy observations. As already stated, the biased part of the mean square error (4.13) is independent of the noise variance. The variance expression for the basis expansion is given as [52, Sec. 6.1.4]

$$\text{var}[m] \approx \sigma_z^2 \boldsymbol{f}^{\mathrm{H}}[m] \boldsymbol{f}[m]\,. \tag{4.36}$$

This equation becomes exact for $\text{bias}^2[m] = 0$. The mean variance for block length M is given by

$$\text{var}_M = \frac{1}{M} \sum_{m=0}^{M-1} \text{var}[m] = \sigma_z^2 \frac{D}{M}\,. \tag{4.37}$$

Equation (4.37) clearly shows that the variance is independent of the used set of orthonormal basis functions and increases linearly with the dimension of the basis expansion D and the noise variance σ_z^2 [52].

The approximate dimension of the signal space D' (4.25) becomes a tight bound for large M (and exact for $M \to \infty$). By insertion of D' into (4.37)

$$\text{var}_M^{(\mathrm{S})} = \sigma_z^2 \frac{\lceil 2\nu_{\mathrm{Dmax}} M \rceil + 1}{M}$$

we are able to obtain a lower tight bound for $\text{var}_M^{(\mathrm{S})}$ in the limit

$$\lim_{M\to\infty} \text{var}_M^{(\mathrm{S})} \geq 2\nu_{\mathrm{Dmax}} \sigma_z^2\,.$$

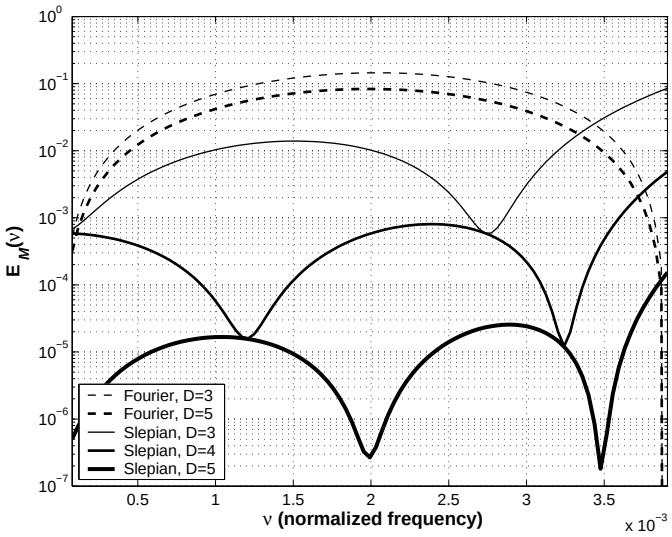

Figure 4.11: Mean error characteristic $E_M(\nu)$ versus normalized frequency ν for the Fourier basis expansion with $D \in \{3, 5\}$ and the Slepian basis expansion with $D \in \{3, 4, 5\}$, $\nu_{\mathrm{Dmax}} = 3.9{\cdot}10^{-3}$ and for block length $M = 256$. The time-bandwidth product for this parameters is $D' = \lceil 2\nu_{\mathrm{Dmax}} M \rceil + 1 = 3$.

4.5.3 Numerical Performance Results

In this section we provide performance results which enable an easy comparison of the Fourier and the Slepian basis expansion. Again we use the parameters given in Section 4.4.1. These system parameters result in $D' = 3$.

If a power spectral density $S_{hh}(\nu)$ is given, the actual bias calculation requires to evaluate (4.34) which depends on the mean error characteristic $E_M(\nu)$. We plot $E_M(\nu)$ in Figure 4.11 to give a direct indication about the performance difference between the Fourier and the Slepian basis expansion. We assume that the support of $S_{hh}(\nu)$ is within $[-\nu_{\mathrm{Dmax}}, \nu_{\mathrm{Dmax}}]$. Figure 4.11 shows $E_M(\nu)$ for positive normalized frequencies $0 \leq \nu \leq 3.9 \cdot 10^{-3}$ ($E_M(\nu)$ is a symmetric function).

Please note that the equations (4.33) ... (4.37) are generic and valid for any basis expansion with orthonormal basis functions $u_i[m]$. Figure 4.11 shows, that the bias of the Fourier basis expansion decays slowly if the basis expansion dimension D is increased above the time bandwidth product D'. For the Slepian basis expansion the bias decrease with increasing D is much faster. This is because of the steep decay of the eigenvalues λ_i for $i > D'$.

Figure 4.12 shows the bias_M^2 (4.34) for the Fourier and the Slepian basis expansion

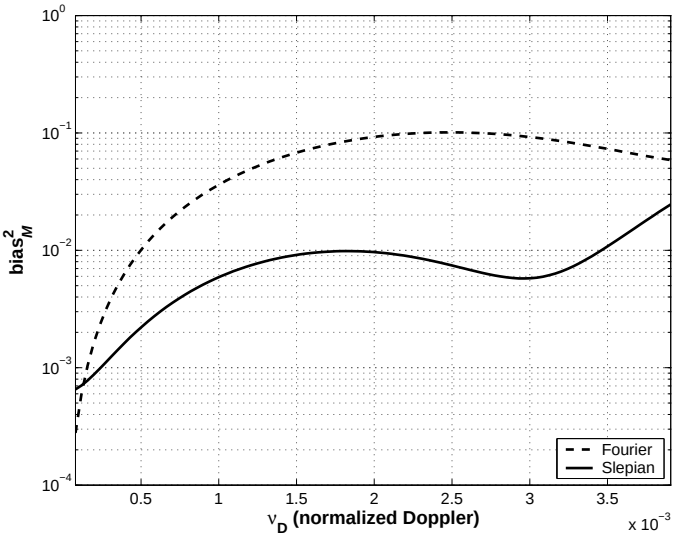

Figure 4.12: Comparison of bias^2_M for the Slepian and the Fourier basis expansion. We use a Jakes' Doppler spectrum and vary the Doppler bandwidth in the range $0 \leq \nu_\text{D} \leq 3.9 \cdot 10^{-3}$ which corresponds to a velocity range of $0 \leq v \leq 102.5\,\text{km/h}$. The basis expansions have dimension $D = 3$. The Slepian sequences are designed according to $\nu_\text{Dmax} = 3.9 \cdot 10^{-3}$ and block length $M = 256$.

when evaluated for the Jakes' Doppler spectrum

$$S_{hh}(\nu) = \begin{cases} \dfrac{1}{\pi\nu_\text{D}\sqrt{1-\left(\frac{\nu}{\nu_\text{D}}\right)^2}} & \text{for } |\nu| < \nu_\text{D}\,, \\ 0 & \text{otherwise.} \end{cases} \tag{4.38}$$

We vary the normalized Doppler bandwidth in the range $0 \leq \nu_\text{D} \leq 3.9 \cdot 10^{-3}$ corresponding to a velocity range of $0 \leq v \leq 102.5\,\text{km/h}$. The results in Figure 4.12 document that the Slepian basis expansion square bias is one magnitude smaller than the square bias of the Fourier basis expansion. The mean variance var_M (4.37) is independent of the chosen set of basis functions $u_i[m]$ but $\text{var}[m]$ (4.36) is not. Figure 4.13 shows $\text{var}[m]/\sigma_z^2$ for the Fourier and the Slepian basis expansion.

We emphasize that the selection of a suitable Slepian basis, defined by M and ν_Dmax, exploits the band-limitation of the Doppler spectrum to ν_Dmax only. The details of the Doppler spectrum for $|\nu| < \nu_\text{Dmax}$ are irrelevant. The necessary dimension of the basis expansion for wireless channels at 2 GHz and vehicular velocities up to 102.5 km/h is in the order of three only. For the calculation of the Slepian sequences efficient methods exists that avoid the numerical instabilities of the eigen-

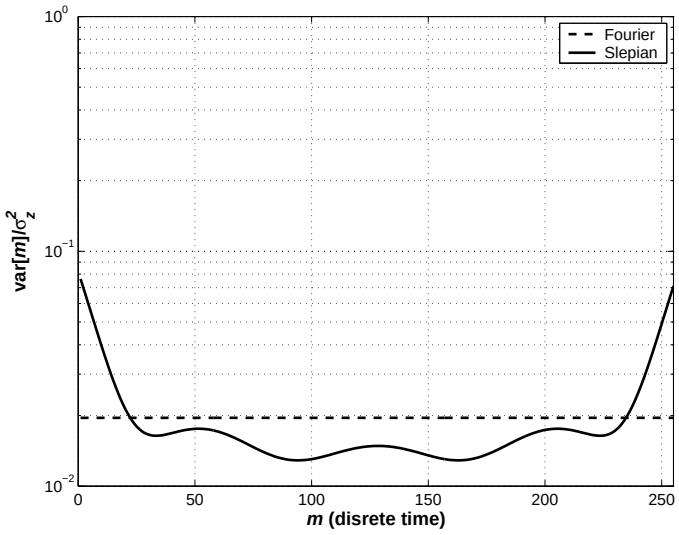

Figure 4.13: Variance multiplication $\mathrm{var}[m]/\sigma_z^2$ for the Fourier and Slepian basis expansion for $m \in \{0, \ldots, 255\}$. Both basis expansions have dimension $D = 3$.

value problem (4.26) due to the rank deficiency of matrix $\boldsymbol{C}$. Our approach therefore differs from a Karhunen-Loève transform which requires *complete* knowledge of the second-order statistics of the fading process.

It was shown by channel sounder measurements that wireless fading channels show stationary behavior for less than 70 wavelengths in a pedestrian typical-urban environment [77, 76]. We doubt that meaningful short-term fading characteristics (second order statistics to begin with) can be acquired in a multi-user system when users move at vehicular speed.

We want to point out that a link between the Slepian basis expansion and the Karhunen-Loève transform exists. Matrix $\boldsymbol{C}$ in (4.26) can be interpreted as covariance matrix of a stochastic process with rectangular power spectral density. Hence, the index limited DPS sequences (i.e. the Slepian sequences) are the eigenvectors which are also found by the Karhunen-Loève transform [41] and the related subspace methods from [67] for a stochastic process with covariance matrix $\boldsymbol{C}$. However, the bandlimited property of the DPS sequences, their double orthogonality and the known asymptotic behavior of the associated eigenvalues are key features for the estimation of time-variant channels with bandlimited Doppler spectrum which can not be inferred from (4.26). Even more, the theory of time-concentrated and bandlimited sequences offers a unifying explanation for the performance results obtained in [34], [17] and [68].

4.6 Pilot Based Channel Estimation

Channel estimation algorithms for the downlink have to be implemented in the mobile equipment and low complexity is a key requirement because of size and battery constraints. Thus, decision feedback structures or iterative receivers with soft-input soft-output decoders are too expensive in terms of resource consumption. We analyze a pilot based channel estimation scheme for time-variant frequency-flat channels. This scheme can be easily extended to an OFDM system in time-variant frequency-selective channels where it is applied on a per-subcarrier basis.

We transmit symbols in blocks of length M. Each block consists of $M - J$ data symbols $b[m]$ with J interleaved pilot symbols $p[m]$

$$d[m] = b[m] + p[m]\,. \tag{4.39}$$

The data symbols satisfy

$$b[m] \in \{\pm 1 \pm \mathrm{j}\}/\sqrt{2} \quad \text{for} \quad m \notin \mathcal{P}\,,$$

and

$$b[m] = 0 \quad \text{for} \quad m \in \mathcal{P}\,.$$

The pilot symbols are i.i.d. chosen from the QPSK symbol set

$$p[m] = \{\pm 1 \pm \mathrm{j}\}/\sqrt{2} \quad \text{for} \quad m \in \mathcal{P}\,,$$

and

$$p[m] = 0 \quad \text{for} \quad m \notin \mathcal{P}\,.$$

The pilot placement is defined through the index set

$$\mathcal{P} = \left\{ \left\lfloor i\frac{M}{J} + \frac{M}{2J} \right\rfloor \;\middle|\; i \in \{0, \ldots, J-1\} \right\}\,. \tag{4.40}$$

Figure 4.14 shows an example for the pilot set $\mathcal{P}$ defined in (4.40). The symbols have constant modulus, their energy is normalized $|d[m]| = \sqrt{E_\mathrm{S}} = 1$.

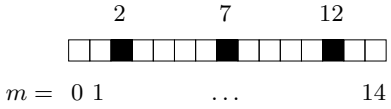

Figure 4.14: Example pilot pattern $\mathcal{P} = \{2, 7, 12\}$ defined by (4.40) for $M = 15$ and $J = 3$.

The basis expansion parameters shall be estimated utilizing the J known pilots at $m \in \mathcal{P}$. We estimate the basis expansion parameters according to:

$$\hat{\gamma}_i = \frac{1}{\sum\limits_{m\in\mathcal{P}} |u_i[m]|^2} \sum_{m\in\mathcal{P}} y[m]p^*[m]u_i^*[m]\,, \tag{4.41}$$

where $i \in \{0,\ldots,D-1\}$. We use a generic notation since (4.41) is valid for any basis expansion.

To achieve high spectral efficiency the percentage of pilot symbols in a data block is required to be as small as possible. We will see in Section 4.8 that the estimator in (4.41) is biased especially for small values of J. This is true not only for the Fourier basis expansion but also for the Slepian basis expansion since the orthogonality of the basis functions is lost. The reason for the lost orthogonality can be seen in (4.41) where the sum is evaluated on the index position defined by the pilot set $\mathcal{P}$ rather than the complete orthogonality set $\{0,\ldots,M-1\}$.

The DPS sequences are bandlimited to $[-\nu_{\mathrm{Dmax}}, \nu_{\mathrm{Dmax}}]$ and mostly concentrated on the time index set $\{0,\ldots,M-1\}$. If we would be able to design sequences $u_i'[m]$ that keep these properties but are orthogonal on the pilot set $\mathcal{P}$

$$\sum_{m\in\mathcal{P}} u_i'[m]u_\ell'[m] = \delta_{i,\ell}\sigma_i'^2 \tag{4.42}$$

we can avoid the bias due to the pilot grid while keeping the simple structure of (4.41).

The derivations of the DPS sequences [69] involve an integral operator for which no easy way was found to incorporate the constraint (4.42) in a numerical stable way. Related approaches for generalization of the DPS sequences were pursued in [22] and [12] in the field of power spectral density estimation. However, the DPS sequences can be approximated by finite discrete prolate spheroidal (FDPS) sequences which are doubly orthogonal over two finite index sets [25, 95].

We introduce the FDPS sequences in Section 4.7. The derivation of the FDPS sequences involves matrix operators which we describe in Section 4.7.1. The matrix operators have a more tractable structure which enables us to incorporate (4.42) more easily. Finally, we obtain generalized FDPS sequences with an orthogonality over the pilot set $\mathcal{P}$ in Section 4.7.2.

4.7 Finite Slepian Basis Expansion

The finite discrete prolate spheroidal (FDPS) sequences $u_i^{(\mathrm{FS})}[m]$ described in [25] and [95] are orthonormal over the *finite* index set $\{0, \ldots, aM-1\}$, i.e.

$$\sum_{m=0}^{aM-1} u_i^{(\mathrm{FS})}[m] u_\ell^{(\mathrm{FS})}[m] = \delta_{i\ell} \quad \text{for} \quad i, \ell \in \{0, \ldots, D^{(\mathrm{FS})}-1\}\,,$$

and orthogonal over the index set $\{0, M-1\}$

$$\sum_{m=0}^{M-1} u_i^{(\mathrm{FS})}[m] u_\ell^{(\mathrm{FS})}[m] = {\sigma_i^{(\mathrm{FS})}}^2 \delta_{i\ell} \quad \text{for} \quad i, \ell \in \{0, \ldots, D^{(\mathrm{FS})}-1\}\,.$$

We link these two intervals through the integer parameter $a > 1$, $a \in \mathbb{Z}^+$. $D^{(\mathrm{FS})}$ is a certain number $D' \leq D^{(\mathrm{FS})}$ defining the dimensionality of the finite Slepian basis expansion. The approximate dimension of the signal space is given by (4.25)

$$D' = \lceil 2\nu_{\mathrm{Dmax}} M \rceil + 1\,.$$

The FDPS sequences $\tilde{\boldsymbol{u}}_i^{(\mathrm{FS})} \in \mathbb{R}^{aM}$ with elements $u_i^{(\mathrm{FS})}[m]$ are the left *singular* vectors of the matrix $\boldsymbol{\mathcal{C}}' \in \mathbb{C}^{aM \times M}$ which is defined as

$$[\boldsymbol{\mathcal{C}}']_{i,\ell} = \frac{1}{aM} \frac{\sin\left[\pi(2\lceil a\nu_{\mathrm{Dmax}} M \rceil + 1)(i-\ell)/(aM)\right]}{\sin\left[\pi(i-\ell)/(aM)\right]}\,.$$

The FDPS sequences deviate here from the DPS sequences, since their defining matrix is non symmetric. Therefore, the eigenvectors do not exist and we have to resort to the singular value decomposition of matrix $\boldsymbol{\mathcal{C}}'$. The left singular vectors of the non symmetric matrix $\boldsymbol{\mathcal{C}}'$ can be calculated as the eigenvectors of the product $\boldsymbol{\mathcal{C}}'\boldsymbol{\mathcal{C}}'^{\mathrm{H}}$ fulfilling [23, Sec. 8.3]

$$\boldsymbol{\mathcal{C}}'\boldsymbol{\mathcal{C}}'^{\mathrm{H}} \tilde{\boldsymbol{u}}_i^{(\mathrm{FS})} = {\sigma_i^{(\mathrm{FS})}}^2 \tilde{\boldsymbol{u}}_i^{(\mathrm{FS})} \quad \text{for} \quad i \in \{0, \ldots, D^{(\mathrm{FS})}-1\}\,. \tag{4.43}$$

The singular values are denoted by $\sigma_i^{(\mathrm{FS})}$.

The rank of matrix $\boldsymbol{\mathcal{C}}'$ is given by

$$\mathrm{rank}(\boldsymbol{\mathcal{C}}') = \min(2a\lceil \nu_{\mathrm{Dmax}} M \rceil + 1, M)\,, \tag{4.44}$$

hence (4.44) defines an upper bound for the dimension of the finite Slepian basis expansion

$$D' \leq D^{(\mathrm{FS})} \leq \min(2a\lceil \nu_{\mathrm{Dmax}} M \rceil + 1, M)\,. \tag{4.45}$$

In analogy to the previous section we define the finite Slepian sequences as the vectors $\boldsymbol{u}_i^{(\mathrm{FS})} \in \mathbb{R}^M$ obtained by index limiting the FDPS sequences $u_i^{(\mathrm{FS})}[m]$ to $\{0, \ldots, M-1\}$.

The finite Slepian sequences $\boldsymbol{u}_i^{(\mathrm{FS})}$ converge to the Slepian sequences $\boldsymbol{u}_i^{(\mathrm{S})}$ for $a \to \infty$ [25]

$$\lim_{a\to\infty} \frac{1}{\sigma_i^{(\mathrm{FS})}} \boldsymbol{u}_i^{(\mathrm{FS})} = \boldsymbol{u}_i^{(\mathrm{S})} , \tag{4.46}$$

The factor $1/\sigma_i^{(\mathrm{FS})}$ in (4.46) is due to the fact, that the Slepian sequences are defined as orthonormal while the DPS sequences are orthogonal [69]. In the finite case the situation is opposite, the finite Slepian sequences are defined as orthogonal while the FDPS sequences are orthonormal.

Matrix $\boldsymbol{\mathcal{C}}'$ is a tall matrix with dimension $aM \times M$. In the limit $a \to \infty$ the first $M \times M$ elements of $\boldsymbol{\mathcal{C}}'$ coincide with $\boldsymbol{C}$

$$\lim_{a\to\infty} [\boldsymbol{\mathcal{C}}']_{i,\ell} = [\boldsymbol{C}]_{i,\ell} \quad \text{for} \quad i,\ell \in \{0,\ldots,M-1\} ,$$

thus matrix $\boldsymbol{\mathcal{C}}'$ has the structure

$$\lim_{a\to\infty} \boldsymbol{\mathcal{C}}' = \begin{bmatrix} \boldsymbol{C} \\ \boldsymbol{B} \end{bmatrix} . \tag{4.47}$$

The square of the singular values of $\boldsymbol{\mathcal{C}}'$ converge to the eigenvalue of $\boldsymbol{C}$

$$\lim_{a\to\infty} {\sigma_i^{(\mathrm{FS})}}^2 = \lambda_i^{(\mathrm{S})} .$$

In the case of finite values $a > 1$ the finite Slepian sequences approximate the Slepian sequences. We will show by numerical simulation in Section 4.8 that a value $a = 2$ is already sufficient for our purposes. Comparing Fig. 4.15 with Fig. 4.9 we can see that there is hardly any difference for an approximation factor $a = 2$.

4.7.1 Operator Representation

The defining matrix for the FDPS sequences $\boldsymbol{\mathcal{C}}'$ can be explained as a concatenation of a time-limiting operator to the discrete index set $\{0,\ldots,M-1\}$ and a band-limiting operator to the frequency range $[-\nu_{\mathrm{Dmax}}, \nu_{\mathrm{Dmax}}]$. Later in Section 4.7.2, we will modify the time-limiting operator for the pilot set $\mathcal{P}$ which allows us to obtain the generalized FDPS sequences.

We define the zero padded matrix

$$\tilde{\boldsymbol{\mathcal{C}}}' = \left[\boldsymbol{\mathcal{C}}', \boldsymbol{0}_{aM\times(a-1)M}\right] \in \mathbb{R}^{aM\times aM} , \tag{4.48}$$

and the time-limiting operator $\boldsymbol{\mathcal{D}}' \in \mathbb{R}^{aM\times aM}$ as the diagonal matrix

$$\boldsymbol{\mathcal{D}}' = \mathrm{diag}\left(\begin{bmatrix} \boldsymbol{1}_M \\ \boldsymbol{0}_{aM-M} \end{bmatrix}\right) . \tag{4.49}$$

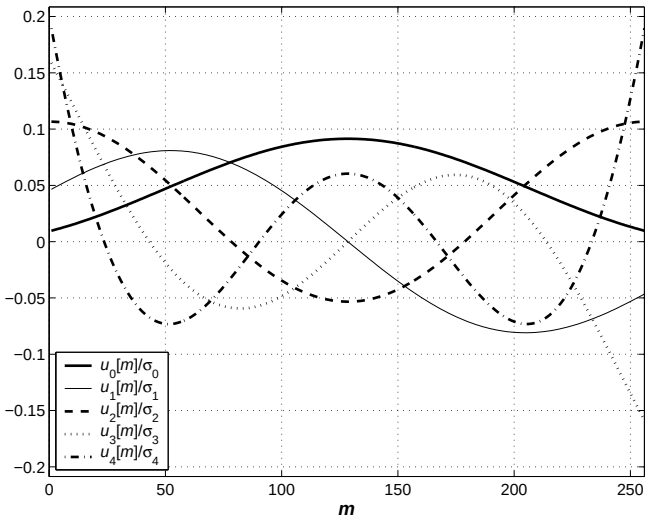

Figure 4.15: Finite Slepian sequences $u_i^{(\mathrm{GS})}[m]/\sigma_i^{(\mathrm{GS})}$ for block length $M = 256$, maximum normalized Doppler bandwidth $\nu_{\mathrm{Dmax}} = 3.9 \cdot 10^{-3}$, and approximation factor $a = 2$.

The band limiting operator $\boldsymbol{\mathcal{B}} \in \mathbb{R}^{aM \times aM}$ in the frequency domain is given by the diagonal matrix

$$\boldsymbol{\mathcal{B}} = \mathrm{diag}\left(\begin{bmatrix} \mathbf{1}_{a\lceil \nu_{\mathrm{Dmax}} M \rceil + 1} \\ \mathbf{0}_{aM - 2a\lceil \nu_{\mathrm{Dmax}} M \rceil - 1} \\ \mathbf{1}_{a\lceil \nu_{\mathrm{Dmax}} M \rceil} \end{bmatrix} \right) .$$

Using these definitions above matrix $\tilde{\boldsymbol{\mathcal{C}}}'$ can be expressed by [95]

$$\tilde{\boldsymbol{\mathcal{C}}}' = \boldsymbol{F}_{aM}^{\mathrm{H}} \boldsymbol{\mathcal{B}} \boldsymbol{F}_{aM} \boldsymbol{\mathcal{D}}' . \tag{4.50}$$

The DFT matrix $\boldsymbol{F}_{aM}$ performs the transformation from the time domain in the frequency domain and back.

The filter operator $\tilde{\boldsymbol{\mathcal{C}}}'$ performs time-limitation to $\{0, \ldots, M-1\}$ and band-limitation to $[-\nu_{\mathrm{Dmax}}, \nu_{\mathrm{Dmax}}]$. If we apply the filter operator on a zero padded, time-limited snapshot of the band-limited sequence of channel values

$$\tilde{\boldsymbol{h}} = [h[0], \ldots, h[M-1]]^{\mathrm{T}} \in \mathbb{C}^{M} \tag{4.51}$$

they remain (practically) unchanged for the the index range $\{0, \ldots, M-1\}$.

$$\begin{bmatrix} \tilde{\boldsymbol{h}} \\ \tilde{\boldsymbol{h}}' \end{bmatrix} \approx \tilde{\boldsymbol{\mathcal{C}}}' \begin{bmatrix} \tilde{\boldsymbol{h}} \\ \mathbf{0}_{aM-M} \end{bmatrix} \tag{4.52}$$

Equation (4.52) becomes exact for $a \to \infty$.

The finite Slepian sequences $\boldsymbol{u}_i^{(\mathrm{FS})}$ are defined as the first M elements of the left singular vector of matrix $\tilde{\boldsymbol{\mathcal{C}}}'$, thus they are optimally suited to define the finite Slepian basis expansion to represent $h[m]$ for $m \in \{0, \ldots, M-1\}$.

4.7.2 Generalized Finite Slepian Basis Expansion

As already mentioned we are interested to obtain generalized finite Slepian sequences that are orthogonal on the pilot set $\mathcal{P}$. The time limiting operator $\boldsymbol{\mathcal{D}}'$ (4.49) defines the inner orthogonality index set $\{0, \ldots, M-1\}$ for the finite Slepian sequences. In order to change the orthogonality set, we define the indicator vector $\boldsymbol{\rho} \in \mathbb{R}^M$ with elements

$$\rho[m] = \begin{cases} 1 & m \in \mathcal{P}, \\ 0 & m \notin \mathcal{P}; \end{cases} \qquad m \in \{0, \ldots, M-1\},$$

and modify the time limiting (4.49) operator according to

$$\boldsymbol{\mathcal{D}} = \mathrm{diag}\left(\begin{bmatrix} \boldsymbol{\rho} \\ \mathbf{0}_{aM-M} \end{bmatrix} \right).$$

Inserting $\boldsymbol{\mathcal{D}}$ in (4.50) provides us with

$$\tilde{\boldsymbol{\mathcal{C}}} = \boldsymbol{F}_{aM}^{\mathrm{H}} \boldsymbol{\mathcal{B}} \boldsymbol{F}_{aM} \boldsymbol{\mathcal{D}}.$$

Since we know the diagonal structure of $\boldsymbol{\mathcal{D}}$ and because of the fact that it multiplies $\boldsymbol{F}_{aM}^{\mathrm{H}} \boldsymbol{\mathcal{B}} \boldsymbol{F}_{aM}$ from the right we know that $\tilde{\boldsymbol{\mathcal{C}}}$ has the following structure

$$\tilde{\boldsymbol{\mathcal{C}}} = \left[\boldsymbol{\mathcal{C}}, \mathbf{0}_{aM \times (a-1)M} \right] \in \mathbb{R}^{aM \times aM}.$$

Omitting all zero columns we calculate the left singular vectors of $\tilde{\boldsymbol{\mathcal{C}}}$ by solving the eigenvalue problem of $\boldsymbol{\mathcal{C}}\boldsymbol{\mathcal{C}}^{\mathrm{H}}$ [23, Sec. 8.3]

$$\boldsymbol{\mathcal{C}}\boldsymbol{\mathcal{C}}^{\mathrm{H}} \tilde{\boldsymbol{u}}_i^{(\mathrm{GS})} = {\sigma_i^{(\mathrm{GS})}}^2 \tilde{\boldsymbol{u}}_i^{(\mathrm{GS})} \quad \text{for} \quad i \in \{0, \ldots, D^{(\mathrm{GS})} - 1\}$$

to obtain the generalized FDPS sequences $\tilde{\boldsymbol{u}}_i^{(\mathrm{GS})} \in \mathbb{R}^{aM}$ with elements $u_i^{(\mathrm{GS})}[m]$.

Figure 4.16 shows the generalized FDPS sequences for block length $M = 256$, maximum Doppler bandwidth $\nu_{\mathrm{Dmax}} = 3.9 \cdot 10^{-3}$, approximation factor $a = 2$, and $J = 30$ pilot symbols. The singular values are denoted by $\sigma_i^{(\mathrm{GS})}$. Figure 4.17 shows the square singular value spectrum corresponding to the generalized FDPS sequences in Figure 4.16.

The rank of $\boldsymbol{\mathcal{C}}$ defines the upper limit for the dimension of the generalized finite Slepian basis expansion

$$D' \leq D^{(\mathrm{GS})} \leq \min(2a\lceil \nu_{\mathrm{Dmax}} M \rceil + 1, M)$$

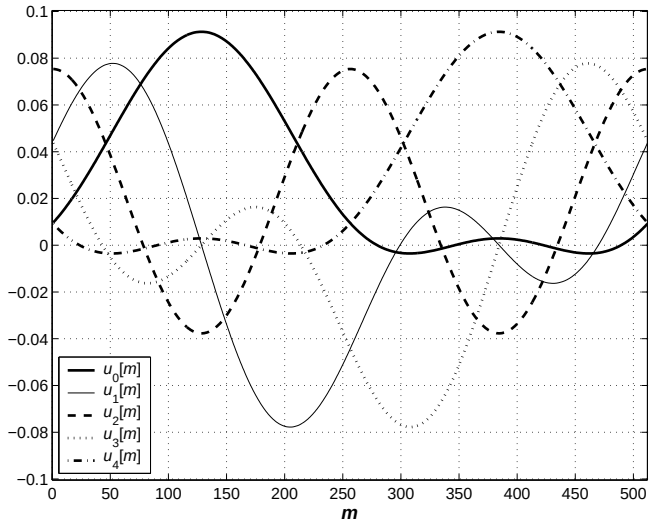

Figure 4.16: Generalized FDPS sequences $u_i^{(\mathrm{GS})}[m]$ for block length $M = 256$, approximation factor $a = 2$, maximum Doppler bandwidth $\nu_{\mathrm{Dmax}} = 3.9 \cdot 10^{-3}$, and $J = 30$ pilot symbols.

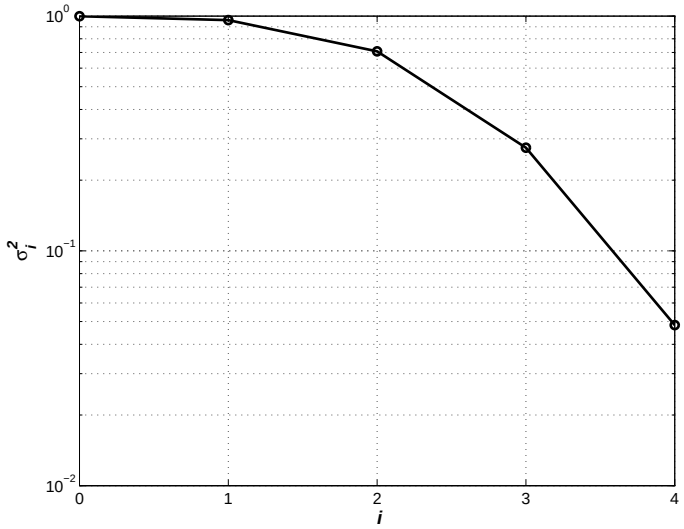

Figure 4.17: Square singular value spectrum ${\sigma_i^{(\mathrm{GS})}}^2$ for the generalized FDPS sequences designed for block length $M = 256$, approximation factor $a = 2$, maximum Doppler bandwidth $\nu_{\mathrm{Dmax}} = 3.9 \cdot 10^{-3}$, and $J = 30$ pilots symbols.

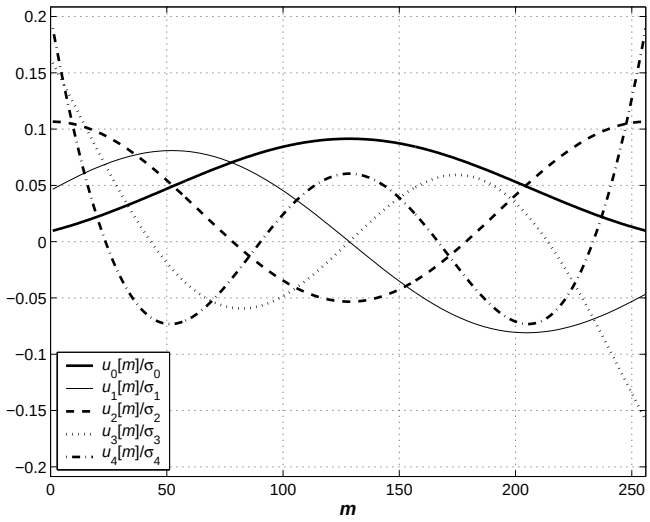

Figure 4.18: Generalized finite Slepian sequences $\frac{1}{\sigma_i^{(\mathrm{GS})}} u_i^{(\mathrm{GS})}[m]$ for block length $M = 256$, approximation factor $a = 2$, maximum normalized Doppler bandwidth $\nu_{\mathrm{Dmax}} = 3.9 \cdot 10^{-3}$, and $J = 30$ pilot symbols.

under the condition

$$\mathrm{tr}(\boldsymbol{\mathcal{B}}) \leq \mathrm{tr}(\boldsymbol{\mathcal{D}})\,, \tag{4.53}$$

which ensures identifiability of the parameters. This means there must be at least as much pilots J than dimensions of the basis expansion $D^{(\mathrm{GS})}$

$$D^{(\mathrm{GS})} \leq J\,.$$

We call the vector $\boldsymbol{u}_i^{(\mathrm{GS})} \in \mathbb{R}^M$, that is obtained by index limiting the generalized FDPS sequence $u_i^{(\mathrm{GS})}[m]$ to $\{0, \ldots, M-1\}$, the generalized finite Slepian sequence. Figure 4.18 depicts the generalized Slepian sequences $u_i^{(\mathrm{GS})}[m]$ for $i \in \{0, \ldots, 4\}$.

The sequences $u_i^{(\mathrm{GS})}[m]$ are orthonormal over the index set $\{0, \ldots, aM-1\}$

$$\sum_{m=0}^{aM-1} u_i^{(\mathrm{GS})}[m] u_\ell^{(\mathrm{GS})}[m] = \delta_{i\ell} \quad \text{for} \quad i, \ell \in \{0, \ldots, D^{(\mathrm{GS})} - 1\}\,,$$

and orthogonal over the pilot set $\mathcal{P}$

$$\sum_{m \in \mathcal{P}} u_i^{(\mathrm{GS})}[m] u_\ell^{(\mathrm{GS})}[m] = {\sigma_i^{(\mathrm{GS})}}^2 \delta_{i\ell} \quad \text{for} \quad i, \ell \in \{0, \ldots, D^{(\mathrm{GS})} - 1\}\,.$$

The generalized finite Slepian basis expansion is given by

$$h[m] \approx \tilde{h}^{(\mathrm{GS})}[m] = \sum_{i=0}^{D^{(\mathrm{GS})}-1} \gamma_i^{(\mathrm{GS})} u_i^{(\mathrm{GS})}[m] \quad \text{for} \quad m \in \{0, \ldots, M-1\}\,.$$

An estimate of parameters $\hat{\gamma}_i^{(\mathrm{GS})}$ is obtained through

$$\begin{aligned}\hat{\gamma}_i^{(\mathrm{GS})} &= \frac{1}{\sum\limits_{m\in\mathcal{P}} \left|u_i^{(\mathrm{GS})}[m]\right|^2} \sum_{m\in\mathcal{P}} y[m]p^*[m]u_i^{(\mathrm{GS})}[m] \\ &= \frac{1}{{\sigma_i^{(\mathrm{GS})}}^2} \sum_{m\in\mathcal{P}} y[m]p^*[m]u_i^{(\mathrm{GS})}[m]\,, \end{aligned} \tag{4.54}$$

where $i \in \{0,\ldots,D^{(\mathrm{GS})}-1\}$. The generalized finite Slepian sequences keep their orthogonality when multiplied with a random pilot sequences as long as $p[m]$ is from an alphabet with constant modulus

$$|p[m]| = \sqrt{E_\mathrm{S}}\,.$$

Without loss of generality we use pilot symbols with $E_\mathrm{S} = 1$. Note that

$$\sum_{m\in\mathcal{P}} \left|u_i^{(\mathrm{GS})}[m]\right|^2 = {\sigma_i^{(\mathrm{GS})}}^2$$

which is the result of the orthogonality of $u_i^{(\mathrm{GS})}[m]$ over the pilot set $\mathcal{P}$. The generalized finite Slepian sequences are *not* orthogonal over the index set $\{0,\ldots,M-1\}$, they are only time-concentrated in this set. Please note that we have designed a basis expansion for the index set $\{0,\ldots,M-1\}$ whose basis functions are not orthogonal on $\{0,\ldots,M-1\}$ but on $\mathcal{P} \subset \{0,\ldots,M-1\}$. Thus, a bandlimited sequence that is time-concentration on a given set is not forced to be orthogonal on the same set.

In conclusion, the generalized finite Slepian sequences in Figure 4.18 are bandlimited and time-concentrated, like the finite Slepian sequences, while having the new orthogonality on the pilot grid. Comparing Figure 4.18 with Figure 4.15 the difference is not directly visible. However, for pilot based channel estimation the curves in Figure 4.18 are evaluated at $J << M$ points only, in order to estimate the basis expansion coefficients γ_i (4.54). Thus, small changes become important. Figure 4.19 shows the relative difference in percent between the finite Slepian sequence $u_0^{(\mathrm{FS})}[m]$ and the generalized finite Slepian sequence $u_0^{(\mathrm{GS,J})}[m]$

$$(u_0^{(\mathrm{FS})}[m] - u_0^{(\mathrm{GS,J})}[m])/u_0^{(\mathrm{FS})}[m]$$

for $J \in \{5,\ldots,10\}$ pilot symbols. Figure 4.19 makes clear that the benefit of the generalized finite Slepian basis expansion over the Slepian basis expansion will be most visible for a small number of pilot symbols. The analysis in the next section will validate this observation.

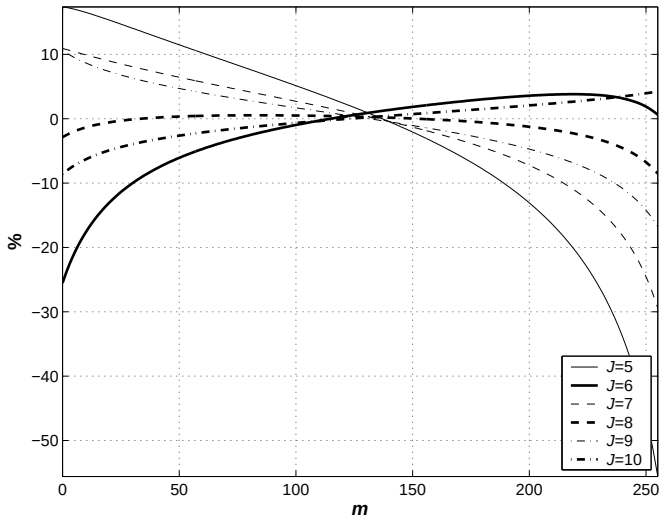

Figure 4.19: Relative difference $(u_0^{(\mathrm{FS})}[m] - u_0^{(\mathrm{GS,J})}[m])/u_0^{(\mathrm{FS})}[m]$ in percent between the finite Slepian sequence $u_0^{(\mathrm{FS})}[m]$ and the generalized finite Slepian sequence $u_0^{(\mathrm{GS,J})}[m]$ for $J \in \{5, \ldots, 10\}$ pilot symbols.

4.8 Basis Expansion Error Analysis for Pilot Based Channel Estimation

In order to demonstrate the merits of the generalized finite Slepian basis expansion and the Slepian basis expansion, we compare their performance to the Fourier basis expansion by means of simulations with the system defined in (4.6). Additionally we will compare the simulation results with analytic results that are derived in the following Section 4.8.1 and Section 4.8.2.

4.8.1 Basis Expansion Bias

We develop an analytic expression for the basis expansion bias for pilot based channel estimation extending Niedzwiecki's results [52, Sec. 6]. We use a generic notation, the results are applicable to all basis expansions presented so far.

We modify the instantaneous frequency response of a basis expansion (4.16) from Section 4.15 for the pilot based case and define

$$H(m,\nu) = \boldsymbol{f}^{\mathrm{T}}[m]\boldsymbol{G}^{-1}\sum_{\ell\in\mathcal{P}}\boldsymbol{f}^{*}[\ell]\mathrm{e}^{-\mathrm{j}2\pi\nu(m-\ell)}\,, \tag{4.55}$$

where $m \in \{0, \ldots, M-1\}$, $|\nu| < 1/2$ and the diagonal correlation matrix is defined

as

$$\boldsymbol{G} = \operatorname{diag}\left([[\boldsymbol{G}']_{0,0}, \ldots, [\boldsymbol{G}']_{D-1,D-1}]\right)$$

with

$$\boldsymbol{G}' = \sum_{\ell \in \mathcal{P}} \boldsymbol{f}[\ell]\boldsymbol{f}^{\mathrm{H}}[\ell]\,. \tag{4.56}$$

We use the diagonal matrix $\boldsymbol{G}$ because we focus on a matched-filter implementation without the need of a matrix inversion so that we can reduce complexity. If a matrix inversion is performed, $\boldsymbol{G}$ has to be replaced by $\boldsymbol{G}'$. The matched filter implementation of (4.54) is exact for the generalized finite Slepian sequences since they are orthogonal on the pilot set $\mathcal{P}$,

$$\boldsymbol{G} = \boldsymbol{G}'^{(\mathrm{GS})}\,.$$

For all other basis expansions the estimator in (4.41) results in a small performance loss.

We repeat here the square bias expressions from Section 4.5.2 for convenience

$$\operatorname{bias}^2[m] = \int_{-\frac{1}{2}}^{\frac{1}{2}} E[m,\nu] S_{hh}(\nu) \mathrm{d}\,\nu\,. \tag{4.57}$$

with the instantaneous error characteristic $E[m,\nu] = |1 - H(m,\nu)|^2$ (4.17) and

$$\operatorname{bias}_M^2 = \frac{1}{M} \sum_{m=0}^{M-1} \operatorname{bias}^2[m]\,. \tag{4.58}$$

4.8.2 Basis Expansion Variance

We define

$$\frac{E_{\mathrm{S}}}{N_0} = \frac{1}{\sigma_z^2} \tag{4.59}$$

for channel estimation purposes. Note that this definition is different from E_{b}/N_0 which we use for data detection, cf. (3.9). Based on the results from [52, Sec. 6.1.4] we can express the basis expansion estimator variance as

$$\operatorname{var}[m] \approx \sigma_z^2 \boldsymbol{f}^{\mathrm{H}}[m] \boldsymbol{G}^{-1} \boldsymbol{f}[m]\,. \tag{4.60}$$

The mean variance for the complete block of length M is given by

$$\operatorname{var}_M \approx \frac{1}{M} \sum_{m=0}^{M-1} \operatorname{var}[m] \tag{4.61}$$

Equation (4.61) becomes exact for $\text{bias}_M^2 = 0$. For the generalized finite Slepian basis expansion (4.61) simplifies to

$$\text{var}_M^{(\text{GS})} \approx \sigma_z^2 \frac{D}{J} .$$

Note that var_M increases with decreasing number of pilot symbols J.

4.8.3 Simulation Model and System Assumption

Again, we use the system parameters from Section 4.4.1. We evaluate the time-variant channel estimator for a channel with autocorrelation

$$\mathbb{E}\{h^*[m+\tilde{m}]h[m]\} = R_{hh}[\tilde{m}] = \text{J}_0(2\pi\nu_\text{D}\tilde{m}) , \tag{4.62}$$

where J_0 is the Bessel function of the first kind and zeroth order. The normalized one-sided Doppler bandwidth

$$\nu_\text{D} = \frac{v f_\text{C}}{c_0} T_\text{S} .$$

The true speed of the user is denoted by v, with $0 \leq v < 102.5\,\text{km/h}$. The related Doppler spectrum is given in (4.38). The range of the normalized Doppler bandwidth is

$$0 \leq \nu_\text{D} < \nu_\text{Dmax} = 3.9 \cdot 10^{-3} .$$

The dimension of the Fourier, the Slepian, and the generalized finite Slepian basis expansion is chosen as $D^{(\text{GS})} = D^{(\text{S})} = D^{(\text{F})} = 5$. For the generalized finite Slepian basis expansion we choose an approximation factor of $a = 2$.

The actual realizations of the time-variant channel $h[m]$ are calculated as the superposition of 20 impinging waves [93]. See Appendix A for more details.

4.8.4 Analytic Results

We evaluate (4.58) for the Jakes' spectrum (4.38) and the transmission of $J = 10$ pilots. Figure 4.20 plots the the square bias of the generalized finite Slepian basis expansion, the Slepian basis expansion and the Fourier basis expansion for $0 \leq \nu_D \leq 3.9{\cdot}10^{-3}$. The analytic results are denoted 'theor.'. The square bias of the generalized finite Slepian basis expansion is three magnitudes smaller than the square bias of the Fourier basis expansion. The square bias of the Fourier basis expansion slightly decays towards $\nu_\text{Dmax} = 3.9 \cdot 10^{-3} = 1/M = 1/256$ since this frequency coincides with the one of the Fourier basis function and thus is a local minimum. The same behavior is also visible in Figure 4.21.

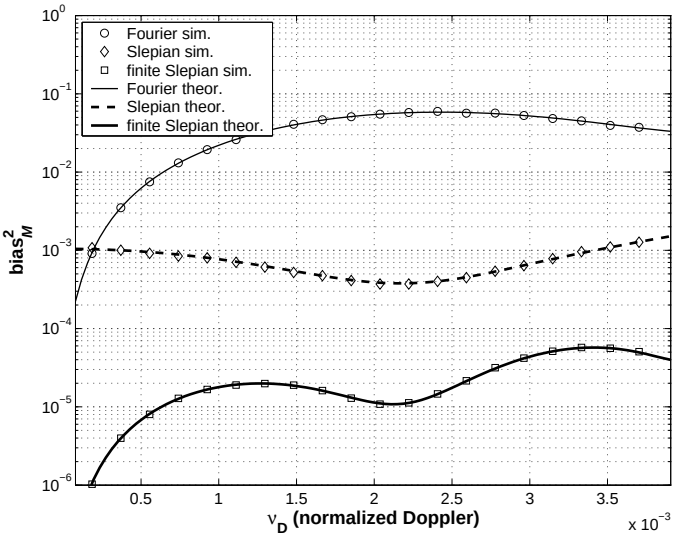

Figure 4.20: bias^2_M for the Fourier, the Slepian, and the generalized finite Slepian basis expansion with dimension $D^{(\text{GS})} = D^{(\text{S})} = D^{(\text{F})} = 5$ and $J = 10$ pilots. We vary the Doppler bandwidth in the range $0 \leq \nu_{\text{D}} \leq 3.9 \cdot 10^{-3}$.

The result in Figure 4.20 also demonstrates that the generalized finite Slepian basis expansion needs less parameters and performs better than the spline approximation investigated in [83].

Note that the generalized finite Slepian basis expansion estimator only exploits that $S_{hh}(\nu) = 0$ for $|\nu| > \nu_{\text{Dmax}}$ and does *not* require any other knowledge about the Doppler spectrum of the time-variant channel. The design parameters for our generalized finite Slepian basis expansion are ν_{Dmax}, M, and $\mathcal{P}$. We use the auto-correlation (4.62) to allow for easier comparison with other publications *only*. Real channels do *not* show a Jake's Doppler spectrum as was shown in [92]. In fact, with (4.57) we are able to evaluate the basis expansion estimator square bias for any Doppler spectrum. In order to achieve optimum performance with the generalized finite Slepian basis expansion the power spectral density has to satisfy

$$S_{hh}(\nu) = 0 \quad \text{for} \quad |\nu| > \nu_{\text{Dmax}} \,,$$

which is ensured by the physical mechanism behind the Doppler effect in a wireless channel.

4.8.5 Numerical Results

To obtain numerical results for the basis expansion square bias we set $\sigma_z = 0$ in (4.6) and perform channel estimation according to (4.54). In Figure 4.20 the Doppler

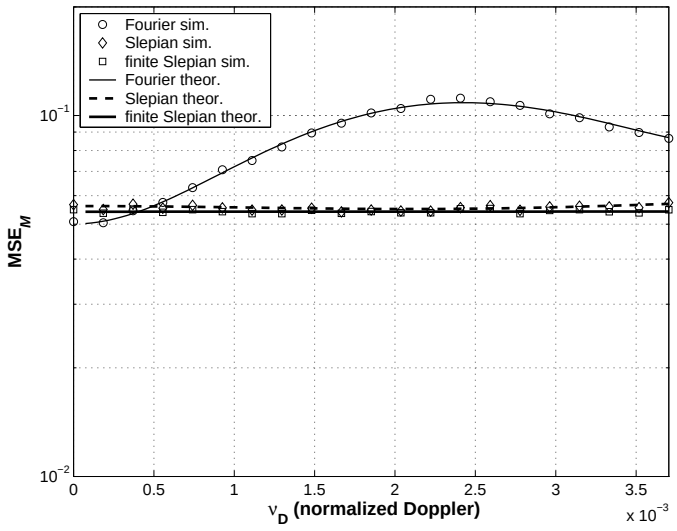

Figure 4.21: MSE_M of the basis expansion estimator with $J = 10$ pilot symbols at an $E_\mathrm{S}/N_0 = 10\,\mathrm{dB}$ for one user moving with $v = 0 \ldots 100\,\mathrm{km/h}$ corresponding to $\nu_\mathrm{D} = 0 \ldots 3.8 \cdot 10^{-3}$.

bandwidth ν_D is varied in the range $0 \leq \nu_\mathrm{D} \leq 3.9 \cdot 10^{-3}$. We plot the square bias of the Fourier, the Slepian and the generalized finite Slepian basis expansion. The results are averaged over 2000 channel realizations. We can observe a perfect match between the numerical (denoted 'sim.') and the analytical results (denoted 'theor.').

We evaluate the basis expansion estimator for a signal to noise ratio of $E_\mathrm{S}/N_0 = 10\,\mathrm{dB}$, $J = 10$ pilot symbols and $0 \leq \nu_\mathrm{D} \leq 3.8 \cdot 10^{-3}$. The simulation result in terms of MSE_M versus ν_D is given in Figure 4.21 together with the analytic results. The square bias of the Fourier basis expansion dominates the mean square error MSE_M, the distance to the generalized finite Slepian basis expansion is reduced because of the present noise level of $E_\mathrm{S}/N_0 = 10\,\mathrm{dB}$.

Figure 4.22 plots the analytic and simulation results for a varying number of pilot symbols $J \in \{5, \ldots, 15\}$ with $\nu_\mathrm{D} = 3.8 \cdot 10^{-3}$ and $E_\mathrm{S}/N_0 = 15\,\mathrm{dB}$. With an increasing number of pilots $J > 10$ the performance difference between the Slepian basis expansion and the generalized finite Slepian basis expansion vanishes. The mean square error of the Slepian basis expansions is smaller than the mean square error of the Fourier basis expansion for $J \geq 7$. The generalized finite Slepian basis expansion has the smallest mean square error down to $J = D = 5$. The difference between the analytic results and the simulations is due to the fact that (4.61) is only exact for $\mathrm{bias}_M^2 = 0$ which is less and less fulfilled for decreasing J.

Finally, we fix $J = 10$, $\nu_\mathrm{D} = 3.8 \cdot 10^{-3}$ and vary E_S/N_0 in the range of 0 to 30 dB. Figure 4.23 shows that the Fourier basis expansion is biased and its mean square

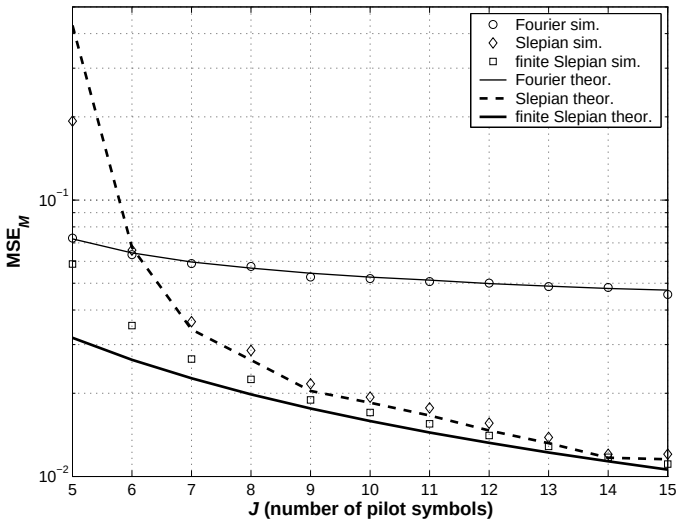

Figure 4.22: MSE_M of the basis expansion estimator with $J = 5, \ldots, 15$ pilot symbols at an $E_\mathrm{S}/N_0 = 15\,\mathrm{dB}$ for one user moving with $v = 100\,\mathrm{km/h}$ corresponding to $\nu_\mathrm{D} = 3.8 \cdot 10^{-3}$.

error saturates for increasing E_S/N_0 at $4 \cdot 10^{-2}$. The same is true for the Slepian basis expansion at a mean square error of about $2 \cdot 10^{-3}$. Only the generalized finite Slepian basis expansion is (practically) unbiased because its basis functions are designed to be orthogonal on the pilot set $\mathcal{P}$.

From this analysis it is clear that the generalized finite Slepian basis expansion offers major performance gains compared to the Fourier basis expansion. Compared to the Slepian basis expansion the performance difference is smaller. The implementation complexity of the Slepian and the generalized finite Slepian basis expansion is exactly the same. Therefore, it is *always* beneficial to use the generalized finite Slepian basis expansion for pilot-based time-variant channel estimation using a low complexity matched-filter implementation.

4.8.6 Further Comparisons and Discussion

So far, all performance results were averaged over a data block with length M. Figure 4.24 gives a comparison of $\mathrm{bias}^2[m]$ (4.57) for the Fourier, the Slepian, and the generalized finite Slepian basis expansions. The variance enhancement per symbol $\mathrm{var}[m]/\sigma_z^2$ is shown in Figure 4.25.

Comparing Figure 4.24 and Figure 4.25 it becomes clearer where the basis expansions obtain their different performance from. The square bias of the Fourier basis expansion is high at the beginning and end of the block. The square bias curves

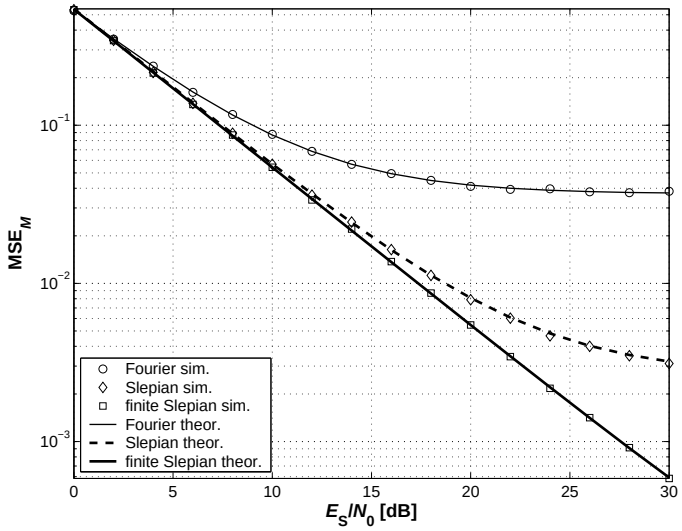

Figure 4.23: MSE_M of the basis expansion estimator for $J = 10$ pilot symbols at an $E_\mathrm{S}/N_0 = 0 \ldots 30\,\mathrm{dB}$ for one user moving with $v = 100\,\mathrm{km/h}$ corresponding to $\nu_\mathrm{D} = 3.8 \cdot 10^{-3}$.

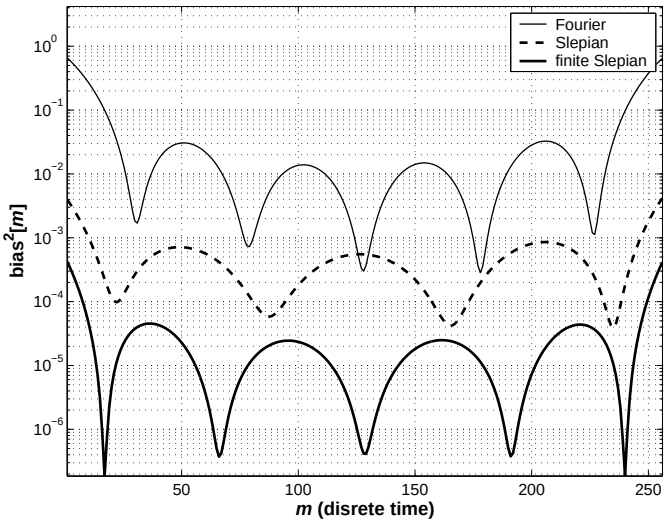

Figure 4.24: Square bias per symbol $\mathrm{bias}^2[m]$ for the Fourier, the Slepian, and the generalized finite Slepian basis expansion with $J = 10$ pilot symbols and $v = 70\,\mathrm{km/h}$.

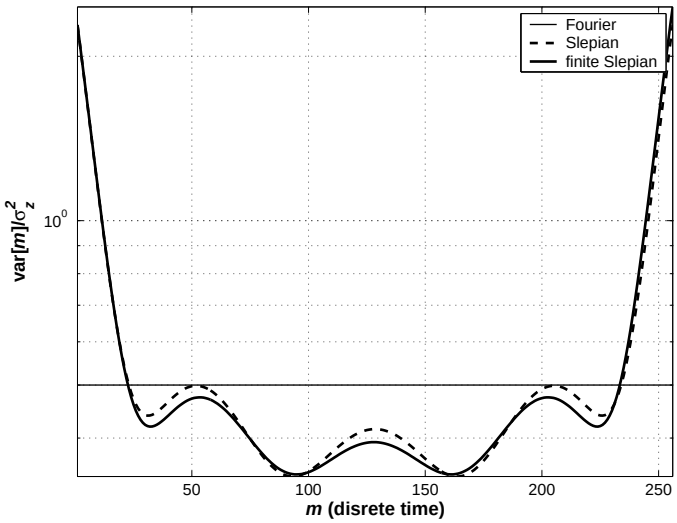

Figure 4.25: Variance multiplier per symbol $\mathrm{var}[m]/\sigma_z^2$ for the Fourier, the Slepian, and the generalized finite Slepian basis expansion with $J = 10$ pilot symbols.

for the Slepian and finite Slepian basis expansions have the same qualitative behavior towards the block boundaries. But the square bias is several magnitudes lower compared to the Fourier basis expansion. The variance multiplication of the Fourier basis expansion is constant over the block length. For the Slepian basis expansion it is largest at the boundaries of the block leading to noise enhancement. However, this effect is smaller than the square bias difference in Figure 4.24.

5 Time-Variant Frequency-Selective Channel Estimation

This chapter describes a low complexity algorithm based on a specially designed basis expansion for time-variant frequency-selective channel estimation in an MC-CDMA downlink. The presentation in this chapter will rely on the notation and the signal model from Chapter 2 for MC-CDMA. Our aim is to establish a channel estimation scheme for a *time-variant frequency-selective* channel that needs only very little knowledge of second order statistics. We will make use of the results presented in Chapter 4 for time-variant frequency-flat channel estimation.

The channel estimation is based on the assumption that the maximum temporal variation of a wireless channel is upper bounded by the maximum (one sided) normalized Doppler bandwidth (4.1)

$$\nu_{\mathrm{Dmax}} = \frac{v_{\max} f_C}{c_0} T_{\mathrm{S}} \,,$$

which is determined by the maximum (supported) velocity $v_{\max}$, the carrier frequency f_{C} and the symbol duration T_{S}.

OFDM transforms the time-variant frequency-selective channel into a set of time-variant frequency-flat subcarriers. We deal with time-variant channels that vary significantly over the duration of a long block of OFDM symbols. However, for the duration of each single OFDM symbol the channel variation is small enough to be neglected. This implies, in other words, a very small inter-carrier interference.

Under the assumption of small inter-carrier interference each time-variant frequency-flat channel (corresponding to each subcarrier) is fully described through a sequence of complex scalars at the OFDM symbol rate $1/T_{\mathrm{S}}$. This sequence is bandlimited by ν_{Dmax}. In order to perform coherent multi-user detection we need to estimate a time limited snapshot of this bandlimited sequence at the receiver side. The length of this snapshot is equal to the length of a data block consisting of OFDM data symbols with interleaved OFDM pilot symbols.

We apply the *generalized finite Slepian basis expansion on a per-subcarrier basis* to estimate the time-variant frequency-selective channel in the MC-CDMA downlink.

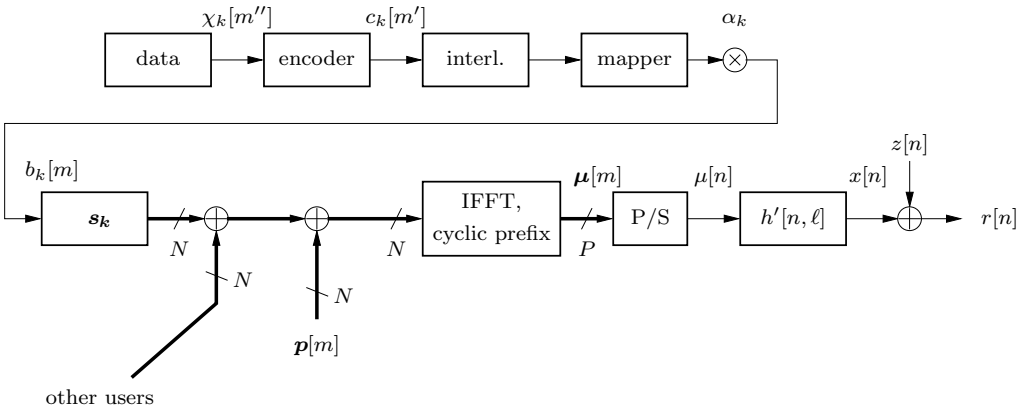

Figure 5.1: Model for the MC-CDMA transmitter in the time-variant downlink.

5.1 Signal Model

We reuse the signal model (2.19) and modify it for the time-variant downlink. This means that all K user signals are transmitted over the *same* time-variant channel. Figure 5.1 depicts the downlink transmitter schematically.

In order to accommodate for time-variant channel estimation the $M - J$ data symbols are distributed over a block of length M allowing for the insertion of J pilot symbols. Thus, the data symbols satisfy

$$b_k[m] \in \{\pm 1 \pm \mathrm{j}\}/\sqrt{2} \quad \text{for} \quad m \notin \mathcal{P} \tag{5.1}$$

and

$$b_k[m] = 0 \quad \text{for} \quad m \in \mathcal{P}\,, \tag{5.2}$$

where the pilot placement is defined through the index set (4.40) which we repeat here for convenience

$$\mathcal{P} = \left\{ \left\lfloor i\frac{M}{J} + \frac{M}{2J} \right\rfloor \;\middle|\; i \in \{0, \ldots, J-1\} \right\}. \tag{5.3}$$

Figure 4.14 shows an example for the pilot placement defined by the pilot set $\mathcal{P}$.

We ignore the effects of path loss and shadow fading,

$$\alpha_k = 1 \quad \text{for} \quad k \in \{1, \ldots, K\}$$

and a perfect power control is assumed. As shown in Figure 5.1, the spread signals of all users are summed up and common pilot symbols $\boldsymbol{p}[m] \in \mathbb{C}^N$ with elements $p[m, q]$ are added

$$\boldsymbol{d}[m] = \boldsymbol{S}\boldsymbol{b}[m] + \boldsymbol{p}[m]\,. \tag{5.4}$$

The elements of the pilot symbol vector $p[m,q]$ for $m \in \mathcal{P}$ and $q \in \{0,\ldots,N-1\}$ are independent identically distributed (i.i.d.) chosen with equal probability from the scaled QPSK symbol set $K\{\pm 1 \pm \mathrm{j}\}/\sqrt{2N}$, otherwise

$$\boldsymbol{p}[m] = \mathbf{0}_N \quad \text{for} \quad m \notin \mathcal{P}\,.$$

By scaling the pilot symbols with the number of users K the energy in the OFDM data-symbols and OFDM pilot-symbols is kept equal.

After OFDM and cyclic prefix insertion we write the chip-vector as

$$\boldsymbol{\mu}[m] = \boldsymbol{T}_{\mathrm{CP}}\boldsymbol{F}_N^{\mathrm{H}}\boldsymbol{d}[m]\,.$$

Then a parallel-serial conversion is performed according to

$$\boldsymbol{\mu}[m] = \begin{bmatrix} \mu[mP] \\ \mu[mP+1] \\ \vdots \\ \mu[mP+P-1] \end{bmatrix}$$

and the chip-stream $\mu[n]$ with chip rate $1/T_{\mathrm{C}} = P/T_{\mathrm{S}}$ is transmitted over a time-variant frequency-selective channel.

The transmit filter, the time-variant channel and the matched receive filter together are represented by $h(t,\tau)$ (4.4). Please refer to Section 2.1 and Section 4.2 for a more detailed background on channel modelling. We denote the chip-rate sampled time-variant impulse response by

$$h'[n,\ell] = h(nT_{\mathrm{C}}, \ell T_{\mathrm{C}})\,.$$

A time-variant channel impulse response generally introduces inter-carrier interference in an OFDM system. However, if the channel variation in time, measured by the normalized Doppler bandwidth, stays below a certain threshold, the inter-carrier interference is small enough to be neglected for the receiver side processing [43]. This condition is fulfilled if the one-sided normalized Doppler bandwidth ν_D is much smaller than the normalized subcarrier bandwidth P/N,

$$\frac{\nu_D N}{P} < 0.01\,. \tag{5.5}$$

In other words the DFT is still applicable [48] although the channel is time-variant. Equation (5.5) is a stronger condition than the more general underspread property [38] which means that the product of Doppler bandwidth and delay spread is smaller than unity

$$\nu_{\mathrm{D}} L_{\mathrm{D}} < 1\,. \tag{5.6}$$

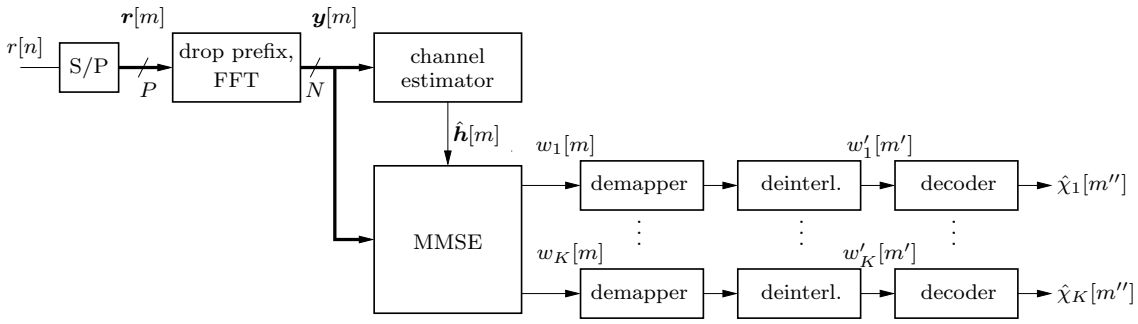

Figure 5.2: Model for the MC-CDMA receiver with channel estimation and time-variant MMSE filter.

We are able to treat the time-variant channel as constant for the duration of each single OFDM symbol if (5.5) is fulfilled. Hence,

$$h[m, \ell] = h'[mP, \ell]\,,$$

respectively

$$\boldsymbol{h}[m] = \begin{bmatrix} h[m,0] \\ \vdots \\ h[m, L-1] \end{bmatrix} \in \mathbb{C}^{L\times 1}$$

in vector notation. The time-variant frequency response $\boldsymbol{g}[m] \in \mathbb{C}^N$ with elements $g[m, q]$ is defined as the DFT of the time-variant impulse response,

$$\boldsymbol{g}[m] = \sqrt{N}\boldsymbol{F}_{N\times L}\boldsymbol{h}[m]\,.$$

The receiver removes the cyclic prefix and performs a DFT. The received signal vector $\boldsymbol{y}[m] \in \mathbb{C}^N$ after these two operations is given by

$$\boldsymbol{y}[m] = \operatorname{diag}(\boldsymbol{g}[m])\,(\boldsymbol{S}\boldsymbol{b}[m] + \boldsymbol{p}[m]) + \boldsymbol{z}[m]\,, \tag{5.7}$$

where complex additive white Gaussian noise with zero mean and covariance $\sigma_z^2\boldsymbol{I}_N$ is denoted by $\boldsymbol{z}[m] \in \mathbb{C}^N$ with elements $z[m, q]$ for $q \in \{0, \ldots, N-1\}$.

5.2 Time-Variant Multi-User Detector

Figure 5.2 shows the schematic structure of the downlink receiver. In contrast to the receiver presented in Section 2.6 for the uplink, we do not use an iterative structure for the downlink. The main reason for this approach is the fact that, in the downlink, all users share the same channel. This allows to obtain much better initial channel

estimates from the pilots alone. Based on these good channel estimates the multi-user detection performance of the linear MMSE filter is sufficient already after the first iteration too. Another key issue for the downlink processing is the space and battery limitation in the mobile handset.

The linear MMSE receiver detects the data using the received vector $\boldsymbol{y}[m]$, the spreading matrix $\boldsymbol{S}$ and the time-variant frequency response $\boldsymbol{g}[m]$ which is assumed to be known for the moment. We define the time-variant effective spreading sequences

$$\tilde{\boldsymbol{s}}_k[m] = \mathrm{diag}\left(\boldsymbol{g}[m]\right)\boldsymbol{s}_k\,, \tag{5.8}$$

and the time-variant effective spreading matrix

$$\tilde{\boldsymbol{S}}[m] = [\tilde{\boldsymbol{s}}_1[m], \ldots, \tilde{\boldsymbol{s}}_K[m]] \in \mathbb{C}^{N\times K}\,,$$

to express the unbiased time-variant linear MMSE filter (cf. (2.29) for the block-fading case).

$$\boldsymbol{f}_k^{\mathrm{H}}[m] = \frac{\tilde{\boldsymbol{s}}_k^{\mathrm{H}}[m](\sigma_z^2\boldsymbol{I}_N + \tilde{\boldsymbol{S}}[m]\tilde{\boldsymbol{S}}^{\mathrm{H}}[m])^{-1}}{\tilde{\boldsymbol{s}}_k^{\mathrm{H}}[m](\sigma_z^2\boldsymbol{I} + \tilde{\boldsymbol{S}}[m]\tilde{\boldsymbol{S}}^{\mathrm{H}}[m])^{-1}\tilde{\boldsymbol{s}}_k[m]}\,. \tag{5.9}$$

The code symbol estimates are given by

$$w_k[m] = \boldsymbol{f}_k^{\mathrm{H}}[m]\boldsymbol{y}[m]\,.$$

After demapping and deinterleaving, the code bit estimates are supplied to the decoder. After the decoder a hard decision is performed to obtain the transmitted data bits $\hat{\chi}_k[m']$.

Please note, that the unbiased linear MMSE filter (5.9) leads to some noise enhancement since the channel energy

$$\|\boldsymbol{h}[m]\|^2 = \|\boldsymbol{g}[m]\|^2/N$$

varies over the duration of a data block.

5.3 Time-Variant Channel Estimator

The performance of the receiver crucially depends on the accurate channel estimates for the time-variant frequency response $\boldsymbol{g}[m]$. The MC-CDMA signal model describes a transmission which takes place over N parallel frequency-flat channels. In order to reflect this we rewrite (5.7) as a set of equations for every subcarrier $q \in \{0, \ldots, N-1\}$,

$$y[m,q] = g[m,q]d[m,q] + z[m,q]\,. \tag{5.10}$$

where $d[m,q]$ are the elements of $\boldsymbol{d}[m]$ (5.4). Comparing (5.10) with (4.6) we see that the structure of these equations is identical. The band-limited property of $h[m,n]$ directly applies to $g[m,q]$ too. This allows to estimate the time-variant frequency-flat subcarrier $g[m,q]$ with the generalized Slepian basis expansion (4.54). We define

$$\hat{\psi}_i[q] = \frac{1}{\sum\limits_{m\in\mathcal{P}} |u_i[m]p[m,q]|^2} \sum_{m\in\mathcal{P}} y[m,q]p^*[m,q]u_i^*[m]\,,$$

where $i \in \{0,\ldots,D-1\}$ and $q \in \{0,\ldots,N-1\}$. Although we will use the generalized Slepian basis expansion, we keep the notation regarding the basis expansion generic. Hence, any basis expansion defined in Chapter 4 can be used for performance comparison.

The estimated time-variant frequency response is given by

$$\hat{g}'[m,q] = \sum_{i=0}^{D-1} u_i[m]\hat{\psi}_i[q]\,.$$

Further noise suppression is obtained if we exploit the correlation between the subcarriers

$$\hat{\boldsymbol{g}}[m] = \boldsymbol{F}_{N\times L}\boldsymbol{F}_{N\times L}^{\mathrm{H}}\hat{\boldsymbol{g}}'[m]\,.$$

Finally, the channel estimates $\hat{\boldsymbol{g}}[m]$ are inserted into (5.8) and multi-user detection can be performed.

5.4 Simulation Results

The realizations of the time-variant frequency-selective channel $h'[n,\ell]$, sampled at the chip-rate $1/T_{\mathrm{C}}$, are generated using an exponentially decaying power-delay profile $\eta^2[\ell]$ defined in (2.4) and the simulation parameters from Section 3.1.1. These are: Number of subcarriers $N = 64$, block length $M = 256$, essential support of the channel impulse response $L = 15$. The discrete time indices n and ℓ denote sampling at rate $1/T_{\mathrm{C}} = 3.84\cdot 10^6\,\mathrm{s}^{-1}$. The exponential decaying power-delay profile corresponds to a normalized delay spread $L_{\mathrm{D}} = T_{\mathrm{D}}/T_{\mathrm{C}} = 1$. The autocorrelation for every channel tap is given by

$$R_{h'h'}[\tilde{n},\ell] = \eta^2[\ell]J_0(2\pi\nu_D P\tilde{n})$$

which results in the classical Jakes' spectrum. We use the enhanced simulation model (A.1) for every channel tap $l \in \{0,\ldots,L-1\}$. The simulation uses a chip-rate sampled time-variant channel, thus any possible effect from residual inter-carrier interference would be visible in the simulation results.

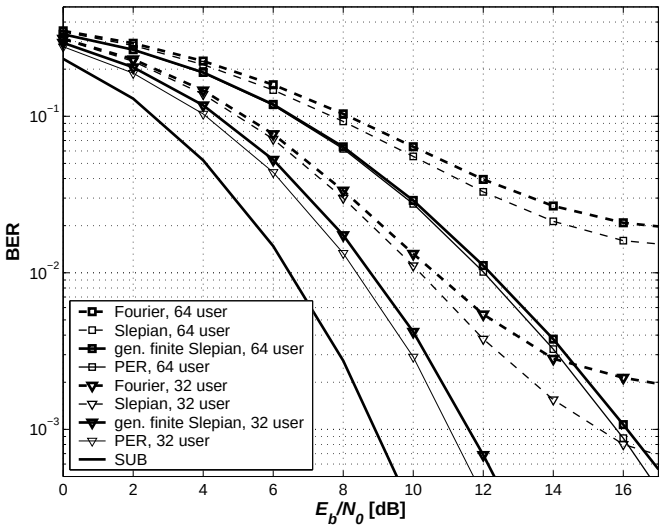

Figure 5.3: Downlink MC-CDMA receiver performance in terms of BER versus E_b/N_0. We compare the generalized finite Slepian basis expansion, the Slepian basis expansion and the Fourier basis expansion, all using $D = 5$ basis functions. The $K \in \{32, 64\}$ users are moving with $v = 70\,\mathrm{km/h}$ and the lowest amount of pilots possible $J = D = 5$ is used. For reference the single-user bound (SUB) and the performance with perfect channel knowledge (PER) are shown.

The system operates at carrier frequency $f_\mathrm{C} = 2\,\mathrm{GHz}$, the users move with velocity $v = 70\,\mathrm{km/h}$, resulting in $B_D = 126\,\mathrm{Hz}$ and $\nu_\mathrm{D} = 0.0026$. The system is designed for $v_\mathrm{max} = 102.5\,\mathrm{km/h}$ which corresponds to $D' = 3$. The generalized finite Slepian basis expansion uses $a = 2$ and $D^{(\mathrm{GS})} = 5$. The Fourier basis expansion and the Slepian basis expansion, both applied for performance comparison, use the same dimensionality $D^{(\mathrm{F})} = D^{(\mathrm{S})} = 5$. We evaluate the performance of the generalized finite Slepian basis expansion channel estimation with the lowest number of pilots possible $J = 5 = D$. Thus, we have as many pilots as basis functions in the basis expansion. The pilot ratio J/M is 2%, which is valid for both the number of pilots and the pilot energy.

In Figure 5.3 we illustrate the downlink MC-CDMA receiver performance with $K \in \{32, 64\}$ users in terms of bit error rate versus E_b/N_0. Additionally, the plot also shows the single-user bound. The results are obtained by averaging over 400 independent channel realizations.

In order to relate the E_b/N_0 values in Figure 5.3 to the channel estimation per-

formance results in Section 4.3 we establish the relation

$$\frac{E_\mathrm{S}}{N_0} = \frac{K^2}{P}\frac{M-J}{M}\frac{E_\mathrm{b}}{N_0} \tag{5.11}$$

where we took the higher pilot energy in the downlink into account. The simulation in Figure 5.3 for $0\,\mathrm{dB} \leq E_\mathrm{b}/N_0 \leq 16\,\mathrm{dB}$ and $K = 32$ users corresponds to E_S/N_0 values in the range $11\,\mathrm{dB} \leq E_\mathrm{S}/N_0 \leq 27\,\mathrm{dB}$. For $K = 64$ users the range is from $17\,\mathrm{dB} \leq E_\mathrm{S}/N_0 \leq 33\,\mathrm{dB}$.

Taking (5.11) into account when referring to Figure 4.23 makes clear, that the drastically smaller MSE_M of the generalized finite Slepian basis expansion than of the Fourier basis expansion leads to a pronounced reduction in bit error rates. This is because, the Fourier basis expansion is biased as is visible for higher E_S/N_0 values in Figure 4.23 which leads to an error floor in Figure 5.3.

Figure 5.3 also shows the receiver performance when using the Slepian basis expansion. As can be seen in Figure 4.22 and as is explained in Section 4.5 the Slepian basis expansion performance degrades because of lost orthogonality due to the pilot grid. At the limit $J = D$ the Slepian basis expansion is hardly better than the Fourier basis expansion. However, this picture changes rapidly with increasing number of pilots. At $J > 10$ pilots the performance of the Slepian basis expansion is practically equivalent to the one of the generalized finite Slepian basis expansion, as is shown in Figure 4.22.

We also plot the receiver performance for a perfectly known channel (denoted 'PER') in Figure 5.3, and we can see that the performance advantage of the generalized finite Slepian basis expansion is strongest at the lowest amount of pilots possible $J = D = 5$. The receiver performance is extremely close to the one with perfect channel knowledge.

5.5 Doppler Diversity in MC-CDMA

In MC-CDMA a data symbol is spread by a user specific spreading code in order to take advantage of multipath diversity V_M. A time-variant channel additionally offers Doppler diversity V_D which can be used in MC-CDMA by convolutional coding and random interleaving [57]. The intuitive reason for Doppler diversity, respectively time diversity, is simply the fact that the fading condition of the channel changes over time. The faster the channel changes the shorter is the duration of a bad channel realization.

However, accurate time-variant channel state information is required at the receiver side so that both sources of diversity can be exploited. The overall diversity of the channel is given by [34]

$$V = V_\mathrm{M} V_\mathrm{D}\,. \tag{5.12}$$

The Doppler diversity depends on the length of the data block the Doppler spectrum and the applied coding scheme. In the next section we derive a measure for the Doppler diversity that an MC-CDMA receiver is able to take advantage of. This measure is validated by means of simulation results.

5.5.1 Diversity Measure

In the literature [34] it has been proposed to measure the Doppler diversity V_{D} of a channel by the product of block length and normalized Doppler bandwidth

$$V_{\mathrm{D}} \approx M \frac{16\pi\nu_{\mathrm{D}}}{9}\,. \tag{5.13}$$

It is obvious that the shape of the Doppler power spectral density $S_{gg}(\nu)$ may have an impact on V_{D} as well. For example the Doppler spectrum caused by the propagation of a single planar wave has the form $S_1(\nu) = \delta(\nu - \nu_{\mathrm{D}})$. Evidently, such a channel will have a lower Doppler diversity than a rich multipath channel in an indoor scenario with three dimensional scattering which typically results in a rectangular Doppler spectrum.

We can interpret a time-variant frequency-flat Rayleigh fading channel $g[m]$ (respectively a subcarrier in an OFDM system) as a stationary Gaussian stochastic process with corresponding power density spectrum $S_{gg}(\nu)$. Its entropy rate is defined as [36]

$$h(S_{gg}) = \log 2\pi\mathrm{e} + \int_{-\frac{1}{2}}^{\frac{1}{2}} \log(S_{gg}(\nu))\mathrm{d}\,\nu\,. \tag{5.14}$$

However, a typical wireless channel is over-sampled with respect to the Doppler bandwidth. This is why the support of $S_{gg}(\nu)$ is much smaller than $[-1/2, +1/2]$ and $S_{gg}(\nu) \equiv 0$ for $\nu_{\mathrm{D}} < |\nu| < 1/2$ which leads to an ill defined entropy rate $h(S_{gg}) = -\infty$ [40] [10, Sec. 4.5]. This fact is the motivation to look for other diversity measures.

A diversity measure for flat-fading multiple-input multiple-output (MIMO) channels was defined in [31]. We will show the applicability of the diversity measure from [31] for time-variant flat-fading single-input single-output channels.

5.5.2 Flat-Fading Multiple-Input Multiple-Output (MIMO) Channel

A flat-fading MIMO channel is described through a matrix $\boldsymbol{H} \in \mathbb{C}^{N_{\mathrm{R}} \times N_{\mathrm{T}}}$ where N_{T} denotes the number of transmit antennas and N_{R} the number of receive antennas. The elements $[\boldsymbol{H}]_{r,t}$ describe the fading coefficient between transmit antenna t and

receive antenna r. We assume that every element $[\boldsymbol{H}]_{r,t}$ is complex, circularly symmetric, zero mean, and Gaussian distributed which leads to Rayleigh fading. The covariance matrix of the MIMO channel is defined as

$$\boldsymbol{R}_{\boldsymbol{H}} = \mathbb{E}\left\{\mathrm{vec}(\boldsymbol{H})\left(\mathrm{vec}(\boldsymbol{H})\right)^{\mathrm{H}}\right\} \tag{5.15}$$

where the operator $\mathrm{vec}(\boldsymbol{H})$ stacks all columns of $\boldsymbol{H}$. The diversity measure of the MIMO channel $\boldsymbol{H}$, given the correlation matrix $\boldsymbol{R}_{\boldsymbol{H}}$, is defined in [31] as

$$\Psi(\boldsymbol{R}_{\boldsymbol{H}}) = \left(\frac{\mathrm{tr}(\boldsymbol{R}_{\boldsymbol{H}})}{\|\boldsymbol{R}_{\boldsymbol{H}}\|_{\mathrm{F}}}\right)^2 . \tag{5.16}$$

In the following section we will show how this measure for a flat-fading MIMO channel can be applied to a time-variant flat-fading single-input single-output channel.

5.5.3 Time-Variant Flat-Fading Single-Input Single-Output Channel

In the case of a time-variant frequency-flat subcarrier q we can stack the channel coefficients $g[m,q]$ in the vector

$$\boldsymbol{g}_q = \begin{bmatrix} g[0,q] \\ \vdots \\ g[M-1,q] \end{bmatrix} \in \mathbb{C}^M ,$$

for the duration of one data block. We define the covariance matrix of $\boldsymbol{g}_q$ as

$$\boldsymbol{R}_{gg} = \mathbb{E}\{\boldsymbol{g}_q \boldsymbol{g}_q^{\mathrm{H}}\} \in \mathbb{C}^{M\times M}$$

which is independent of subcarrier q if we assume the same Doppler spectrum for every channel tap.

The elements of $g[m,q]$ fulfill the same statistic properties as the elements of the MIMO channel matrix $[\boldsymbol{H}]_{r,t}$. This is why we are able to insert $\boldsymbol{R}_{gg}$ into (5.16) in order to define the *diversity measure for a time-variant frequency-flat subcarrier* as

$$\Psi(\boldsymbol{R}_{gg}) = \left(\frac{\mathrm{tr}(\boldsymbol{R}_{\boldsymbol{gg}})}{\|\boldsymbol{R}_{\boldsymbol{gg}}\|_{\mathrm{F}}}\right)^2 . \tag{5.17}$$

We can express (5.17) through the eigenvalues of matrix $\boldsymbol{R}_{gg}$. The trace of an $M \times M$ matrix in terms of its eigenvalues is given by

$$\mathrm{tr}(\boldsymbol{R}_{\boldsymbol{gg}}) = \sum_{i=0}^{M-1} \lambda_i . \tag{5.18}$$

An equivalent expression for the Frobenius norm is found through

$$\|\boldsymbol{R}_{\boldsymbol{gg}}\|_{\mathrm{F}} = \sqrt{\sum_{i=0}^{M-1} \lambda_i^2}\,. \tag{5.19}$$

Inserting (5.18) and (5.19) into (5.17) results in

$$\Psi(\boldsymbol{R}_{\boldsymbol{gg}}) = \left(\frac{\sum_{i=0}^{M-1} \lambda_i}{\sqrt{\sum_{i=0}^{M-1} \lambda_i^2}} \right)^2 . \tag{5.20}$$

This diversity measure has the property

$$1 \leq \Psi(\boldsymbol{R}_{gg}) \leq M\,. \tag{5.21}$$

The lower bound is reached for a constant (block fading) channel $\boldsymbol{g} = g\mathbf{1}_M$ which gives a covariance matrix $\boldsymbol{R}_{gg} = \sigma_g^2 \mathbf{1}_{M\times M}$. Inserting $\boldsymbol{R}_{gg}$ in (5.17) we see that $\Psi = 1$. The upper bound is is reached if the channel coefficients are uncorrelated for a block of length M.

We have evidence that $V_{\mathrm{D}} = \Psi(\boldsymbol{R}_{gg})$ but no final proof, thus we continue to use two different symbols.

5.5.4 Maximum Diversity for a Given Doppler Bandwidth

We assume that every subcarrier has a rectangular Doppler power density spectrum

$$S_{gg}(\nu) = \begin{cases} \frac{1}{2\nu_{\mathrm{D}}} & \text{for } |\nu| < \nu_{\mathrm{D}}\,, \\ 0 & \text{otherwise.} \end{cases} \tag{5.22}$$

With this assumption we are able to apply the knowledge about the asymptotic behavior of the eigenvalues from the DPS sequence theory in order to obtain closed form results.

The covariance matrix per subcarrier is given by

$$\boldsymbol{R}_{gg} = 1/(2\nu_{\mathrm{D}})\boldsymbol{C}_{gg}\,,$$

where $\boldsymbol{C}_{gg}$ is similar to the defining matrix for the DPS sequences (see Section 4.5) with elements

$$[\boldsymbol{C}_{gg}]_{i,\ell} = \frac{\sin\left[2\pi(i-\ell)\nu_{\mathrm{D}}\right]}{\pi(i-\ell)}\,.$$

We know that the eigenvalues λ_i of matrix $\boldsymbol{C}_{gg}$ rapidly drop to zero for

$$i > \lceil 2\nu_{\mathrm{D}} M \rceil + 1\,.$$

Thus, we can give an analytic upper bound for the Doppler diversity measure

$$\Psi(\boldsymbol{R}_{gg}) \leq \lceil 2\nu_{\mathrm{D}} M \rceil + 1\,. \tag{5.23}$$

For $\nu_{\mathrm{D}} M = c$ and $M \to \infty$ Equation (5.23) becomes a tight bound, since $\lambda_i = 1$ for $i \leq \lceil 2\nu_{\mathrm{D}} M \rceil$ and $\lambda_i = 0$ for $i > \lceil 2\nu_{\mathrm{D}} M \rceil$ [69] [24, Sec. 5.2]. For arbitrary Doppler power density spectra with support $[-\nu_{\mathrm{D}}, \nu_{\mathrm{D}}]$ (5.23) is an upper bound.

Definition (5.23) gives a rigorous formulation of the observations made in [47] where the Fourier basis expansion [60] was used.

5.5.5 Simulation Results

Using the same system parameters as defined in Section 5.4 we simulate a system with $K = 32$ users moving with velocity $v \in \{0, 50, 100\}\,\mathrm{km/h}$ which gives $B_{\mathrm{D}} \in \{0, 93, 185\}\,\mathrm{Hz}$ and $\nu_{\mathrm{D}} \in \{0, 1.9 \cdot 10^{-3}, 3.8 \cdot 10^{-3}\}$. We use $J = 10$ OFDM pilot symbols. The system is designed for $v_{\max} = 102.5\,\mathrm{km/h}$ which results in a signal space dimension of $D' = 3$. We choose an approximation factor $a = 2$ and a basis expansion dimension $D^{(\mathrm{GS})} = 5$ for the generalized finite Slepian basis expansion. The results are obtained by averaging over 2000 independent channel realizations.

In Figure 5.4 we illustrate the downlink MC-CDMA receiver performance in terms of bit error rate versus E_{b}/N_0. With increasing velocity the receiver performs better because the Doppler diversity V_{D} increases too. For velocities in the range $0 < v < 100\mathrm{km/h}$ the Doppler diversity measure (5.23) is in the range $1 < \Psi < 3$ predicting a similar Doppler diversity V_{D}. In the following we will analyze to which extend our receiver algorithm is able to take advantage of the predicted Doppler diversity.

The *diversity* V is defined as the slope of the bit error rate versus E_{b}/N_0 curve in log-log scale. The power-delay profile defining the multipath diversity V_{M} is kept constant in this simulation. For velocity $v = 0\,\mathrm{km/h}$, the Doppler diversity $V_{\mathrm{D}} = 1 = \Psi$, which follows from the multiplicative assumption in (5.12) and the bound (5.21). This allows to calculate the additional Doppler diversity that the MC-CDMA receiver is able to exploit as

$$V_{\mathrm{D}}(v) = V(v)/V(0).$$

where v denotes the users velocity.

Figure 5.5 plots the Doppler diversity V_{D} versus E_{b}/N_0 for velocity $v \in \{50, 100\}\mathrm{km/h}$ and a single user $K = 1$. For the simulations Jakes' spectrum was used, for which the diversity measure (5.17) predicts a Doppler diversity of $\Psi(50\mathrm{km/h}) = 1.7$ and $\Psi(100\mathrm{km/h}) = 2.8$. The obtained Doppler diversity V_{D} as depicted in Figure 5.5 is clearly much smaller. The reason may be that the selected transmission and coding scheme does not allow to exploit all diversity. The slight

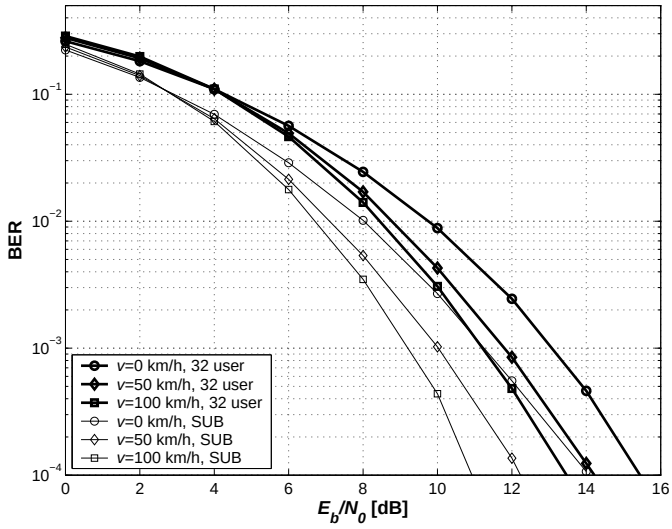

Figure 5.4: Downlink MC-CDMA receiver performance in terms of bit-error rate (BER) versus E_b/N_0 for $K = 32$ users moving with $v \in \{0, 50, 100\}$ km/h. For reference the single-user bounds (SUB) are shown too.

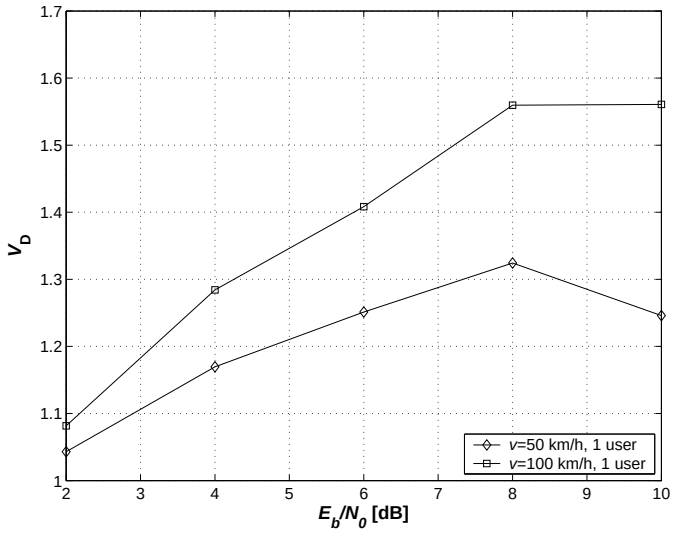

Figure 5.5: Doppler diversity V_D exploited by the MC-CDMA system. The diversity $V = V_\mathrm{D}V_\mathrm{M}$ (5.12) is defined as the slope of the bit-error rate versus E_b/N_0 curve in Figure 5.4.

decay at higher E_b/N_0 values might be due to the bias of the applied time-variant channel estimation method.

The block-interleaving described in Section 3.3 for block-fading channels results in a similar diversity increase as the one obtained through Doppler diversity in the time-variant case.

6 Iterative Multi-User Detection and Time-Variant Channel Estimation

This chapter deals with iterative time-variant channel estimation and multi-user detection for the uplink of an MC-CDMA system. In iterative receivers the soft information gained about the transmitted data symbols is used to enhance the channel estimation and data detection in consecutive iterations. Iterative multi-user detection and channel estimation for an MC-CDMA uplink was shown in Chapter 3 to achieve the single-user bound under high load for a block-fading channel. However, if users are moving at vehicular speed the wireless channel coefficients vary significantly over the duration of a single data block. In this chapter we extend the concept of iterative detection and channel estimation to the time-variant case.

Our results will challenge the reasoning in [5, 72] where a comparison between different combinations of OFDM and DS-CDMA for cellular communication systems is given. It is stated that MC-CDMA is best suited for the downlink. For the uplink MC/DS-CDMA is favored which uses time domain spreading in parallel carriers with rather large bandwidth per carrier. In [5, 72] MC-CDMA is deprecated for the uplink mainly because the orthogonality of the spreading sequences is destroyed due to the frequency selective channel. This leads to bad performance for a matched filter receiver. Furthermore, it is stated that the channel estimation does not perform well for MC-CDMA.

The results of this chapter will show that MC-CDMA is an *excellent* choice for the uplink which allows to exploit both, multipath and Doppler diversity. The basic prerequisite is iterative multi-user detection. By applying this technique the orthogonality of the spreading codes is no necessity any more. Thus, the diversity of the frequency selective channel can be exploited without drawbacks. However, the enhanced performance obtained by multi-user detection does not come at no cost. The computational complexity is increased since a matrix inversion needs to be performed. Our results are applicable to an isolated-cell scenario since no scrambling code is applied.

Accurate channel estimates are mandatory for iterative multi-user detection algorithms. In the following sections we use the iterative multi-user receiver structure to

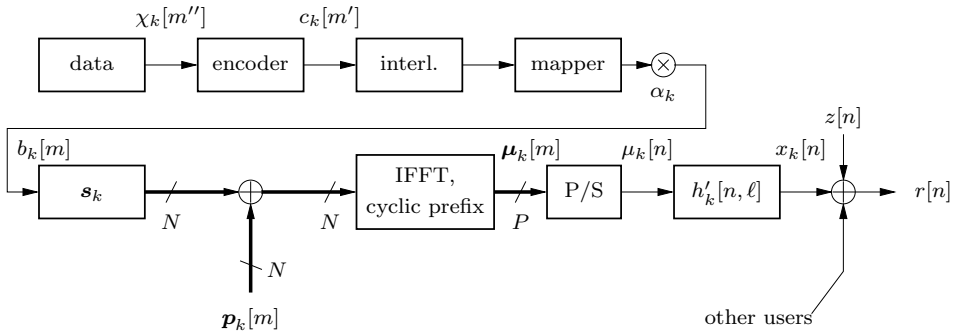

Figure 6.1: Model for the MC-CDMA transmitter and the channel in the uplink.

design a new iterative time-variant channel estimation scheme. This iterative time-variant channel estimation scheme uses the feedback soft symbols, that are derived from the output of the soft-in soft-out decoder, in order to enhance the channel estimates. The channel estimation itself is performed individually for every subcarrier but jointly for all users. The time-variant subcarrier is modelled by the Slepian basis expansion from Section 4.5. By using the Slepian basis expansion the dimensionality of the time-variant estimation problem can be drastically reduced and we do *not* need the detailed knowledge of second order statistics.

6.1 Uplink Signal Model for Time-Variant Frequency-Selective Channels

We extend the downlink signal model (5.7) to the uplink case where every user transmits over a different channel and uses a unique (random) pilot sequence. Figure 6.1 shows the schematic transmitter and channel model for the uplink. The $M - J$ data symbols are distributed over a block of length M fulfilling

$$b_k[m] \in \{\pm 1 \pm \mathrm{j}\}/\sqrt{2} \quad \text{for} \quad m \notin \mathcal{P} \tag{6.1}$$

and

$$b_k[m] = 0 \quad \text{for} \quad m \in \mathcal{P} \tag{6.2}$$

allowing for pilot symbol insertion. The pilot placement is defined through the pilot set $\mathcal{P}$ (4.40), see also Figure 4.14.

After spreading, pilot symbols $\boldsymbol{p}_k[m] \in \mathbb{C}^N$ with elements $p_k[m,q]$ are added

$$\boldsymbol{d}_k[m] = \boldsymbol{s}_k b_k[m] + \boldsymbol{p}_k[m]\,. \tag{6.3}$$

The elements of the pilot symbols $p_k[m,q]$ for $m \in \mathcal{P}$ and $q \in \{0,\ldots,N-1\}$ are i.i.d. chosen with equal probability from the QPSK symbol set $\{\pm 1 \pm \mathrm{j}\}\sqrt{2N}$, otherwise

$$\boldsymbol{p}_k[m] = \mathbf{0}_N \quad \text{for} \quad m \notin \mathcal{P}\,.$$

Then, an N point inverse DFT is performed and a cyclic prefix of length G is inserted. Each single OFDM symbol together with the cyclic prefix is represented by $\boldsymbol{\mu}_k[m] \in \mathbb{C}^{\,P}$ and has length $P = N + G$ chips. We write

$$\boldsymbol{\mu}_k[m] = \boldsymbol{T}_{\mathrm{CP}} \boldsymbol{F}_N^{\mathrm{H}} \boldsymbol{d}_k[m]\,.$$

After parallel-serial conversion according to

$$\boldsymbol{\mu}_k[m] = \begin{bmatrix} \mu_k[mP] \\ \mu_k[mP+1] \\ \vdots \\ \mu_k[mP+P-1] \end{bmatrix}$$

the chip stream $\mu_k[n]$ with chip rate $1/T_{\mathrm{C}} = P/T_{\mathrm{S}}$ is transmitted over a time-variant frequency-selective channel $\boldsymbol{h}_k[m]$. We assume the same channel conditions as defined in Section 5.1 with (5.5), so that the inter-carrier interference is negligibly small.

At the receive antenna all K user signals add up. The receiver removes the cyclic prefix and performs a DFT. The received signal vector after these two operations is given by

$$\boldsymbol{y}[m] = \sum_{k=1}^{K} \mathrm{diag}\left(\boldsymbol{g}_k[m]\right)\left(\boldsymbol{s}_k b_k[m] + \boldsymbol{p}_k[m]\right) + \boldsymbol{z}[m]\,, \tag{6.4}$$

where complex additive white Gaussian noise with zero mean and covariance $\sigma_z^2 \boldsymbol{I}_N$ is denoted by $\boldsymbol{z}[m] \in \mathbb{C}^{\,N}$ with elements $z[m,q]$.

6.2 Iterative Time-Variant Multi-User Detection

We define the time-variant effective spreading sequences

$$\tilde{\boldsymbol{s}}_k[m] = \mathrm{diag}\left(\boldsymbol{g}_k[m]\right)\boldsymbol{s}_k\,, \tag{6.5}$$

and the time-variant effective spreading matrix

$$\tilde{\boldsymbol{S}}[m] = [\tilde{\boldsymbol{s}}_1[m],\ldots,\tilde{\boldsymbol{s}}_K[m]] \in \mathbb{C}^{\,N\times K}\,.$$

Using these definitions we write a signal model for data detection

$$\boldsymbol{y}[m] = \tilde{\boldsymbol{S}}_k[m]\boldsymbol{b}[m] + \boldsymbol{z}[m] \quad \text{for} \quad m \notin \mathcal{P}$$

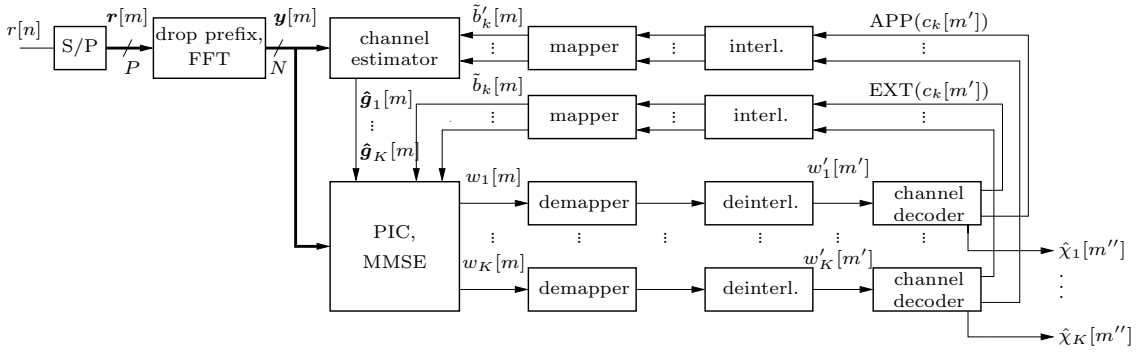

Figure 6.2: Model for the MC-CDMA joint time-variant channel-estimation and decoding multi-user receiver.

where $\boldsymbol{b}[m]$ (2.20) contains the stacked data symbols for K users.

Figure 6.2 shows the structure of the iterative receiver. The receiver detects the data $\boldsymbol{b}[m]$ using the received vector $\boldsymbol{y}[m]$, the spreading matrix $\tilde{\boldsymbol{S}}^{(i)}[m]$, and the feedback extrinsic information $\Pr^{(\mathrm{EXT})}(c_k^{(i)}[m'] = +1)$ on the code bits at iteration i. The time-variant frequency-selective nature of the channel requires to build a filter which is matched to the time-variant effective spreading sequence $\tilde{\boldsymbol{s}}_k^{(i)}[m]$. For Section 6.2, it is only of interest that the channel estimator supplies an estimate $\hat{\boldsymbol{g}}_k[m]$ for the time-variant channel frequency response for every user. The general optimization problem is therefore reduced to the estimation of $\boldsymbol{b}[m]$ only (for the time-invariant case see Section 2.6).

6.2.1 Time-Variant Parallel Interference Cancellation

To cancel the multi-access interference, we perform soft cancellation for user k

$$\tilde{\boldsymbol{y}}_k^{(i)}[m] = \boldsymbol{y}[m] + \tilde{\boldsymbol{s}}_k^{(i)}[m]\tilde{b}_k^{(i)}[m] - \tilde{\boldsymbol{S}}^{(i)}[m]\tilde{\boldsymbol{b}}^{(i)}[m]. \tag{6.6}$$

Vector $\tilde{\boldsymbol{b}}^{(i)}[m]$ contains the soft bit estimates that are computed from the extrinsic information supplied by the decoding stage. The mapping for the QPSK alphabet is specified in (2.26).

6.2.2 Time-Variant Unbiased Conditional MMSE Filter

The output of the interference canceller $\tilde{\boldsymbol{y}}_k^{(i)}[m]$ is further cleaned from noise and multi-access interference with a successive linear MMSE filter

$$\tilde{w}_k^{(i)}[m] = (\boldsymbol{f}_k^{(i)}[m])^{\mathrm{H}}\tilde{\boldsymbol{y}}_k^{(i)}[m]$$

to obtain an estimate of the transmitted symbol $b_k[m]$. A time-variant unbiased conditional MMSE filter for the MC-CDMA system can be found similarly to the

MMSE detector given in Section 2.6. In order to simplify the notation we omit the iteration index i for the filter. It has the form

$$\boldsymbol{f}_k^{\mathrm{H}}[m] = \frac{\tilde{\boldsymbol{s}}_k^{\mathrm{H}}[m](\sigma_z^2 \boldsymbol{I}_N + \tilde{\boldsymbol{S}}[m]\boldsymbol{V}[m]\tilde{\boldsymbol{S}}^{\mathrm{H}}[m])^{-1}}{\tilde{\boldsymbol{s}}_k^{\mathrm{H}}[m](\sigma_z^2 \boldsymbol{I} + \tilde{\boldsymbol{S}}[m]\boldsymbol{V}[m]\tilde{\boldsymbol{S}}^{\mathrm{H}}[m])^{-1}\tilde{\boldsymbol{s}}_k[m]},$$

cf. (2.29) for the block-fading case.

Matrix $\boldsymbol{V}[m]$ denotes the error covariance matrix

$$\boldsymbol{V}[m] = \mathop{\mathbb{E}}_{b}\left\{(\boldsymbol{b}[m] - \tilde{\boldsymbol{b}}[m])(\boldsymbol{b}[m] - \tilde{\boldsymbol{b}}[m])^{\mathrm{H}}\right\} \tag{6.7}$$

with diagonal elements

$$[\boldsymbol{V}\,[m]]_{k,k} = 1 - |\tilde{b}_k^{(i)}[m]|^2\,, \tag{6.8}$$

the non-diagonal elements are assumed to be zero. In this case we calculate the variance for the symbol at time instant m belonging to user k and consider the filter conditional.

6.3 Iterative Time-Variant Channel Estimation

The performance of the iterative receiver crucially depends on the accurate channel estimates for the time-variant frequency response $\boldsymbol{g}_k[m]$. The MC-CDMA signal model (6.4) shows that the transmission takes place over N parallel frequency-flat channels. We rewrite (6.4) as a set of equations for every subcarrier $q \in \{0, \ldots, N-1\}$,

$$y[m,q] = \sum_{k=1}^{K} g_k[m,q](s_k[q]b_k[m] + p_k[m,q]) + z[m,q]\,. \tag{6.9}$$

Comparing (6.9) with (5.10) makes clear why the channel estimation in the uplink is substantially more complicated than in the downlink. For every subcarrier q we need to estimate the additive mixture of K bandlimited processes $g_k[m,q]$. We describe the band limited property of each users' process by the Slepian basis expansion from Section 4.5. A linear MMSE filter is applied to estimate the basis expansion coefficients using pilots and soft symbols in an iterative process.

6.3.1 Signal Model for Time-Variant Channel Estimation

For the downlink, as described in Section 5, we used the generalized finite Slepian basis expansion without iterative processing to perform channel estimation. In the downlink all users share the same channel, thus the effective E_{S}/N_0 for the channel estimation is high enough in order to obtain time-variant channel estimates with

good accuracy, see Section 5.4. The generalized finite Slepian basis expansion performs channel estimation using the pilot pattern $\mathcal{P}$ and interpolation between the pilot positions.

In the uplink the E_S/N_0 is drastically reduced since channels for K individual users have to be estimated. In the uplink the available processing power is much higher such we can afford iterative processing. During the iterative process channel knowledge for the full data block may be obtained, thus the orthogonality of the Slepian basis functions can be maintained. The higher amount of pilots necessary for the uplink due to the small E_S/N_0 reduces the performance gain of the generalized finite Slepian basis expansion (see Section 4.8.5). This is why we use the Slepian basis expansion also for the first iteration where only pilots are used for the initial channel estimate.

Substituting the Slepian basis expansion (4.28) for the time-variant subcarrier coefficients $g_k[m,q]$ into the system model (6.9) we obtain

$$y[m,q] = \sum_{k=1}^{K} \sum_{i=0}^{D-1} u_i[m]\psi_k[i,q]d_k[m,q] + z[m,q]\,, \tag{6.10}$$

where

$$d_k[m,q] = s_k[q]b_k[m] + p_k[m,q]\,. \tag{6.11}$$

An estimate of the subcarrier coefficients $\hat{\psi}_k[i,q]$ can be obtained jointly for all K users but individually for every subcarrier q. We define the vector

$$\boldsymbol{\psi}_q = \begin{bmatrix} \psi_1[0,q] \\ \vdots \\ \psi_K[0,q] \\ \vdots \\ \psi_1[D-1,q] \\ \vdots \\ \psi_K[D-1,q] \end{bmatrix} \in \mathbb{C}^{KD}$$

containing the basis expansion coefficients of all K users for subcarrier q. Furthermore, we introduce

$$\boldsymbol{y}_q = \begin{bmatrix} y[0,q] \\ \vdots \\ y[M-1,q] \end{bmatrix} \in \mathbb{C}^{M}$$

for the received symbol sequence on subcarrier q for each single data block. Using these definitions we write

$$\boldsymbol{y}_q = \boldsymbol{\mathcal{D}}_q\boldsymbol{\psi}_q + \boldsymbol{z}_q\,, \tag{6.12}$$

where

$$\boldsymbol{\mathcal{D}}_q = [\mathrm{diag}\,(\boldsymbol{u}_0)\,\boldsymbol{D}_q, \ldots, \mathrm{diag}\,(\boldsymbol{u}_{D-1})\,\boldsymbol{D}_q] \in \mathbb{C}^{M\times KD}\,, \tag{6.13}$$

and $\boldsymbol{D}_q \in \mathbb{C}^{M\times K}$ (3.3) contains the transmitted symbols for all K users on subcarrier q which we repeat here for convenience

$$\boldsymbol{D}_q = \begin{bmatrix} d_1[0,q] & \ldots & d_K[0,q] \\ \vdots & \ddots & \vdots \\ d_1[M-1,q] & \ldots & d_K[M-1,q] \end{bmatrix}.$$

For channel estimation, J pilot symbols in (6.11) are known. The remaining $M-J$ data symbols are not known. We replace them by soft symbols, calculated from the a-posteriori probability (3.5) obtained in the previous iteration. This enables us to obtain refined channel estimates if the soft symbols get more certain from iteration to iteration. For the first iteration the soft symbols $\tilde{b}'_k[m]$ for $m \notin \mathcal{P}$ are set to zero.

We define the soft symbol matrix $\tilde{\boldsymbol{D}}_q \in \mathbb{C}^{M\times K}$ according to (3.3) by replacing $d_k[m,q]$ with

$$\tilde{d}_k[m,q] = s_k[q]\tilde{b}'_k[m] + p_k[m,q]\,.$$

The soft symbols $\tilde{b}'_k[m]$ are defined according to (3.5). Finally we define $\tilde{\boldsymbol{\mathcal{D}}}_q \in \mathbb{C}^{M\times KD}$ according to (6.13) by replacing $\boldsymbol{D}_q$ with $\tilde{\boldsymbol{D}}_q$. The matrix $\tilde{\boldsymbol{\mathcal{D}}}_q$ contains deterministic pilot symbols and statistical information about the transmitted data symbols.

6.3.2 Linear MMSE Channel Estimation

We extend the results obtained in Section 3.2 to the time-variant case. The linear MMSE estimate of $\boldsymbol{\psi}_q$ in (6.12) is given by (with the subcarrier index q omitted)

$$\hat{\boldsymbol{\psi}}_{\mathrm{LMMSE}} = \tilde{\boldsymbol{\mathcal{D}}}^{\mathrm{H}} \left(\tilde{\boldsymbol{\mathcal{D}}}\tilde{\boldsymbol{\mathcal{D}}}^{\mathrm{H}} + \underbrace{\boldsymbol{\Lambda}' + \sigma_z^2 \boldsymbol{I}_M}_{\triangleq \boldsymbol{\Delta}'} \right)^{-1} \boldsymbol{y}. \tag{6.14}$$

where the elements of the diagonal matrix $\boldsymbol{\Lambda}'$ are defined as

$$[\boldsymbol{\Lambda}']_{m,m} = \sum_{k=1}^{K} \sum_{i=0}^{D-1} \frac{1}{N} u_i^2[m] \mathrm{var}\{b_k[m]\}, \tag{6.15}$$

and the symbol variance is

$$\mathrm{var}\{b_k[m]\} = \mathop{\mathbb{E}}_{\boldsymbol{b}} \left\{ \left(b_k[m] - \mathop{\mathbb{E}}_{\boldsymbol{b}}\{b_k[m]\} \right)^2 \right\} = 1 - \tilde{b}_k^2[m].$$

The elements of the basis function are denoted by $u_i[m]$ (see Section 4.5).

For evaluation of this estimator it is necessary to invert an M-dimensional matrix, which is computationally expensive. To avoid this, we apply the matrix inversion lemma to (6.14), yielding

$$\hat{\boldsymbol{\psi}}_{\mathrm{LMMSE}} = \left(\tilde{\boldsymbol{\mathcal{D}}}^{\mathrm{H}} \boldsymbol{\Delta}'^{-1} \tilde{\boldsymbol{\mathcal{D}}} + \boldsymbol{I}_K\right)^{-1} \tilde{\boldsymbol{\mathcal{D}}}^{\mathrm{H}} \boldsymbol{\Delta}'^{-1} \boldsymbol{y}. \tag{6.16}$$

The rows of matrix $\tilde{\boldsymbol{\mathcal{D}}}$ are scaled by the diagonal matrix $\boldsymbol{\Delta}'$, taking into account the variances of the noise and the variance of the soft symbol estimates.

After estimating $\hat{\boldsymbol{\psi}}_q$ for all $q \in \{0, \ldots, N-1\}$ an estimate for the time-variant frequency response is given by

$$\hat{g}'_k[m, q] = \sum_{i=0}^{D-1} u_i[m] \hat{\psi}_k[i, q] \,.$$

Further noise suppression is obtained if we exploit the correlation between the subcarriers

$$\hat{\boldsymbol{g}}_k[m] = \boldsymbol{F}_{N \times L} \boldsymbol{F}^{\mathrm{H}}_{N \times L} \hat{\boldsymbol{g}}'_k[m] \,.$$

Finally, this allows to perform data detection by inserting the channel estimates $\hat{\boldsymbol{g}}_k[m]$ into (6.5). Figure 6.3 shows a summary of the iterative channel estimation algorithm.

Input:
$\boldsymbol{y} \in \mathbb{C}^N$, $\tilde{b}'_k[m] \in \mathbb{C}$, $\sigma_z^2 \in \mathbb{R}$.
Uses:
$p_k[m, q] \in \mathbb{C}$, $s_k[q] \in \mathbb{C}$, $u_i[m] \in \mathbb{R}$ for $i \in \{0, \ldots, D-1\}$.
Index ranges:
$k \in \{1, \ldots, K\}$, $m \in \{0, \ldots, M-1\}$, $q \in \{0, \ldots, N-1\}$.
Channel estimation:
$[\boldsymbol{\Lambda}']_{m,m} = \sum_{k=1}^{K} \sum_{i=0}^{D-1} \frac{1}{N} u_i^2[m](1 - \tilde{b}_k^2[m])$,
$\boldsymbol{\Delta}' = \boldsymbol{\Lambda}' - \sigma_z^2 \boldsymbol{I}_M$,
$[\boldsymbol{D}_q]_{m,k} = s_k[q] \tilde{b}'_k[m] + p_k[m, q]$,
$\hat{\boldsymbol{\psi}}_{q,\mathrm{LMMSE}} = \left(\tilde{\boldsymbol{\mathcal{D}}}_q^{\mathrm{H}} \boldsymbol{\Delta}'^{-1} \tilde{\boldsymbol{\mathcal{D}}}_q + \boldsymbol{I}_K\right)^{-1} \tilde{\boldsymbol{\mathcal{D}}}_q^{\mathrm{H}} \boldsymbol{\Delta}'^{-1} \boldsymbol{y}$,
$\hat{g}'_k[m, q] = \sum_{i=0}^{D-1} u_i[m] \hat{\psi}_k[i, q]$,
$\hat{\boldsymbol{g}}_k[m] = \boldsymbol{F}_{N \times L} \boldsymbol{F}^{\mathrm{H}}_{N \times L} \hat{\boldsymbol{g}}'_k[m]$.
Output:
$\hat{\boldsymbol{g}}_k[m] \in \mathbb{C}^N$.

Figure 6.3: Iterative channel estimation algorithm. Each line is evaluated for the defined index ranges if a certain index appears on the left hand side.

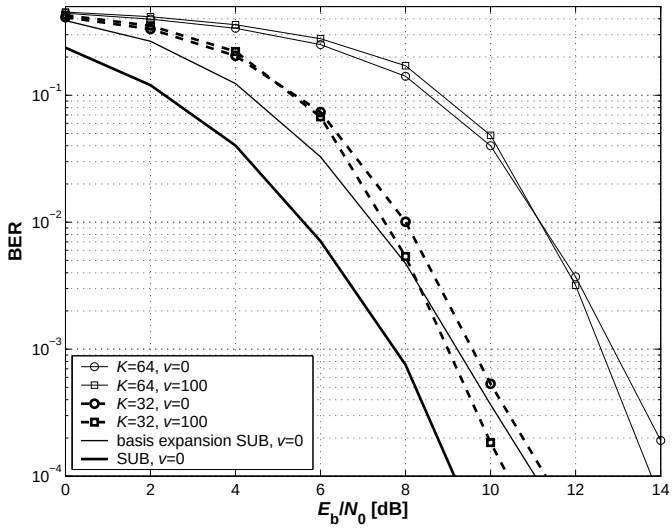

Figure 6.4: MC-CDMA uplink performance in terms of bit error rate (BER) versus E_b/N_0 after 4 iterations. The Slepian basis expansion uses $D' = D = 3$ basis functions. The $K \in \{32, 64\}$ users are moving with $v \in \{0, 100\}\,\mathrm{km/h}$. The normalized delay spread $L_\mathrm{D} = 4$. For reference, the single-user bound (SUB) and the basis expansion single-user bound both for $v = 0\,\mathrm{km/h}$ are shown too.

6.3.3 Simulation Results

The realizations of the time-variant frequency-selective channel $h'_k[n, \ell]$, sampled at the chip-rate $1/T_\mathrm{C}$, are generated using the parameters from Section 5.4.

The system operates at carrier frequency $f_C = 2\,\mathrm{GHz}$ and the $K \in \{32, 64\}$ users move with velocity $v \in \{0, 100\}\,\mathrm{km/h}$. This gives a Doppler frequency $B_\mathrm{D} \in \{0, 190\}\,\mathrm{Hz}$ and $\nu_\mathrm{D} \in \{0, 3.8 \cdot 10^{-3}\}$. The number of subcarriers $N = 64$ and the OFDM symbol with cyclic prefix has length of $P = G + N = 79$. The data block consists of $M = 256$ OFDM symbols with $J = 60$ OFDM pilot symbols. The system is designed for $v_\mathrm{max} = 102.5\,\mathrm{km/h}$ which results in $D = D' = 3$ for the Slepian basis expansion. The simulation results are obtained by averaging over 100 independent channel realizations.

Figure 6.4 illustrates the MC-CDMA uplink performance with iterative time-variant channel estimation based on the Slepian basis expansion in term of bit error rate versus E_b/N_0 after four iterations. The plot also shows the single-user bound which is defined as the performance for one user $K = 1$ and a perfectly known channel $\boldsymbol{g}_k[m]$. Additionally, we plot the basis expansion single-user bound. This is the performance which can be achieved with the Slepian basis expansion channel-

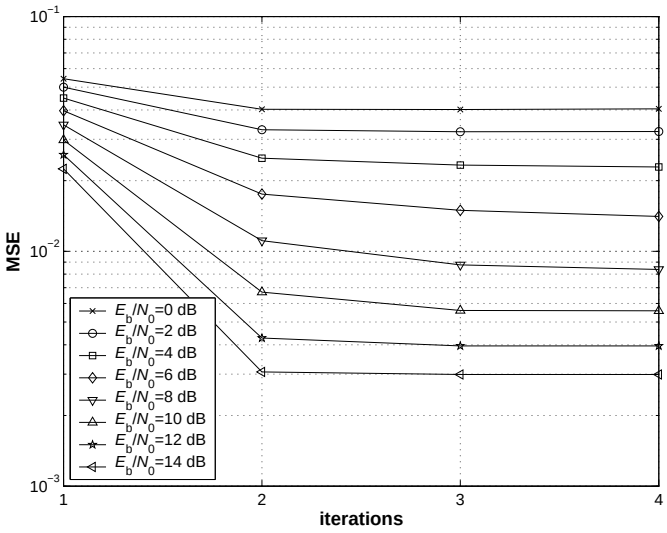

Figure 6.5: Mean square channel estimation error MSE_M versus number of iteration $i \in \{1, \ldots, 4\}$ for the uplink of an MC-CDMA system. The Slepian basis expansion uses $D = 3$ basis functions. The $K = 32$ users are moving with $v = 100\,\mathrm{km/h}$.

estimation algorithm.

In order to obtain the simulation results for the basis-expansion single-user bound, we supply the receiver with channel values according to

$$\hat{h}_k[m, \ell] = \boldsymbol{f}^{\mathrm{T}}[m] \sum_{\check{m}=0}^{M-1} \boldsymbol{f}^{*}[\check{m}] h_k[\check{m}, \ell] + \sqrt{\frac{D}{J}} z[m, \ell]\,.$$

Thus, we project the time-variant channel onto the orthogonal basis function taking into account the bias^2_M (4.58) and an additive noise term the variance var_M (4.61).

The distance between the single-user bound and the basis expansion single-user bound is explained by the energy that is used for the pilot symbols and the mean square error of the basis expansion channel estimates MSE_M.

For every subcarrier, KD coefficients have to be estimated. Under full load $KD = 192$ comes near to the overall number of symbols in a single data block $M = 256$. This is why the uncertainty of the channel estimates increases as the number of users approaches full load. This explains the performance gap between $K = 32$ and $K = 64$ users.

Figure 6.5 shows the mean square channel estimation error MSE_M versus number of iterations i for $K = 32$ user. This plot shows that after four iterations the channel estimation error does not decrease further.

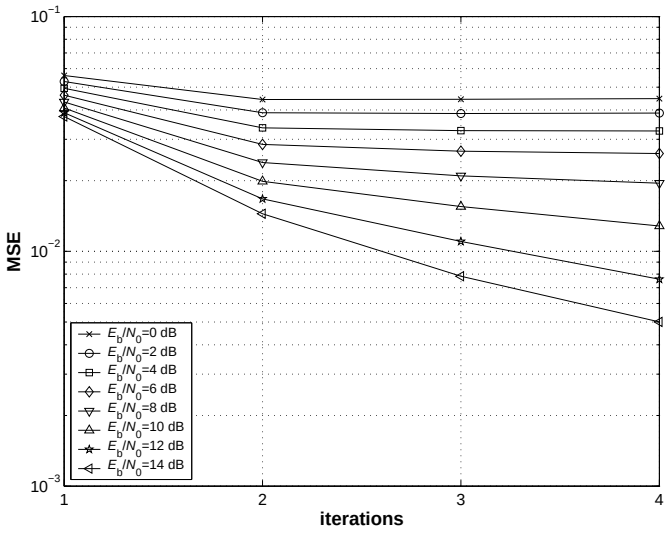

Figure 6.6: Means square channel estimation error MSE_M versus number of iteration $i \in \{1, \ldots, 4\}$ for the uplink of an MC-CDMA system. The Slepian basis expansion uses $D = 3$ basis functions. The $K = 64$ users are moving with $v = 100\,\mathrm{km/h}$.

The picture is different for $K = 64$ users as is shown in Figure 6.6. Here it can be seen that it would be beneficial to perform more iterations at higher E_b/N_0 values.

7 Conclusions

This thesis deals with OFDM multi-user communication over time-variant channels. We investigated MC-CDMA that combines OFDM with frequency domain spreading. We applied iterative multi-user detection based on parallel interference cancellation and MMSE filtering.

Instrumental for any multi-user detection algorithm are accurate channel estimates. We developed new iterative channel estimation methods that combine pilots with feedback soft-symbols to enhance the quality of the channel estimates. Furthermore, statistical information about the soft-symbols, like the mean and the variance, are exploited using a channel estimator based on the MMSE criterion.

The thesis can be divided into two parts. The first part in Chapter 2 and 3 deals with block fading channels where the channel is assumed to stay constant for the duration of a data block. The second part in Chapter 4, 5 and 6 deals with time-variant channels which vary significantly over the duration of data block.

Block Fading Channels

In the following we list key findings and conclusions specific to block fading channels:

- We showed that an MC-CDMA system, while having the same complexity for data-detection as DS-CDMA, has a drastically reduced channel estimation complexity especially at high bit rates. This is due to the fact that the channel estimation complexity for MC-CDMA grows linearly with the essential support of the channel impulse response L. While in DS-CDMA, because of time domain processing, the complexity increases with L^3.

- The performance increase through block interleaving is not linear in the number of blocks. This is linked to the constrained length of the applied code.

Time-Variant Channels

In the following we will present key findings and conclusions for time-variant channels:

- OFDM transmission over time-variant channels is susceptible to inter-carrier interference. But, the delay spread of mobile-communication channels is still short enough so that the subcarrier bandwidth can be chosen much larger than the Doppler bandwidth while retaining acceptable spectral efficiency. Such a design results in time-variant frequency-flat subcarriers that are independent of each other.

- We investigated time-variant channel estimation methods that do *not* need knowledge of detailed second order statistics. We assumed an upper bound for the maximum Doppler bandwidth only. The classical Fourier basis expansion was analyzed and its weaknesses which stems from windowing and the associated spectral leakage were discussed.

- We introduced the concepts from the theory of time-concentrated and band-limited sequences to the field of channel estimation and modelling by designing a Slepian basis expansion. The Slepian basis expansion is characterized by two parameters only: the maximum velocity of the users and the block length. For practical communication systems at 2 GHz with users at vehicular velocities up to 100 km/h the Slepian basis expansion needs as few as three basis functions in order to describe the time-variant channel. The basis expansion is suitable for a whole ensemble of channel realization as long as the velocity of the user is below the chosen upper bound.

- Analytic performance results for time-variant frequency-flat channels, respectively subcarriers, were established. We could show that the square bias of the Slepian basis expansion is more than a magnitude smaller than the square bias of the Fourier basis expansion.

- We derived a novel generalized finite Slepian basis expansion and applied it to pilot-based time-variant channel estimation on a per-subcarrier basis for an MC-CDMA downlink. With the generalized finite Slepian basis expansion we are able to perform low complexity time-variant channel estimation for each single data block using evenly distributed pilots. Additionally, interpolation between the pilot positions is performed by the basis expansion too.

- We extended the iterative MC-CDMA receiver for the uplink to the time-variant case using the Slepian basis expansion, achieving a consistent performance for a wide range of velocities.

- It is important to emphasize that the situation in a mobile communication system is different to the one in a single-frequency broadcasting network that uses DVB-T or DAB. Such broadcasting systems have a more pronounced

inter-carrier interference problem since the overall design has to accommodate for the large distances between individual transmitters that all use the same carrier frequency.

- We derived a simulation model with correct Rayleigh fading statistics over the full velocity range. We found that the receiver performance strongly depends on the statistical fading property of the channel.

- The results presented in this thesis for the uplink scenario can be easily extend to a MIMO multi-user system where every user has one transmit antenna and the base station has N_{R} receive antennas. First work on this issue can be found in [49]. Further analysis using a geometry based stochastic channel model was performed in [28].

- We showed that Doppler diversity can be exploited by an MC-CDMA system if accurate time-variant channel estimation based on the Slepian basis expansion is used. Thus the receiver performs *better* at higher speed.

- In [5, 72] it is stated that MC-CDMA has several drawbacks which hinders its application in the uplink. This drawbacks are namely the destroyed orthogonality of the spreading codes due to the frequency selective channels and the not adequate channel estimation quality. However, the analysis in [5, 72] was conducted for an receiver based on a single user matched filter. We showed in this thesis that by applying iterative multi-user detection and iterative time-variant channel estimation MC-CDMA becomes a very interesting candidate for future 4G systems. We showed that MC-CDMA can achieve excellent performance for time-variant channels in the uplink.

A Simulation Model for Time-Variant Channels with Jakes' Spectrum

We use the model from [93] and correct it so that the Rayleigh distribution of $h[m]$ is maintained at low velocities and at $v = 0\,\mathrm{km/h}$. The detailed simulation model for $h[m]$ is defined as follows:

$$h[m] = \frac{1}{\sqrt{2}}(h_c[m] + \mathrm{j}h_s[m]) \tag{A.1}$$

$$h_c[m] = \frac{2}{\sqrt{A}} \sum_{i=1}^{A} \cos(\psi_i) \cdot \cos(2\pi\nu_\mathrm{D} m \cos\alpha_i + \phi_i) \tag{A.2}$$

$$h_s[m] = \frac{2}{\sqrt{A}} \sum_{i=1}^{A} \sin(\psi_i) \cdot \cos(2\pi\nu_\mathrm{D} m \cos\alpha_i + \phi_i)$$

with

$$\alpha_i = \frac{2\pi i - \pi + \phi}{4A} \quad \text{for} \quad i \in \{1, \ldots, A\}$$

where ϕ, ϕ_i, and ψ_i are independent and uniformly distributed over $[-\pi, \pi)$ for all i. For the numerical simulations we fix the number of interfering paths to $A = 20$.

In the limit $\nu_\mathrm{D} = 0$ equation (A.2) reduces to

$$h_c[m] = \frac{2}{\sqrt{A}} \sum_{i=1}^{A} \cos(\psi_i) \cdot \cos(\phi_i)\,. \tag{A.3}$$

Because of the central limit theorem and the independence of all ψ_i and ϕ_i the channel coefficients $h_c[m]$ are normally distributed. Therefore, the model converges to a block fading channel.

In [93] ϕ_i is replaced by a common phase ϕ. In this case the components of the sum in (A.3) are not independent and the channel coefficients $h_c[m]$ are not normally distributed.

B List of Abbreviations

We list all abbreviations used in this thesis in Table B.1 and Table B.2.

Abbreviation	Description
ADSL	asymmetric digital subscriber line
APP	a-posteriori probability
BPSK	binary phase shift keying
CDMA	code division multiple access
DAB	digital audio broadcast
DFT	discrete Fourier transform
DPS	discrete prolate spheroidal
DRM	digital radio mondial
DS	direct sequence
DVB-T	digital video broadcast terrestrial
EXT	extrinsic probability
FDPS	finite discrete prolate spheroidal
GSM	Global System for Mobile Communications
IEEE	Institute of Electrical and Electronics Engineers
i.i.d.	independent identical distributed
ISI	inter-symbol interference

Table B.1: Abbreviations A-K and their full description.

Abbreviation	Description
LAN	local area networks
LMMSE	liner minimum mean square error
MC-CDMA	multi-carrier code division multiple access
MIMO	multiple-input multiple-output
MMSE	minimum mean square error
MSE	mean square error
OFDM	orthogonal frequency division multiplexing
QPSK	quadrature phase shift keying
SUB	single-user bound
TDD	time division duplex
TDMA	time division multiple access
UMTS	Universal Mobile Telecommunications System

Table B.2: Abbreviations L-Z and their full description.

C List of Symbols

We list here symbols that are generally used throughout the thesis. Locally used symbols are omitted. We list Greek symbols in Table C.1, lower case symbols in Table C.2, and upper case symbols in Table C.3.

Symbol	Description
α	user power
β	load in a communication system
γ	time domain basis expansion coefficient
η^2	power delay profile
λ	eigenvalue
μ	transmitted chip
ν	normalized frequency
ν_{D}	normalized Doppler bandwidth (frequency)
ξ	sufficient statistic
σ^2, σ	variance, singular value
ψ	frequency domain basis expansion coefficient
Ψ	diversity measure
χ	information bit

Table C.1: Greek symbols.

Symbol	Description
a	approximation factor for finite Slepian basis expansion
b	data symbol
$\tilde{b}$	soft symbol
c	code bit
c_0	speed of light
d	transmitted symbol
f_C	carrier frequency
g	channel frequency response
h	channel impulse response
i, ℓ	general index
j	$\sqrt{-1}$
k	user index
m	discrete time at symbol rate $1/T_\mathrm{S}$
n	discrete time at chip rate $1/T_\mathrm{C}$
p	pilot symbol
q	subcarrier index
r	received chip with noise
$\boldsymbol{s}$	spreading sequence
$\tilde{\boldsymbol{s}}$	effective spreading sequence
u	basis function
v	velocity
w	channel value after detector
x	received chip without noise
y	received symbol after cyclic prefix removal and DFT
z	noise

Table C.2: Lower case symbols.

Symbol	Description
A	number of interfering paths per channel tap
B	number of data blocks used for interleaving
B_{D}	one sided Doppler bandwidth
D	dimension of the basis expansion
E_{b}	energy per information bit
E_{S}	energy per data symbol
G	length of cyclic prefix
J	number of pilot symbols per data block
K	number of users
L	essential support of the channel impulse response
L_{D}	root mean square delay spread normalized to the sampling rate
T_{D}	root mean square delay spread
M	number of symbols per data block
N	number of subcarriers, length of spreading sequence
N_0	noise power spectral density
N_{R}	number of receive antennas
N_{T}	number of transmit antennas
P	length of an OFDM symbol including the cyclic prefix
$\mathcal{P}$	set of pilot positions
R	autocorrelation
$\boldsymbol{R}$	covariance matrix
R_{C}	code rate of the convolutional encoder
R_{S}	code rate of the symbol mapper
S	power spectral density
$\boldsymbol{S}$	spreading matrix
$\tilde{\boldsymbol{S}}$	effective spreading matrix
T_{C}	chip duration
T_{D}	root mean square delay spread
T_{S}	symbol duration
V	diversity
V_{D}	Doppler diversity
V_{M}	multipath diversity
$\mathcal{X}$	set of data sybols

Table C.3: Upper case symbols.

Bibliography

[1] 3GPP, "Third Generation Partnership Project (3GPP)." [Online]. Available: http://www.3gpp.org/ 1

[2] ——, "Feasibility study for OFDM for UTRAN enhancement," 3GPP TR 25.892 V1.1.0, March 2004. [Online]. Available: http://www.3gpp.org/ 2

[3] C. H. Aldana, E. de Carvalho, and J. M. Cioffi, "Channel estimation for multicarrier multiple input single output systems using the EM algorithm," *IEEE Transactions on Signal Processing*, vol. 51, no. 12, pp. 3280–3292, December 2003. 33

[4] H. Artés, F. Hlawatsch, and G. Matz, "Efficient POCS algorithms for deterministic blind equalization of time-varying channels," in *IEEE Global Telecommunication Conference (GLOBECOM)*, vol. 2, San Francisco (CA), USA, November 2000, pp. 1031–1035. 49

[5] H. Atarashi, S. Abeta, and M. Sawahashi, "Broadband packet wireless access appropriate for high-speed and high-capacity throughput," in *IEEE Vehicular Technology Conference (VTC)*, vol. 1, May 2001, pp. 566–570. 91, 105

[6] L. R. Bahl, J. Cocke, F. Jelinek, and J. Raviv, "Optimal decoding of linear codes for minimizing symbol error rate," *IEEE Transactions on Information Theory*, vol. 20, no. 2, pp. 284–287, Mar. 1974. 2, 21, 24

[7] S. Barbarossa and A. Scaglione, *Signal Processing Advances in Wireless and Mobile Communications*. Upper Saddle River (NJ), USA: Prentice-Hall, Inc., 2000, vol. 2, ch. Time-Varying Fading Channels. 41

[8] I. Barhumi, G. Leus, and M. Moonen, "Time-varying FIR equalization of doubly-selective channels," in *IEEE International Conference on Communications (ICC)*, vol. 5, Anchorage (AK), USA, May 2003, pp. 3246–3250. 49

[9] P. Bello, "Characterization of randomly time-variant linear channels," *IEEE Trans. Comm. Syst.*, vol. CS-11, no. 4, pp. 360–393, December 1963. 3, 42

[10] T. Berger, *Rate Distortion Theory*, T. Kailath, Ed. Englewood Cliffs (NJ), USA: Prentice-Hall, Inc., 1971. 85

[11] J. A. C. Bingham, "Multicarrier modulation for data transmission: An idea whose time has come," *IEEE Transactions on Communications*, vol. 28, no. 5, pp. 5–14, 1990. 2, 10

[12] T. P. Bronez, "Spectral estimation of irregularly sampled multideminsional processes by generalized prolate spheroidal sequences," *IEEE Transactions on Acoustics, Speech, and Signal Processing*, vol. 36, no. 12, pp. 1862–1873, December 1988. 60

[13] G. Caire and U. Mitra, "Structured multiuser channel estimation for block-synchronous DS/CDMA," *IEEE Transactions on Communications*, vol. 49, no. 9, pp. 1605–1617, September 2001. 25

[14] G. Caire, R. R. Müller, and T. Tanaka, "Iterative multiuser joint decoding: Optimal power allocation and low-complexity implementation," *IEEE Transactions on Information Theory*, to appear. 21, 23, 31

[15] L. M. Correia, *Wireless Flexible Personalised Communications*. Wiley, 2001. 8, 9

[16] M. Debbah, "Linear precoders for OFDM," Ph.D. dissertation, Ecole Normale Suprieure de Cachan, France, 2002. 2, 16

[17] O. Edfors, M. Sandell, J.-J. van de Beek, S. K. Wilson, and P. O. Börjesson, "OFDM channel estimation by singular value decomposition," *IEEE Transactions on Communications*, vol. 46, no. 7, pp. 931–939, July 1998. 40, 58

[18] ETSI, "Digital audio broadcasting (DAB) to mobile, portable and fixed receivers," ETSI EN 300 401, May 2001. [Online]. Available: http://www.etsi.org 1

[19] ——, "Digital video broadcasting (DVB); framing structure, channel coding and modulation for digital terrestrial television," ETSI EN 300 744 V1.4.1, January 2001. [Online]. Available: http://www.etsi.org 1, 16

[20] ——, "Digital radio mondiale (DRM); system specification," ETSI ES 201 980 V2.1.1, April 2004. [Online]. Available: http://www.etsi.org 1

[21] B. L. Floch, M. Alard, and C. Berrou, "Coded orthogonal frequency division multiplex," *Proceedings of the IEEE*, vol. 83, no. 6, pp. 982–996, June 1995. 16

[22] I. K. Fodor and P. B. Stark, "Multitaper spectrum estimation for time series with gaps," *IEEE Transactions on Signal Processing*, vol. 48, no. 12, pp. 3472–3483, December 2000. 60

[23] G. H. Golub and C. F. V. Loan, *Matrix Computations*, 2nd ed. Baltimore (MD), USA: Johns Hopkins University Press, 1989. 61, 64

[24] U. Grenander and G. Szegö, *Toeplitz Forms and Their Applications*. Berkley and Los Angeles (CA), USA: Universtiy of California Press, 1958. 88

[25] A. Grünbaum, "Eigenvectors of a Toeplitz matrix: Discrete version of the prolate spheroidal wave functions," *SIAM J. Alg. Disc. Meth.*, vol. 2, no. 2, pp. 136–141, June 1981. 60, 61, 62

[26] P. Hoeher, "A statistical discrete-time model for the WSSUS multipath channel," *IEEE Transactions on Vehicular Technology*, vol. 41, no. 4, pp. 461–468, November 1992. 41

[27] H. Hofstetter and P. H. Lehne, "Documentation of the measurement campaign - part 1: 2.1 GHz, annex 1: Results listings," IST-2001-32125 FLOWS, Tech. Rep. D10, April 2003. 9, 10

[28] H. Hofstetter, T. Zemen, J. Wehinger, and G. Steinböck, "Iterative MIMO multi-user detection: Performance evaluation with COST 259 channel model," in *Seventh International Symposium on Wireless Personal Multimedia Communications*, Abano Terme, Italy, 12-15 Sept. 2004, invited, to be presented. 105

[29] IEEE, "Part 11: Wireless LAN medium access control (MAC) and physical layer (PHY) specifications," IEEE Std 802.11a, 1999. [Online]. Available: http://grouper.ieee.org/groups/802/11/ 1, 16

[30] ——, "Mobile broadband wireless access (MBWA)," IEEE 802.20, December 2002. [Online]. Available: http://grouper.ieee.org/groups/802/20/ 2

[31] M. T. Ivrlac and J. A. Nossek, "Quantifying diversity and correlation in Rayleigh fading MIMO communication systems," in *3rd International Symposium on Signal Processing and Information Technology (ISSPIT)*, Darmstadt, Germany, 2003. 85, 86

[32] W. Jakes, *Microwave Mobile Communications*. New York, USA: John Wiley & Sons, 1974. 40

[33] P. L. Kafle and A. S. Sesay, "Iterative semi-blind multiuser detection using subspace approach for MC-CDMA uplink," in *Proceedings of the 2002 Canadian Conference on Electrical and Computer Engineering (CCECE)*, vol. 3, May 2002, pp. 1374–1379. 25

[34] S. Kaiser, *Multi-Carrier CDMA Mobile Radio Systems - Analysis and Optimization of Detection, Decoding, and Channel Estimation*, ser. Fortschritts-Berichte VDI Reihe. Düsseldorf, Germany: VDI Verlag GmbH, 1998, vol. 10, no. 531. 2, 16, 40, 58, 84, 85

[35] M. Kobayashi, J. Boutros, and G. Caire, "Successive interference cancellation with SISO decoding and EM channel estimation," *IEEE Journal on Selected Areas in Communications*, vol. 19, no. 8, pp. 1450 – 1460, Aug. 2001. 23

[36] A. N. Kolomogrov, "On the Shannon theory of information transmission in the case of continuous signals," *IRE Transactions on Information Theory*, vol. 2, no. 4, pp. 102–108, December 1956. 85

[37] C. Komninakis, C. Fragouli, A. H. Sayed, and R. D. Wesel, "Multi-input multi-output fading channel tracking and equalization using Kalman estimation," *IEEE Transactions on Signal Processing*, vol. 50, no. 5, pp. 1065–1076, May 2002. 40

[38] W. Kozek, "On the transfer function calculus for underspread LTV channels," *IEEE Transactions on Signal Processing*, vol. 45, no. 1, pp. 219–223, January 1997. 79

[39] V. Kühn, "Iterative interference cancellation and channel estimation for coded OFDM-CDMA," in *IEEE International Conference on Communications (ICC), Anchorage (AK), USA*, vol. 4, May 2003, pp. 2465–2469. 37

[40] A. Lapidoth, "On the high SNR capacity of stationary Gaussian fading channels," in *41st Annual Allerton Conference on Communication, Control, and Computing*, Monticello (IL), USA, October 2003. 85

[41] A. Leon-Garcia, *Probability and Random Processes for Electrical Engineering*. Addison-Wesley Publishing Company, 1994. 58

[42] G. Leus, S. Zhou, and G. B. Giannakis, "Orthogonal multiple access over time- and frequency-selective channels," *IEEE Transactions on Information Theory*, vol. 49, no. 8, pp. 1942–1950, August 2003. 49

[43] Y. G. Li and L. J. Cimini, "Bounds on the interchannel interference of OFDM in time-varying impairments," *IEEE Transactions on Communications*, vol. 49, no. 3, pp. 401–404, March 2001. 79

[44] H. Liu, *Signal processing applications in CDMA communications*. Artech House, 2000. 25

[45] H. Liu and G. Xu, "A subspace method for signature waveform estimation in synchronous CDMA systems," *IEEE Transactions on Communications*, vol. 44, no. 10, pp. 1346–1354, October 1996. 25

[46] M. Lončar, R. Müller, J. Wehinger, C. Mecklenbräuker, and T. Abe, "Iterative channel estimation and data detection in frequency selective fading MIMO channels," *European Transcations on Telecommunications*, 2004, to appear. 36

[47] X. Ma and G. B. Giannakis, "Maximum-diversity transmission over doubly selective wireless channels," *IEEE Transactions on Information Theory*, vol. 49, no. 7, pp. 1832–1840, July 2003. 49, 88

[48] G. Matz and F. Hlawatsch, "Time-frequency transfer function calculus (symbolic calculus) of linear time-varying systems (linear operators) based on generalized underspread theory," *J. Math. Phys.*, vol. 39, pp. 4041–4071, August 1998. 79

[49] C. F. Mecklenbräuker, J. Wehinger, T. Zemen, H. Artés, and F. Hlawatsch, *Smart Antennas in Europe - State of the Art*. EURASIP, to appear 2004, ch. Multiuser MIMO Channel Equalization. 105

[50] R. R. Müller, "Multi-user communications," Lecture notes, 2003. 2, 19, 31

[51] R. R. Müller and G. Caire, "The optimal received power distribution for IC-based iterative multiuser joint decoders," in *39th Annual Allerton Conference on Communication, Control and Computing*, Monticello (IL), USA, August 2001. 2, 23

[52] M. Niedzwiecki, *Identification of Time-Varying Processes*. John Wiley & Sons, 2000. 3, 40, 46, 55, 68, 69

[53] D. B. Percival and A. T. Walden, *Spectral Analysis for Physical Applications*. Cambridge University Press, 1963. 43, 52

[54] J. G. Proakis, *Digital Communications*, 4th ed. New York, USA: McGraw-Hill, 2000. 8, 16

[55] J. G. Proakis and D. G. Manolakis, *Digital Signal Processing*, 3rd ed. Prentice-Hall, 1996. 43, 49

[56] T. Rappaport, *Wireless Communications - Principles & Practice*. Upper Saddle River (NJ), USA: Prentice Hall, 1996. 8, 40, 42

[57] R. Raulefs, A. Dammann, and S. Kaiser, "The Doppler spread - gaining diversity for future mobile radio systems," in *IEEE Global Communications Conference (GLOBECOM)*, vol. 3, San Francisco (CA), USA, December 2003, pp. 1301–1305. 84

[58] H. Rohling, R. Grünheid, and D. Galda, "OFDM air interface for the 4th generation of mobile communication systems," in *Proceedings of the 6th International OFDM-Workshop*, Hamburg, Germany, 2001, pp. 1–28. 1

[59] H. Sari, G. Karam, and I. Jeanclaude, "Transmission techniques for digital terrestrial time-variant broadcasting," *IEEE Communications Magazine*, vol. 33, no. 2, pp. 100–109, February 1995. 1

[60] A. M. Sayeed and B. Aazhang, "Joint multipath-Doppler diversity in mobile wireless communications," *IEEE Transactions on Communications*, vol. 47, no. 1, pp. 123–132, January 1999. 40, 44, 49, 88

[61] A. M. Sayeed, A. Sendonaris, and B. Aazhang, "Multiuser detection in fast-fading multipath environment," *IEEE Journal on Selected Areas in Communications*, vol. 16, no. 9, pp. 1691–1701, December 1998. 40, 44, 49

[62] D. Schafhuber, "Wireless OFDM systems: Channel prediction and system capacity," Ph.D. dissertation, Vienna Technical University, Vienna, March 2003. 40

[63] D. Schafhuber and G. Matz, "MMSE and adaptive prediction of time-varying channels for OFDM systems," *IEEE Transactions on Wireless Communications*, 2004, to appear. 40

[64] D. Schafhuber, G. Matz, and F. Hlawatsch, "Adaptive Wiener filters for time-varying channel estimation in wireless OFDM systems," in *IEEE International Conference on Acoustics, Speech, and Signal Processing (ICASSP)*, vol. 4, April 2003, pp. 688–691. 40

[65] D. Schafhuber, M. Rupp, G. Matz, and F. Hlawatsch, "Adaptive identification and tracking of doubly selective fading channels for wireless MIMO-OFDM systems," in *IEEE Workshop on Signal Processing Advances in Wireless Communications*, Rome, Italy, June 2003. 40

[66] L. L. Scharf, *Statistical Signal Processing: Detection, Estimation, and Time Series Analysis*. Reading (MA), USA: Addison-Wesley Publishing Company, Inc., 1991. 55

[67] L. L. Scharf and D. W. Tufts, "Rank reduction for modeling stationary signals," *IEEE Transactions on Acoustics, Speech, and Signal Processing*, vol. ASSP-35, no. 3, pp. 350–355, March 1987. 58

[68] M. Siala, "Maximum a posteriori semi-blind channel estimation for OFDM systems operating on highly frequency selective channels," *Annals of telecommunications*, vol. 57, no. 9/10, pp. 873–924, September/October 2002. 40, 58

[69] D. Slepian, "Prolate spheroidal wave functions, Fourier analysis, and uncertainty - V: The discrete case," *The Bell System Technical Journal*, vol. 57, no. 5, pp. 1371–1430, May-June 1978. 3, 40, 50, 51, 52, 60, 62, 88

[70] D. Slepian and H. O. Pollak, "Prolate spheroidal wave functions, Fourier analysis, and uncertainty - I," *The Bell System Technical Journal*, vol. 40, no. 1, pp. 43–64, January 1961. 3, 50

[71] D. Slepian, "Some comments on Fourier analysis, uncertainty and modeling," *SIAM Review*, vol. 25, no. 3, pp. 379–393, July 1983. 50

[72] S. Suwa, H. Atarashi, and M. Sawahashi, "Performance comparison between MC/DS-CDMA and MC-CDMA for reverse link broadband packet wireless access," in *56th IEEE Vehicular Technology Conference (VTC)*, vol. 4, 24-28 Sept. 2002, pp. 2076–2080. 91, 105

[73] L. Tong, G. Xu, and T. Kailath, "Blind identification and equalization based on second-order statistics: A time domain approach," *IEEE Transactions on Information Theory*, vol. 40, no. 2, pp. 340–349, March 1994. 25

[74] M. Tüchler, R. Koetter, and A. Singer, "Turbo equalization: Principles and new results," *IEEE Transactions on Communications*, vol. 50, no. 5, pp. 754–767, May 2002. 33

[75] S. Verdú, *Mulituser Detection*. New York, USA: Cambridge University Press, 1998. 2, 19, 20

[76] I. Viering, *Analysis of Second Order Statistics for Improved Channel Estimation in Wireless Communications*, ser. Fortschritts-Berichte VDI Reihe. Düsseldorf, Germany: VDI Verlag GmbH, 2003, no. 733. 58

[77] I. Viering and H. Hofstetter, "Potential of coefficient reduction in delay, space and time based on measurements," in *Conference on Information Sciences and Systems (CISS)*, Baltimore, USA, March 2003. 40, 58

[78] Z. Wang and G. B. Giannakis, "Wireless multicarrier communications," *IEEE Signal Processing Magazine*, vol. 17, no. 3, pp. 29–48, May 2000. 13, 14

[79] J. Wehinger, C. F. Mecklenbräuker, R. R. Müller, T. Zemen, and M. Lončar, "On channel estimators for iterative CDMA multi-user receivers in flat fading," in *IEEE International Conference on Communications (ICC)*, 2004. 36

[80] J. Wehinger, R. R. Müller, M. Lončar, and C. F. Mecklenbräuker, "Performance of iterative CDMA receivers with channel estimation in multipath environments," in *36th Asilomar Conference on Signals, Systems and Computers*, vol. 2, Pacific Grove (CA), USA, 2002, pp. 1439 – 1443. 2, 23, 25, 31

[81] S. B. Weinstein and P. M. Ebert, "Data transmission by frequency-divison multiplexing using the discrete fourier transform," *IEEE Transactions on Communications*, vol. 19, no. 5, pp. 628–634, October 1971. 1, 10

[82] X. Wu, Q. Yin, J. Zhang, and K. Deng, "Time-domain multiuser detection for MC-CDMA systems without cyclic prefix," in *IEEE International Conference on Communications (ICC)*, vol. 2, April 2002, pp. 921–925. 25

[83] Y. V. Zakharov, T. C. Tozer, and J. F. Adlard, "Polynomial spline-approximation of Clarke's model," *IEEE Transactions on Signal Processing*, vol. 52, no. 5, pp. 1198–1208, May 2004. 71

[84] T. Zemen, M. Lončar, J. Wehinger, C. F. Mecklenbräuker, and R. R. Müller, "Improved channel estimation for iterative receivers," in *IEEE Global Communications Conference (GLOBECOM)*, vol. 1, San Francisco (CA), USA, December 2003, pp. 257–261. 3

[85] T. Zemen and C. F. Mecklenbräuker, "Time-variant channel equalization via discrete prolate spheroidal sequences," in *37th Asilomar Conference on Signals, Systems and Computers*, Pacific Grove (CA), USA, November 2003, pp. 1288–1292, invited. 3, 40

[86] ——, "Doppler diversity in MC-CDMA using the Slepian basis expansion model," in *12th European Signal Processing Conference (EUSIPCO)*, Vienna, Austria, September 2004, to be presented. 3, 4

[87] ——, "Time-variant channel estimation for MC-CDMA using prolate spheroidal sequences," *IEEE Transactions on Signal Processing*, revised. 3, 4, 40

[88] T. Zemen, C. F. Mecklenbräuker, and R. R. Müller, "Time variant channel equalization for MC-CDMA via Fourier basis functions," in *Multi-Carrier Spread-Spectrum Workshop*, Oberpaffenhofen, Germany, September 2003, pp. 451–454. 3, 49

[89] T. Zemen, C. F. Mecklenbräuker, J. Wehinger, and R. R. Müller, "Iterative multi-user decoding with time-variant channel estimation for MC-CDMA," in *Fifth International Conference on 3G Mobile Communication Technologies*, London, United Kingdom, invited, to be presented. 4

[90] ——, "Iterative multi-user decoding with time-variant channel estimation for MC-CDMA," *IEEE Transactions on Wireless Communications*, submitted. 4

[91] T. Zemen, J. Wehinger, C. F. Mecklenbräuker, and R. R. Müller, "Iterative detection and channel estimation for MC-CDMA," in *IEEE International Conference on Communications (ICC)*, vol. 5, Anchorage (AK), USA, May 2003, pp. 3462–3466. 2

[92] X. Zhao, J. Kivinen, P. Vainikainen, and K. Skog, "Characterization of Doppler spectra for mobile communications at 5.3 GHz," *IEEE Transactions on Vehicular Technology*, vol. 52, no. 1, pp. 14–23, January 2003. 3, 40, 71

[93] Y. R. Zheng and C. Xiao, "Simulation models with correct statistical properties for Rayleigh fading channels," *IEEE Transactions on Communications*, vol. 51, no. 6, pp. 920–928, June 2003. 3, 70, 107

[94] S. Zhou, G. B. Giannakis, and A. Swami, "Digital multi-carrier spread spectrum versus direct sequence spread spectrum for resistance to jamming and multipath," *IEEE Transactions on Communications*, vol. 50, no. 4, pp. 643–655, April 2002. 13, 14, 25

[95] Y. Zhou, C. K. Rushforth, and R. L. Frost, "Singular value decomposition, singular vectors, and the discrete prolate spheroidal sequences," in *IEEE International Conference on Acoustics, Speech, and Signal Processing (ICASSP)*, vol. 9, 1984, pp. 92–95. 60, 61, 63

[96] W. Y. Zou and Y. Wu, "COFDM: An overview," *IEEE Transactions on Broadcasting*, vol. 41, no. 1, pp. 1–8, March 1995. 2, 16